UNOBTRUSIVE DETECTION OF BREATHING USING LOAD CELLS AND THE APPLICATION TO SLEEP APNEA DETECTION

By

Zachary Todd Beattie

A DISSERTATION

Presented to the Department of Biomedical Engineering
and the Oregon Health & Science University
School of Medicine
in partial fulfillment of
the requirements for the degree of

Doctor of Philosophy

September 2013

Oregon Health & Science University

CERTIFICATE OF APPROVAL

This is to certify that the PhD dissertation of

Zachary T. Beattie

has been approved

For the late Tamara L. Hayes, Ph.D.:
Owen J. T. McCarty, Ph.D.
Associate Professor
Thesis Research Advisor

Robert J. Peterka, Ph.D.
Associate Professor

Chad C. Hagen, M.D.
Assistant Professor

Monica T. Hinds, Ph.D.
Associate Professor

Peter G. Jacobs, Ph.D.
Assistant Professor

Jeffrey A. Kaye, M.D.
Professor

TABLE OF CONTENTS

List of Tables

List of Figures

List of Abbreviations

AASM	American Academy of Sleep Medicine
ACC_{sum}	summed accelerometer signal
AHI	apnea-hypopnea index
AHI-LC	apnea-hypopnea index from load cell signal
$AHI\text{-}LC_{AUTO}$	apnea-hypopnea index automatically calculated from load cell data
AHI-PSG	apnea-hypopnea index from polysomnography
ANOVA	analysis of variance
AUC	area under receiver operating characteristic curve
BMI	body mass index
CA-LC	central apnea from load cell signal
CM	center of mass
CoP	center of pressure
CPAP	continuous positive airway pressure
cV	coefficient of variation
DBI	disordered breathing index
EDF	European Data Format
FPR	false positive rate
ICA	independent component analysis
LC	load cell
LC_{sum}	summed load cell signal
LL	lower left
LR	lower right

MANOVA	multivariate analysis of variance
MI	movement index
OA-LC	obstructive apnea from load cell signal
OH-LC	obstructive hypopnea from load cell signal
OHSU	Oregon Health & Science University
POCL	Point of Care Lab
PSD	power spectral density
PSG	polysomnography
PSP	Pacific Sleep Program
RDI-LC	respiratory disturbance index from load cell signal
$RDI\text{-}LC_{AUTO}$	respiratory disturbance index automatically calculated from load cell data
RDI-PSG	respiratory disturbance index from polysomnography
RERA	respiratory effort related arousal
RIP	respiratory inductance plethysmography
ROC	receiver operating characteristic
RR_{FLOW}	respiration rate from nasal pressure cannula signal
RR_{LC}	respiration rate from load cell breathing signal
SAS	sleep apnea syndrome
SCSB	static charge sensitive bed
TPR	true positive rate
UL	upper left
UR	upper right
VID	video data

Acknowledgements

One of the main reasons that I came to the Biomedical Engineering Department at Oregon Health & Science University (OHSU) was to have the opportunity to work with Tamara Hayes, Ph.D. From the first time that I met Tamara, I could tell that she was a highly motivated, hardworking professor who, as an advisor, would care about my success. Over the years she taught me how to think critically and how to consider what I was trying to accomplish and break things down into their "1st principles". I couldn't have asked for a better mentor and friend. I hope she is proud.

My dissertation would not be what it is without the enthusiastic help from Chad Hagen, M.D. It was Chad who convinced Tamara and me that using the load cell technology to unobtrusively detect sleep apnea would be "awesome". His knowledge of the sleep medicine field and his ability to "think outside the box" were invaluable to this project. Tamara and I were so impressed with Chad as a collaborator that we followed him from OHSU, to private practice, and back to OHSU. I am especially grateful for Chad's help during the last few weeks of writing this dissertation. I could always count on him for an encouraging email that was "*never sarcastic"*.

I would also like to thank the other members of my dissertation committee: Bob Peterka, Ph.D., Jeff Kaye, M.D., Pete Jacobs, Ph.D., and Monica Hinds, Ph.D. I appreciate everyone's willingness to sacrifice so much of their time and effort in order to help me with the graduating process.

The load cell system only exists because of the technical expertise of John Hunt, M.S.E.E. I am thankful for his assistance in designing the load cell electronics and for pretending to let me help. John also taught me how to solder, graciously allowed me to

spend several weeks in his lab while I meticulously put the load cell electronics together, and helped me out of several binds during the process. It is a testament to John's tutelage that the original sets of load cells still work today. I was convinced that most of my soldering would have shorted out by now.

I would be amiss if I did not acknowledge all the members of the Point of Care Lab team. I think I recruited everyone at some point to help me move mattresses, assist in data collection, or participate as a test subject. I cannot name everyone by name in fear that I would leave someone out, however, I would like to mention Nicole Larimer, Jon Yeargers, and Thomas Riley. Nicole was always happy to edit papers, help with IRBs, and answer a myriad of random questions that I always had. Jon graciously helped solder and assemble the electronics for the more recent load cell assemblies. Thomas was instrumental in helping me collect data at the OHSU and Pacific Sleep program Sleep labs. He helped me calibrate the load cells; he helped me set up the load cell system at both sleep labs; and he wrote software to replace my original code that streamlined the load cell data collection process.

The sleep technologists and other personnel at the OHSU and Pacific Sleep Program sleep labs were very helpful. They took time out of their busy schedules to consent patients, generate sleep study summary data, and remake beds. It seemed that Thomas and I were always adjusting the load cell system, and we could never put the bedding back exactly the way we found it. We have yet to master our "Hospital Corners".

Finally, I would like to thank the ARCS Foundation along with my sponsor Jensen Investment Management represented by Bob and Happy Millen. All the members

of the ARCS Foundation (Portland Chapter) have been so nice and encouraging. In addition, the financial support I received as an ARCS scholar helped keep my ever growing family afloat during my first few years as a graduate student.

Abstract

Unobtrusive Detection of Breathing using Load Cells and the Application to Sleep Apnea Detection

Zachary T. Beattie

Department of Biomedical Engineering
School of Medicine
Oregon Health & Science University

September 2013
Thesis Advisor: Tamara L. Hayes, Ph.D.

The Institute of Medicine reports that "50 to 70 million Americans chronically suffer from a disorder of sleep and wakefulness." Many of these individuals have sleep apnea which is thought to occur in 24% of middle aged men and 9% of middle aged women. It has been estimated that approximately 80% of individuals with moderate to severe sleep apnea syndrome have not been diagnosed. Unfortunately, even those suspected to have this sleep disorder can expect on average to wait several months for diagnosis and treatment due to the inadequate prevalence of overnight polysomnography (PSG).

Polysomnography is the gold standard for detecting sleep disorders. However, an overnight PSG is expensive and obtrusive. Patients admitted for PSG are wired up to several devices. Typically, electrodes are placed on both legs, on the chest, by the eyes, on the chin, and on the scalp. Respiratory induced plethysmography belts are placed around the chest and abdomen. A pulse oximeter is attached to one finger. A nasal pressure cannula and a thermistor are inserted into the nose with the tubing wrapped behind the ears and taped to the face in order to stay in place. Then the patient, who is

already having a difficult time sleeping, is asked to sleep normally in a strange bed while being recorded with both video and audio.

I am interested in being able to unobtrusively monitor sleep, either during PSG or in patients' own homes outside of PSG. Over the years, several devices have been developed to 'unobtrusively' detect respiration while an individual is lying in bed. However, the majority of these devices are either placed on top of or just under the mattress. I theorize that these devices would either disrupt the sleep of the patient or be disrupted by the patient during routine bed sheet changes. Load cells, however, can be placed completely under the bed in a manner that they would rarely, if ever, come in contact with the patient.

In this dissertation, I report the work that I have done to characterize the frequency of response and damping characteristics of the bed/mattress system for several different mattress types. I also describe a novel method for detecting and monitoring the breathing of an individual lying on the bed using a center of pressure signal derived from the load cell data. Finally, I present results showing the ability of the load cell system to be used in the detection and diagnosis of sleep apnea. The load cell system has potential to replace obtrusive breathing sensors in the sleep lab and to be used as a prescreening tool for patients suspected of having sleep apnea. This technology is currently patent pending.

Chapter 1: Introduction

Problem Statement:

Sleep apnea

Sleep is a vital part of living. It consumes, ideally, about one third of everyone's life. While many are able to enjoy the restorative effects of a 'good night sleep', there are a significant number of others who, plagued by various sleep disorders, cannot. The Institute of Medicine reports that 50 to 70 million Americans suffer from what they refer to as a "disorder of sleep and wakefulness" [1]. One of the most common sleep disorders is sleep apnea. Sleep apnea is defined as the cessation of breathing during sleep and is categorized as 'obstructive' when coupled with upper airway obstruction or as 'central' when the pause in breathing coincides with a lack of respiratory effort [2]. When breathing during sleep is only attenuated but associated with a decrease in blood-oxygen saturation, the respiratory event is considered a hypopnea [3].

Sleep apnea is prevalent, associated with several serious medical conditions, and severely under-diagnosed. Sleep apnea is commonly quantified by the number of apnea and hypopnea events that occur per hour otherwise known as the apnea-hypopnea index (AHI). It is estimated that 9% of middle aged women and 24% of middle aged men have an AHI of 5 or more and that 2% of middle aged women and 4% of middle aged men have sleep apnea syndrome (SAS) defined as an AHI of 5 or more associated with

daytime hypersomnolence (i.e. sleepiness) [4]. The overall impact from the prevalence of sleep apnea is compounded by the various health issues that it has been linked to. After a thorough investigation of the literature, Redline et al. concluded that sleep apnea is associated with hypertension, myocardial dysfunction, coronary artery disease, and cardiac arrhythmias [5]. They also pointed out evidence for possible relationships between sleep apnea and a patient's neurocognitive condition, health related quality of life, and mood [5]. Despite the widespread nature of sleep apnea and its negative effects on an individual's health and life, sleep apnea is under-diagnosed. It has been estimated that 80% of middle aged men and women with moderate to severe SAS (AHI $\geq$ 15 with daytime hypersomnolence) have not been diagnosed [6]. All of these results indicate that there is a large population of underserved individuals with a serious health condition.

Clinical assessment of sleep apnea

The accepted gold standard for clinically detecting and diagnosing sleep apnea is polysomnography (PSG). During PSG several electrodes and wires are attached to the patient. Patient brainwaves are monitored using 12 electrodes placed on the head. Eye, chin, and leg movements are tracked using electrodes attached to the patient's face and legs. A nasal cannula placed in each nostril and two respiratory inductance plethysmography (RIP) belts placed around the chest and abdomen are utilized to observe patient respiration. Finally, blood-oxygen saturation is obtained using a pulse oximeter attached to the finger. During an overnight PSG sleep test, a patient who is already having difficulties with their sleep is 'wired up' to all these different devices and then asked to sleep normally in a strange bed in a strange environment while being recorded

with both video and audio. Patients typically sleep differently their first night in the sleep lab [7, 8] likely due in some degree to the sensors that the patient is required to wear [9].

Along with being obtrusive and inconvenient, PSG is also expensive and is not always readily available. Flemons et al. estimate that the number of PSGs performed in the United States each year is too low to sufficiently address sleep apnea [10]. They also found that in the United States the wait time for an individual with sleep apnea to be diagnosed and treated with continuous positive airway pressure (CPAP) can range from 2 to 10 months. The prevalence of SAS and limited access to PSG necessitates supplemental methods for monitoring patients with suspected sleep apnea.

Alternative methods of assessing respiration and sleep apnea

To date many methods have been implemented and several devices have been developed in an attempt to unobtrusively monitor respiration. The design and methodology of these devices have been highly variable. Sensors have been developed to be placed under the patient's pillow [11-16]. Various designs involve monitoring the air pressure in an air mattress or an air bladder [17-22]. Conductive textiles have been placed between the bed sheet and the mattress [23]. Pressure sensors have been integrated into sheets that go on the bed [24, 25]. A couple of groups have placed arrays of several sensors under the mattress to detect the pressure applied to the mattress at various locations [26, 27]. A foam pad sandwiched between two plastic plates that utilizes an array of optical sensors to detect pressure at several points has been positioned between the bed sheet and mattress [28, 29]. Piezoelectric sensors [30-33] and electret foils [34] have been utilized by placing these sensors under the subject's back either just below the bed sheet or beneath a small pad placed on the mattress. Video [35, 36] and

radar [37, 38] have been placed above the bed to track rhythmic movements of the torso due to respiration. The static charge sensitive bed (SCSB), which measures potential differences between two metal plates separated by an insulator and is placed under the mattress, has also been applied to detect respiration [39].

The SCSB has obtained clinical use in Scandinavia with well over a hundred papers reporting its use and effectiveness. However, the SCSB is typically used under a foam mattress and may not work effectively under typical US mattresses. This would necessitate a foam mattress being added to the top of the subject's bed which would alter their normal sleeping arrangement. The SCSB placed under a foam mattress in this manner also has the risk of being moved or altered by the subject during their normal bedding changing procedures. This complication would also be present even if the SCSB could be placed under the subject's normal mattress.

The validation of the remaining devices' ability to detect respiration has significantly varied in depth and quality, and only a few of the devices have been meticulously tested and validated. However, all of them have at least one shortcoming. Any kind of video [35, 36] in the bedroom would be considered obtrusive and unacceptable by many, and some subjects may also object to attaching a radar device [37, 38] to their ceiling or hanging it over their bed in plain view. It is also likely that anything such as bedding that blocks the radio waves from the radar device or the view of the video recorder would affect the use of these devices. The majority of the other devices must be placed between the subject and their mattress [11-19, 21, 23-25, 28-34] which interferes with the normal sleeping arrangement of the subject, runs the risk of the device setup being altered by the subject, and are dependent on the patient lying correctly

over the sensors. The remaining devices that are placed under the mattress [20, 22, 26, 27] also run the risk of subject interference during routine bedding changes.

Unobtrusive Monitoring of Sleep with Load Cells

In recent years several groups including our own lab have begun investigating the use of pressure sensitive load cells placed under the bed to monitor various aspects of sleep. Load cells can be placed under a subject's bed where they will not come in contact with the subject or affect the subject's normal sleep or living routines. They are also very versatile in their applications. Load cells have been used to monitor sleep hygiene [40], detect lying position [41], and distinguish between when an individual is in-bed or out-of-bed [42]. They have also been implemented to detect [43-46] and classify movement [47-49]. Our lab and other groups have shown that load cells can classify a subject's sleep and wake state [50-52] and possibly detect slow-wave sleep [53]. Load cells are also sensitive enough to detect heart rate [44, 52-57] and respiration [44, 58]. However, a load cell system including algorithms that can unobtrusively detect sleep apnea has not been developed.

Contributions to Unobtrusive Breathing and Sleep Apnea Detection

I have developed a system where load cells are placed under the supports of the bed in order to detect the breathing of an individual lying on the bed. While developing this system, I used the load cells to characterize the frequency and damping response of the bed/mattress system which has never been done. In this dissertation I will introduce a new method for using center of pressure (*CoP*) calculations from the load cell data to detect and monitor the breathing of an individual lying on the bed. I am the first to

demonstrate the utility of using load cells placed under the supports of a bed in order to detect sleep apnea. I have shown that load cells are a valid replacement for traditional obtrusive breathing sensors when an overnight PSG sleep study is visually scored by a registered polysomnography technologist for sleep apnea. I have also developed a system to automatically detect sleep apnea only using overnight load cell signals. This is the first time that load cells have been utilized in this manner, the developed techniques are patent pending, and my approach and algorithms could also be applicable to other types of unobtrusive sensors for detecting breathing signals.

This dissertation outlines the development of this load cell system and highlights my contributions to the unobtrusive breathing and sleep apnea detection field. Chapter 2 describes the development and calibration of the load cell system. Chapter 3 presents a mathematical discussion about the theory behind how the load cells can be used to detect the breathing signal of an individual lying on the bed using the *CoP* signal. Chapter 4 contains the experiments and results used to characterize the bed/mattress system. In chapter 5 the ability of the load cell *CoP* signal to accurately detect the breathing of individuals lying on the bed/mattress system independent of lying position and mattress type is demonstrated. A detection algorithm used to detect and remove large movement artifacts when analyzing entire nights of load cell data is outlined in chapter 6. Chapter 7 is comprised of the experiments and results showing how the load cell system can be utilized to detect sleep apnea. Lastly, the summary and conclusions of my dissertation are presented in chapter 8.

Chapter 2: Device Development

Introduction

An important part of this work was to develop a load cell system that could be used to collect data in the Point of Care Lab (POCL) here at Oregon Health & Science University (OHSU), at the sleep center, and in patients' homes. The load cell system can be divided into two parts: the electronics and the connection between the load cells and the bed.

Load Cell Electronics

Several sets of load cells were developed in order to collect data. An initial set of load cells (version 1 or V1) was used to collect data at the OHSU sleep lab and initially at POCL. A second set of load cells (version 2 or V2) was constructed to collect data at the Pacific Sleep Program (PSP) sleep lab. Finally, four sets of load cells (version 3 or V3) were developed to collect additional data at POCL and in study participant's homes. All of the load cell sets are similarly designed, and the slight variations between the three versions are noted in the following description.

The load cell design consists of five to seven single point load cells (AG 100C3SH5eU, SCAIME, Annemasse, France) with 100 kg capacities. Each load cell is connected to a signal conditioning box via DB9M serial connectors. The signal condition

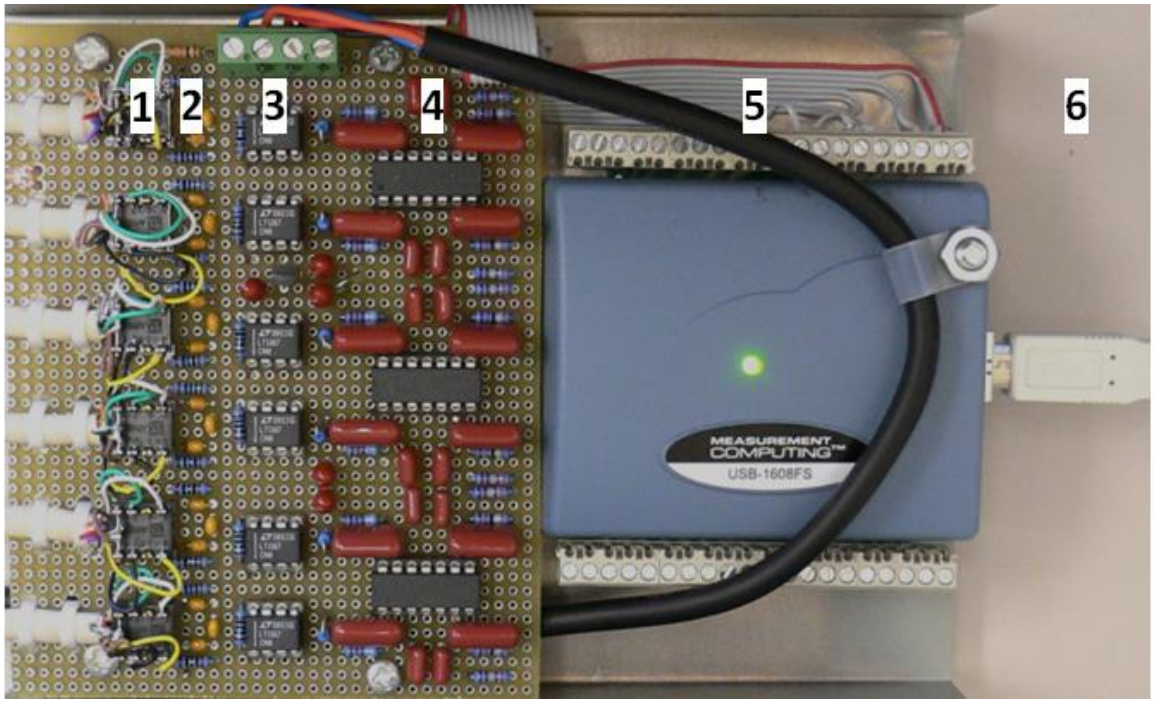

Figure 2-1. Signal conditioning box circuitry. Signal flow is from left to right. (**1**) Signal from load cell. (**2**) RF filter. (**3**) Signal amplification. (**4**) Four pole Butterworth filter. (**5**) Sixteen-bit A/D converter. (**6**) Signal sent to laptop via USB connector.

box contains circuitry assembled in house and a commercially available 16-bit A/D converter (USB-1608FS, Measurement Computing, Norton, MA). Figure 2-1 contains a close-up image of the circuitry from the V1 load cells. The signals from the load cells are first passed through an RF filter that attenuates any radio frequencies. The signals are then amplified with a gain of 265 by an LT1167 instrumentation amplifier. A -4V offset is applied to each signal so that the expected range of the load cells is from -4V at a 0kg load to +3.95V at a 100kg load. Each load cell signal is then filtered using a 4 pole Butterworth filter before being sent to the 16-bit A/D converter. The cutoff frequency for the V1 load cells is set at 150 Hz while the cutoff frequency for the V2 and V3 load cells is set at 50 Hz. Finally, in order to avoid aliasing, the 16-bit A/D converter digitizes each load cell signal at a specified sampling rate (V1 = 2000 Hz and V2/V3 = 500 Hz), and the load cell data is saved on a computer that is connected to the A/D converter via a USB

connection. With the exception of a commercial A/D converter, the electronics used for conditioning the load cell signals were designed and assembled in-house with the assistance of John Hunt M.S.E.E.

Due to observed drift in the time clocks that was different for the computer used to collect PSG data and the laptop used to collected load cell data, a unique synchronization feature was added to the V2 load cells used to collect data at the PSP sleep lab. A synchronization signal consisting of packets that contained five square waves with amplitudes ranging from 1 volt to 5 volts was continuously generated (see figure 2-2). The synchronization signal was recorded by both the PSP PSG computer and

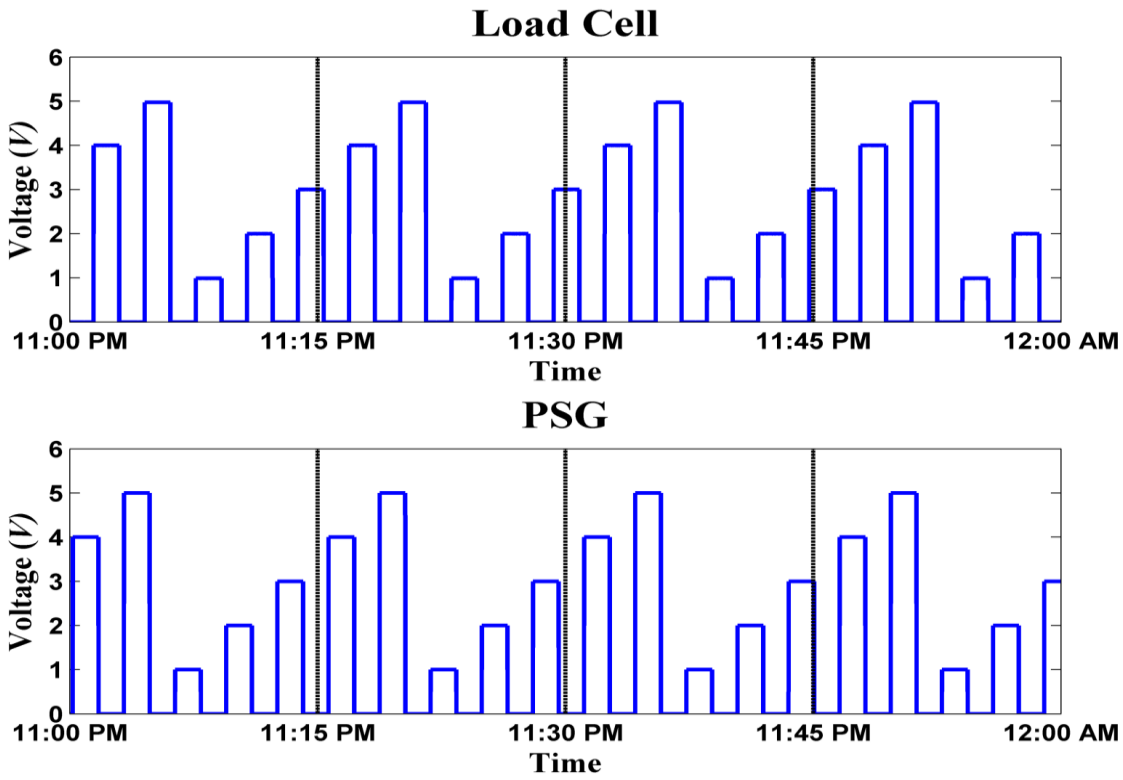

Figure 2-2. The same synchronization signal as recorded by the load cell computer (upper) and the PSG computer (lower). The differing locations of the synchronization signal at the same computer time stamps, as exemplified by the vertical black dashed lines, illustrates the time difference between the computers' clocks used to record the load cell data and PSG data. By aligning the synchronization signal as recorded by both computers using a method such as cross-correlation, the time difference between the two computer clocks can be estimated, and the load cell signal time points can be adjusted to temporally match those of other PSG signals recorded by the PSG computer.

the load cell computer allowing for the offset between the two computer clocks to be estimated. Time alignment between the PSG signals and the load cell signals could then be achieved, post-hoc, by adjusting the timestamps for the load cell data in order to match the timestamps from the PSG data.

Load Cell Bed Supports

An important aspect of the load cell systems was the mode in which the load cells were placed under the supports of the bed. Determining the method to attach the load cells to the bed supports was difficult because the load cell/bed connection needed to be safe, secure, and sturdy while still being simple to install; generalizable across different bed frames; and not too altering of the original bed setup. An example of the first bed / load cell attachments is shown in figure 2-3. A small block of cedar with a hole bored

Figure 2-3. Resistive load cell design (V1). Six single point load cells shown on the right are connected to a signal conditioning box shown in the upper left via serial connectors. The upper most load cell is attached to the cedar bed attachments. The cedar block attached to the top of the upper most load cell is designed to support and contain the foot of the bed support. The base of the load cell rests in another cedar block. Not shown in the image are the 1.27cm thick steel plates bolted to the bottom of the load cells or the bolt and washer system used to securely clamp the load cells into the bottom cedar support.

partially through one side was bolted to the top of the load cell. A 1.27cm thick steel bar is bolted to the bottom of the load cell and this entire setup is placed in a 20 cm long cedar block that has had the centered hollowed out. The load cells were clamped securely to this cedar block using bolts and washers. With this system, the supports of the bed simply rested inside the hole bored out of the cedar block. These bed connections were simple to install and fairly generalizable. However, I discovered that the design did not support the bed in a completely stable manner.

In order to improve how safe, secure, and sturdy the bed connections were, a new design was developed. This new design was still easy to install and did not significantly alter the original setup. However, the new load cell bed connections were specifically designed to be used with a standard metal frame leading to a loss of some generalizability, but the connections should be functional with most brands and sizes of metal bed frames. A metal piece was fabricated that could be bolted to the load cell on one end and securely attached to the leg of the metal bed frame on the other end. This metal piece was bolted to a 2.3 cm by 2.5 cm by 5 cm metal block that is attached to the load cell. A 12.7 cm by 25.7 cm by 1.2 cm metal slab was bolted to the bottom of the load cell. A protective aluminum casing was placed over the load cell and secured to the aluminum slab. The aluminum slab corners were rounded to match the shape of the protective casing, and two holes were cut out of the casing for the metal bed connector and the load cell cord. An example of the load cell system actually set up under a bed with the new bed attachments is shown in figure 2-4.

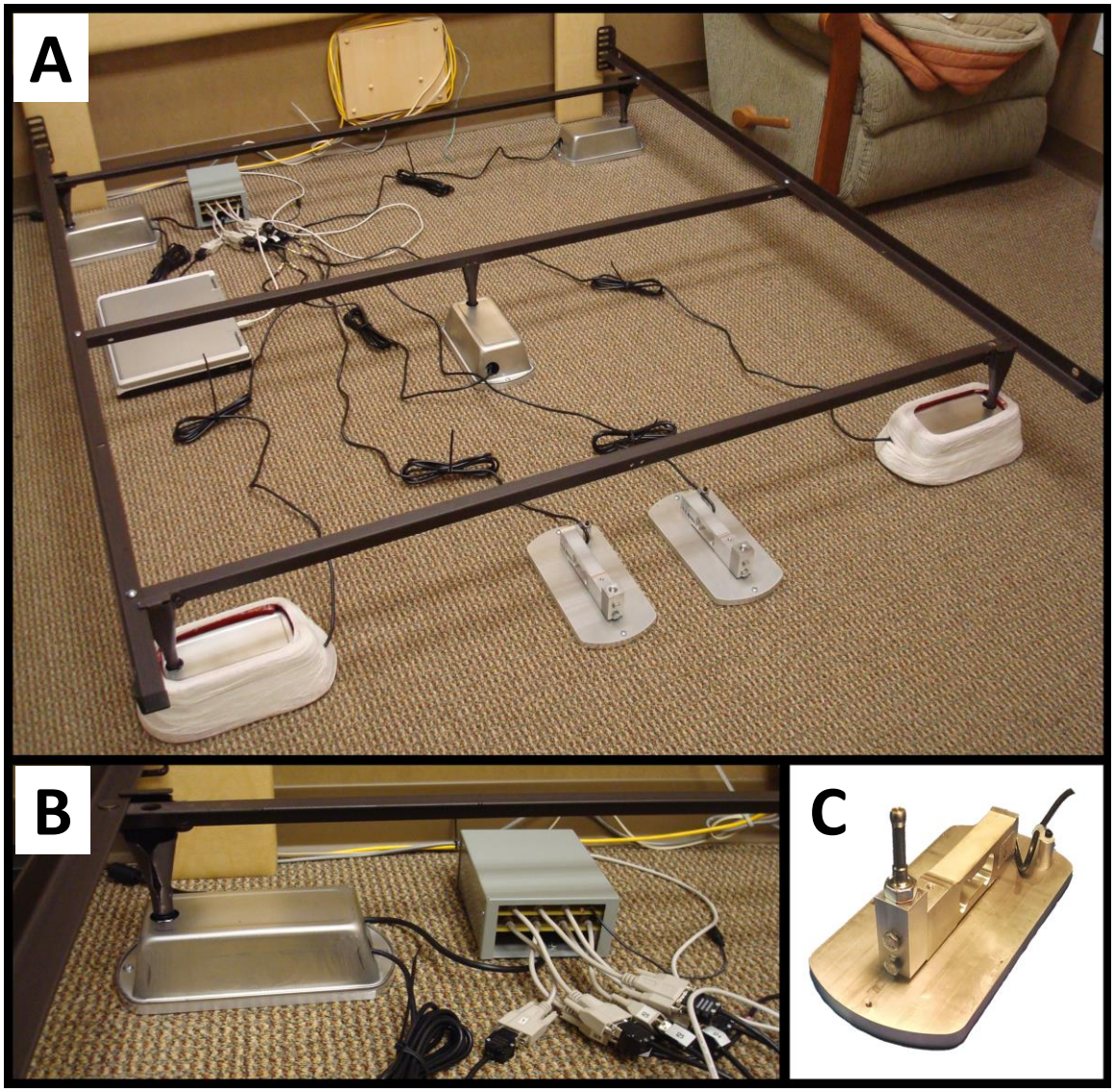

Figure 2-4. (**A**) Load cell setup at the Pacific Sleep Program sleep lab. Five load cells were attached to the supports of the metal bed frame (mattress and box spring have been removed). Each load cell was connected to the signal conditioning box in the upper left corner. The A/D converter (inside the signal conditioning box) exported the load cell data to a laptop via a USB connection. The two load cells attached to the bed supports at the foot of the bed were wrapped with padding in case a patient inadvertently bumped into the load cell with their foot. Two load cells (without aluminum casings) are shown but were not attached to the bedframe or utilized. (**B**) Close up of the signal conditioning box and a load cell attached to a support of the bed. (**C**) Image of a load cell without its aluminum casing. The image illustrates how the load cell is attached to the aluminum base and shows the metal piece that is bolted to the top of the load cell allowing for a secure attachment to a metal bedframe.

Load Cell Calibration

The raw output of each load cell is a digitized voltage signal ranging from approximately -4 V to 4 V. In order to be able to interpret the load cell data using meaningful units, the load cells were calibrated to ascertain the relationship between the voltage output of each load cell and the corresponding force applied to the load cell.

A small plate of 14.2 N was attached to the load cell that was being calibrated. Data was collected for 10 seconds, and then an approximately 107 N weight was placed on the platform. Data was again collected for 10 seconds. This process of adding an additional approximately 107 N weight and collecting 10 seconds of load cell data was repeated until the load cell was loaded with eight 107 N weights. Data was collected with the load cell loaded with eight weights for two 10 second periods and then 10 seconds of data was collected again as each weight was sequentially removed. This process of loading and unloading the load cell was repeated two times resulting in four 10 second periods of data being collected for each loading of the load cell from no weights on the platform to a total of eight weights on the platform. This calibration was repeated for each load cell.

The means were calculated for each 10 second period of data collected from the load cells. The calibration for each load cell was found by determining the relationship between the known force applied to the load cell and the recorded output of the load cell. Assuming that the load cell output was linearly related to the applied force, this relationship was defined using a least squares regression line fit to the load cell output and applied force data pairs. The coefficients for *a* (slope) and *b* (intercept) from the least squares regression line $y = ax + b$, where x is the load cell output and y is the

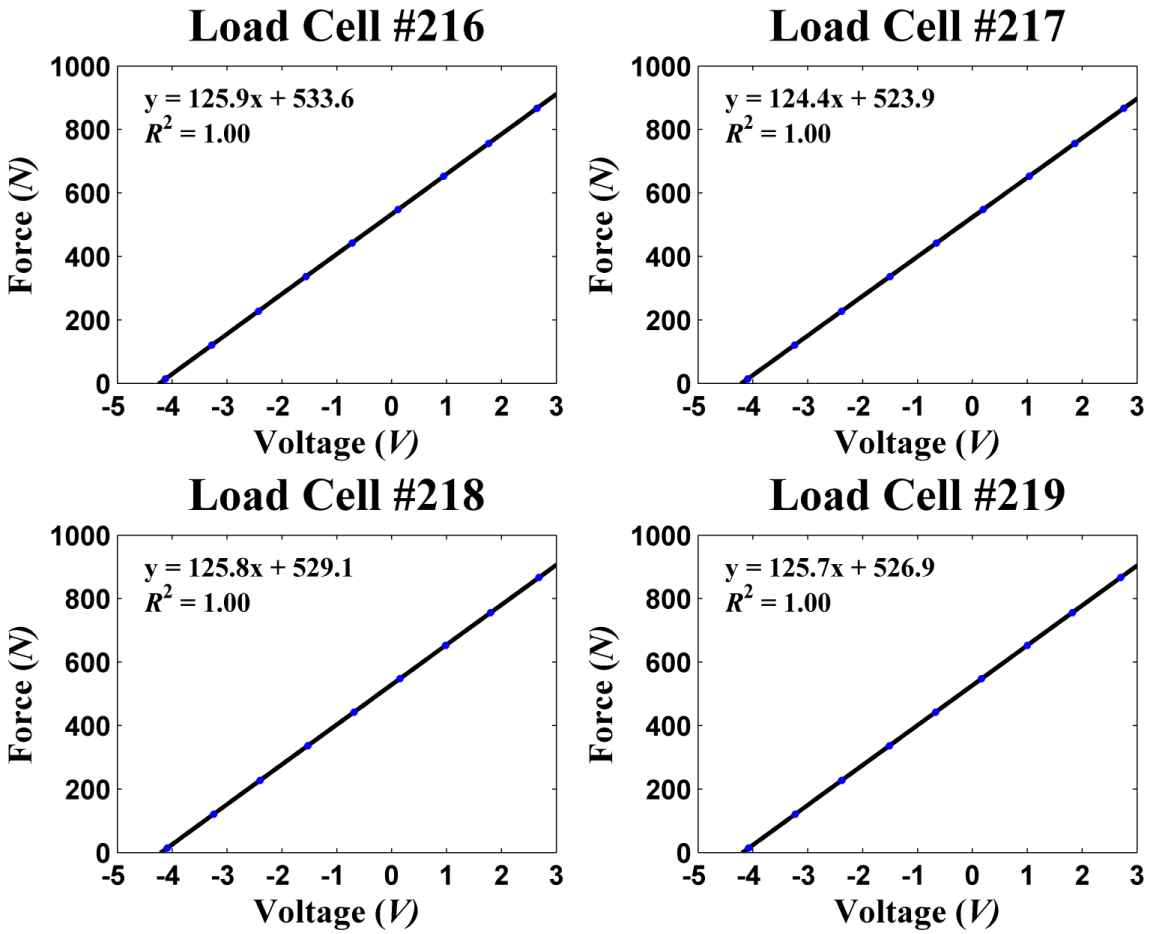

Figure 2-5. Calibration for four load cells (V3) showing the resulting slopes (*a*) and intercepts (*b*) for converting the load cell output in voltage (*V*) to the known applied force (*N*). The averaged output for each 10 second load cell data collection is shown as a blue circle. Error bars calculated as ± one standard deviation for each 10 second segment are plotted but are too small to be visible. The results of the linear regression for all 36 data segments (4 ten-second load cell data segments for each of the 9 loading conditions) is represented using a black line. These load cells were placed under the four supports of various bed/mattress systems at the POCL, and were used to collect data during the "Bed/Mattress System Characterization" experiment in chapter 4, the "Bed/Mattress System Response to Low Speed Mass Movement" experiment also in chapter 4, and the "Breathing Detection Validation Experiment 2: Different Mattress Types" experiment in chapter 5.

predicted load on the load cell, are found by minimizing the error $\sum_i \left(Y_i - y_i\right)^2$ where Y is the actual weight applied to the load cell. The calibrations for four load cells (V3) are shown in figure 2-5. The calibrations for the remaining load cells (V1 & V2) used to collect data for the experiments presented herein are contained in tables 2-1 thru 2-3.

Table 2-1

Calibration for the six load cells (V1) placed under the supports of the bed at the OHSU sleep lab. These load cells were used to collect part of the data used during the "Sleep Apnea Detection: Automatic Scoring" experiment in chapter 7.

Load Cell	Slope (*a*)	Intercept (*b*)
1	125.3	512.0
2	124.7	504.6
3	124.7	498.2
4	125.8	510.3
5	122.9	488.6
6	123.9	498.6

Table 2-2

Calibration for the 4 load cells (V1) used to collect data for some experiments at the POCL. These load cells were used to collect the data used for the "Movement Detection and Removal" experiment in chapter 6 and the "Breathing Detecting Validation Experiment 1: Different Lying Positions" in chapter 5.

Load Cell	Slope (*a*)	Intercept (*b*)
131	125.3	511.0
132	124.7	503.4
133	124.6	497.1
135	125.5	508.6

Table 2-3

Calibration for the five load cells (V2) placed under the supports of the bed at the PSP sleep lab. At one point the fittings on these load cells were re-tightened and the calibration process was repeated. These load cells (using calibration #1) were used to collect the data used during the "Sleep Apnea Detection: Visual Scoring" experiment in chapter 7 and for part of the data (using a mixture of calibration #1 and calibration #2) used during the "Sleep Apnea Detection: Automatic Scoring" experiment in chapter 7.

Load Cell	Slope (*a*) #1/#2	Intercept (*b*) #1/#2
121	124.2/124.7	509.3/511.8
123	125.1/125.1	513.6/513.5
124	123.9/123.8	507.6/507.3
125	125.4/125.6	510.8/511.7
127	125.3/125.3	515.7/515.6

Chapter 3: Load Cell Breathing Signal Origin

Introduction

The load cell system is comprised of force sensors (i.e. load cells) that are placed under each support of a bedframe (figure 2-4). The load cells are transducers that convert the amount of weight (or force) supported by each bed leg into an electrical signal measured in volts. The electrical signal is amplified, filtered, and digitized using the electronics described in chapter 2 and then logged using a laptop or other computer. The calibration procedure also described in chapter 2 is used to convert the voltage signal from the load cells into units of force (Newton). In this chapter, I describe how the force readings from each load cell under the supports of the bed can be used to detect small movements of mass that represent the breathing of a person lying on the bed.

How the Breathing Signal is captured by Load Cells

As an individual lies on the bed, the load cells detect the forces supported by each bed leg. When the individual breathes in, their diaphragm displaces several visceral organs towards the foot of the bed. Hence, the load cells at the foot of the bed see a relative increase in force, and the load cells at the head of the bed see a relative decrease in force. Conversely, when the individual breathes out, the mass of the visceral organs are displaced towards the head of the bed leading to a relative increase in forces

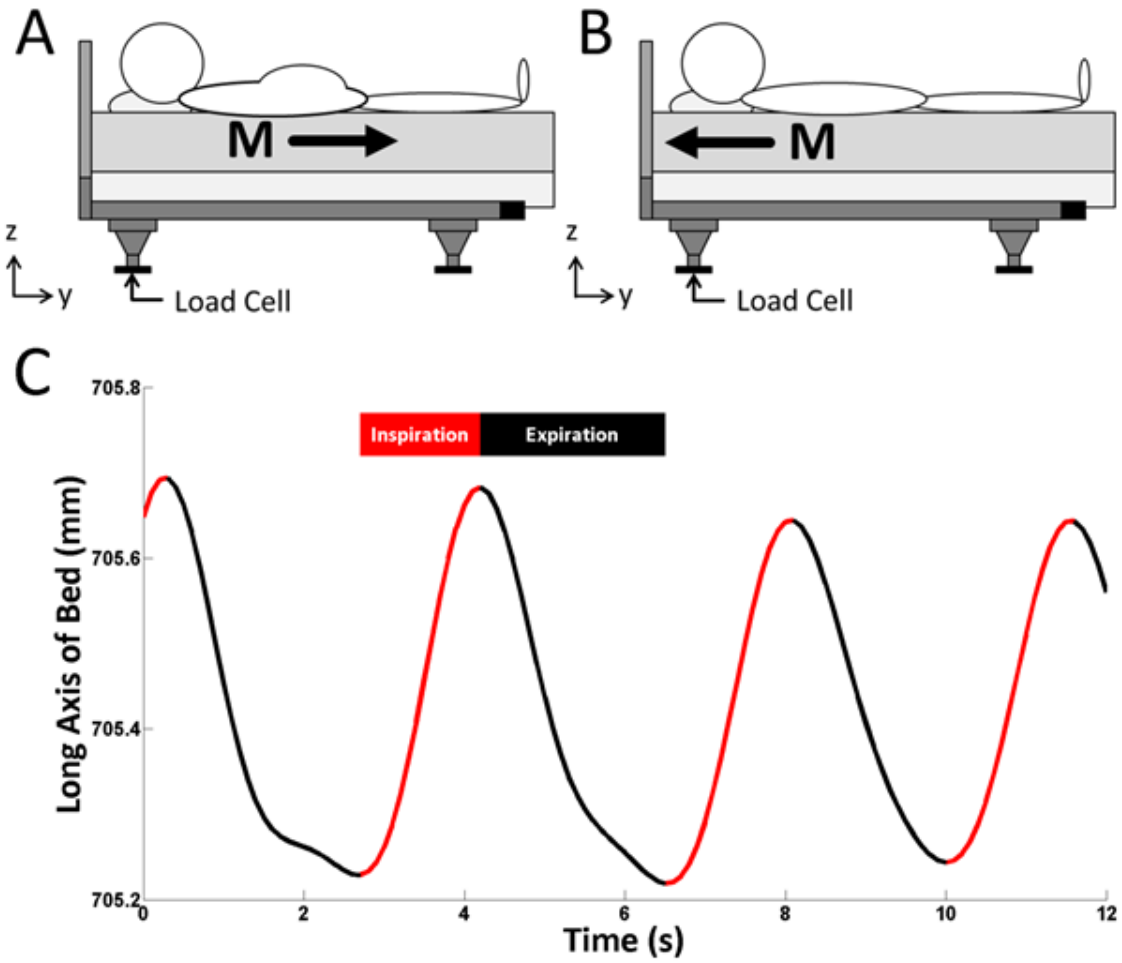

Figure 3-1. (**A-B**) Illustration of how the load cells detect breathing via small mass (M) displacements. As an individual lies on the bed, the load cells detect the forces supported by each bed leg. (**A**) During inspiration mass is displaced towards the foot of the bed. (**B**) During expiration mass is displaced towards the head of the bed. (**C**) An example of a load cell breathing signal collected from an individual lying on the bed is shown. Periods of inspiration are marked in red and periods of expiration are marked in black.

measured at the head of the bed and a relative decrease to forces measured at the foot of the bed. These quasi-periodic changes in the relative forces detected by the load cells represent the breathing signal of the individual lying on the bed (see figure 3-1 (A & B) [59]).

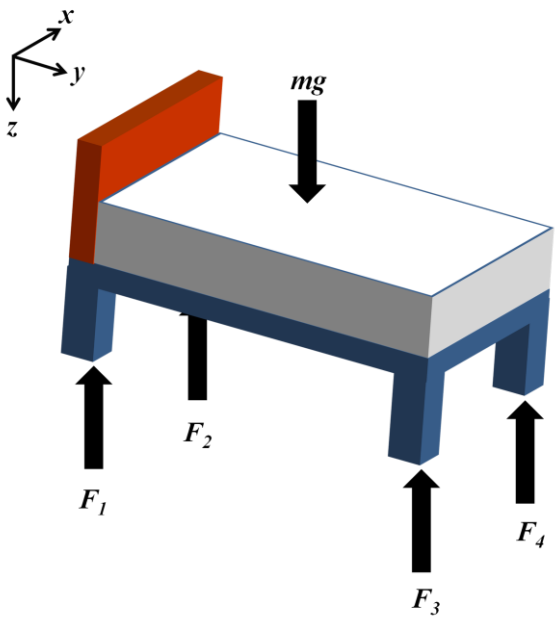

Figure 3-2. A generic bed/mattress system with four supports. The force of the bed, mattress, and individual lying on the bed is shown as ***mg***. The reaction forces that support the system are represented as $\boldsymbol{F_1}$, $\boldsymbol{F_2}$, $\boldsymbol{F_3}$, and $\boldsymbol{F_4}$.

With the load cells placed under each support of a bed effectively supporting its entire weight, the load cells can theoretically be utilized to track the changes in the center of mass caused by an individual breathing while lying on top of the bed/mattress system. A generic bed/mattress system with four supports is shown in figure 3-2. The weight of the bed, mattress, and individual lying on the bed are represented as the force ***mg*** which is located at the center of mass (CM) for the entire system. The ground reaction forces that support the bed and everything else are represented as $\boldsymbol{F_1}$, $\boldsymbol{F_2}$, $\boldsymbol{F_3}$, and $\boldsymbol{F_4}$ and they act in the z-direction opposite to ***mg***. The locations of each force in the 3 dimensional Cartesian coordinate are represented as $\boldsymbol{r_{1\text{-}4}}$, and $\boldsymbol{r_{CM}}$ is the location of the overall CM for the bed, mattress, and individual. If we assume that the system is in mechanical equilibrium, then the sum of the moments (***M***) about an arbitrary point *p* must be 0 [60].

$$\sum \boldsymbol{M}_p = 0 = \boldsymbol{r}_1 \times \boldsymbol{F}_1 + \boldsymbol{r}_2 \times \boldsymbol{F}_2 + \boldsymbol{r}_3 \times \boldsymbol{F}_3 + \boldsymbol{r}_4 \times \boldsymbol{F}_4 + \boldsymbol{r}_{CM} \times \boldsymbol{mg} \tag{3.1}$$

The cross product for each force (***F***) and moment arm (***r***) can be solved using the following determinants [61]:

$$0 = \det\left(\begin{bmatrix} \boldsymbol{i} & \boldsymbol{j} & \boldsymbol{k} \\ r_1^x & r_1^y & r_1^z \\ F_1^x & F_1^y & -F_1^z \end{bmatrix}\right) + \det\left(\begin{bmatrix} \boldsymbol{i} & \boldsymbol{j} & \boldsymbol{k} \\ r_2^x & r_2^y & r_2^z \\ F_2^x & F_2^y & -F_2^z \end{bmatrix}\right) + \det\left(\begin{bmatrix} \boldsymbol{i} & \boldsymbol{j} & \boldsymbol{k} \\ r_3^x & r_3^y & r_3^z \\ F_3^x & F_3^y & -F_3^z \end{bmatrix}\right) + \det\left(\begin{bmatrix} \boldsymbol{i} & \boldsymbol{j} & \boldsymbol{k} \\ r_4^x & r_4^y & r_4^z \\ F_4^x & F_4^y & -F_4^z \end{bmatrix}\right) + \det\left(\begin{bmatrix} \boldsymbol{i} & \boldsymbol{j} & \boldsymbol{k} \\ r_{CM}^x & r_{CM}^y & r_{CM}^z \\ mg^x & mg^y & mg^z \end{bmatrix}\right) \tag{3.2}$$

where $\boldsymbol{i}$, $\boldsymbol{j}$, and $\boldsymbol{k}$ represent unit vectors in the respective x, y and z axes, and the force vectors ($\boldsymbol{F}$) and moment arms ($\boldsymbol{r}$) have been broken down into their x, y, and z components. Each individual determinant can be expanded.

$$\begin{aligned} 0 = {} & -F_1^z r_1^y \boldsymbol{i} + F_1^x r_1^z \boldsymbol{j} + F_1^y r_1^x \boldsymbol{k} - F_1^x r_1^y \boldsymbol{k} - F_1^y r_1^z \boldsymbol{i} + F_1^z r_1^x \boldsymbol{j} - \\ & F_2^z r_2^y \boldsymbol{i} + F_2^x r_2^z \boldsymbol{j} + F_2^y r_2^x \boldsymbol{k} - F_2^x r_2^y \boldsymbol{k} - F_2^y r_2^z \boldsymbol{i} + F_2^z r_2^x \boldsymbol{j} - \\ & F_3^z r_3^y \boldsymbol{i} + F_3^x r_3^z \boldsymbol{j} + F_3^y r_3^x \boldsymbol{k} - F_3^x r_3^y \boldsymbol{k} - F_3^y r_3^z \boldsymbol{i} + F_3^z r_3^x \boldsymbol{j} - \\ & F_4^z r_4^y \boldsymbol{i} + F_4^x r_4^z \boldsymbol{j} + F_4^y r_4^x \boldsymbol{k} - F_4^x r_4^y \boldsymbol{k} - F_4^y r_4^z \boldsymbol{i} + F_4^z r_4^x \boldsymbol{j} + \\ & mg^z r_{CM}^y \boldsymbol{i} + mg^x r_{CM}^z \boldsymbol{j} + mg^y r_{CM}^x \boldsymbol{k} - mg^x r_{CM}^y \boldsymbol{k} - mg^y r_{CM}^z \boldsymbol{i} - mg^z r_{CM}^x \boldsymbol{j} \end{aligned} \tag{3.3}$$

Equation 3.3 can be simplified by assuming that the forces ($\boldsymbol{F}$) supporting the bed and $\boldsymbol{mg}$ act only in the z-direction and are 0 in the x and y-directions.

$$\begin{aligned} 0 = {} & -F_1^z r_1^y \boldsymbol{i} + F_1^z r_1^x \boldsymbol{j} - F_2^z r_2^y \boldsymbol{i} + F_2^z r_2^x \boldsymbol{j} - F_3^z r_3^y \boldsymbol{i} + F_3^z r_3^x \boldsymbol{j} - \\ & F_4^z r_4^y \boldsymbol{i} + F_4^z r_4^x \boldsymbol{j} + mg^z r_{CM}^y \boldsymbol{i} - mg^z r_{CM}^x \boldsymbol{j} \end{aligned} \tag{3.4}$$

Separating the equation into its $\boldsymbol{i}$ and $\boldsymbol{j}$ components

$$0 = -F_1^z r_1^y \boldsymbol{i} - F_2^z r_2^y \boldsymbol{i} - F_3^z r_3^y \boldsymbol{i} - F_4^z r_4^y \boldsymbol{i} + mg^z r_{CM}^y \boldsymbol{i} \tag{3.5}$$

$$0 = F_1^z r_1^x \boldsymbol{j} + F_2^z r_2^x \boldsymbol{j} + F_3^z r_3^x \boldsymbol{j} + F_4^z r_4^x \boldsymbol{j} - mg^z r_{CM}^x \boldsymbol{j} \tag{3.6}$$

and then solving for $\boldsymbol{r_{CM}}$ leaves

$$r_{CM}^y = \frac{\left(F_1^z r_1^y + F_2^z r_2^y + F_3^z r_3^y + F_4^z r_4^y\right)}{mg^z} \tag{3.7}$$

$$r_{CM}^x = \frac{\left(F_1^z r_1^x + F_2^z r_2^x + F_3^z r_3^x + F_4^z r_4^x\right)}{mg^z} \tag{3.8}$$

showing that the forces detected by the load cells supporting the bed can be used to estimate the CM of the entire bed/mattress system with an individual lying on the mattress. Assuming that mg^z is equivalent to the sum of the output from all the load cells, this relationship is represented by

$$\boldsymbol{CM} = \frac{\sum_{i=1}^{N} LC_i \left[x_i, y_i\right]}{\sum_{i=1}^{N} LC_i} \tag{3.9}$$

where $\boldsymbol{CM}$ is the xy coordinates of the center of mass , LC_i is the force measurement recorded by the i^{th} load cell, N is the number of load cells, and x_i and y_i are the coordinate locations of the i^{th} load cell. However, when an individual is lying even quiescent on the bed/mattress system, movements of mass caused by respiration are likely to generate forces that were not accounted for in the model represented in equation (3.1). Therefore, some error will be introduced when using the load cells to estimate the mass movement resulting from the individual's breathing. Consequently, CM estimates acquired using the load cell data will be referred to as center of pressure (*CoP*) measurements:

$$CoP(t) = \frac{\sum_{i=1}^{N} LC_i(t)\left[x_i, y_i\right]}{\sum_{i=1}^{N} LC_i(t)} \tag{3.10}$$

where $LC_i(t)$ is the force measurement recorded by the i^{th} load cell at time *t*.

The load cell *CoP* signal was utilized to validate the assumption that the load cells detect the breathing of an individual on the bed by tracking the displacement of the organs towards the foot of the bed during inspiration and conversely towards the head of the bed during expiration. Ten minutes of load cell data were collected while an individual lay quiescently on their back on the bed/mattress system. At approximately the 0.5, 1.5 2.5, 3.5, and 4.5 minute marks, the subject was instructed to hold their breath

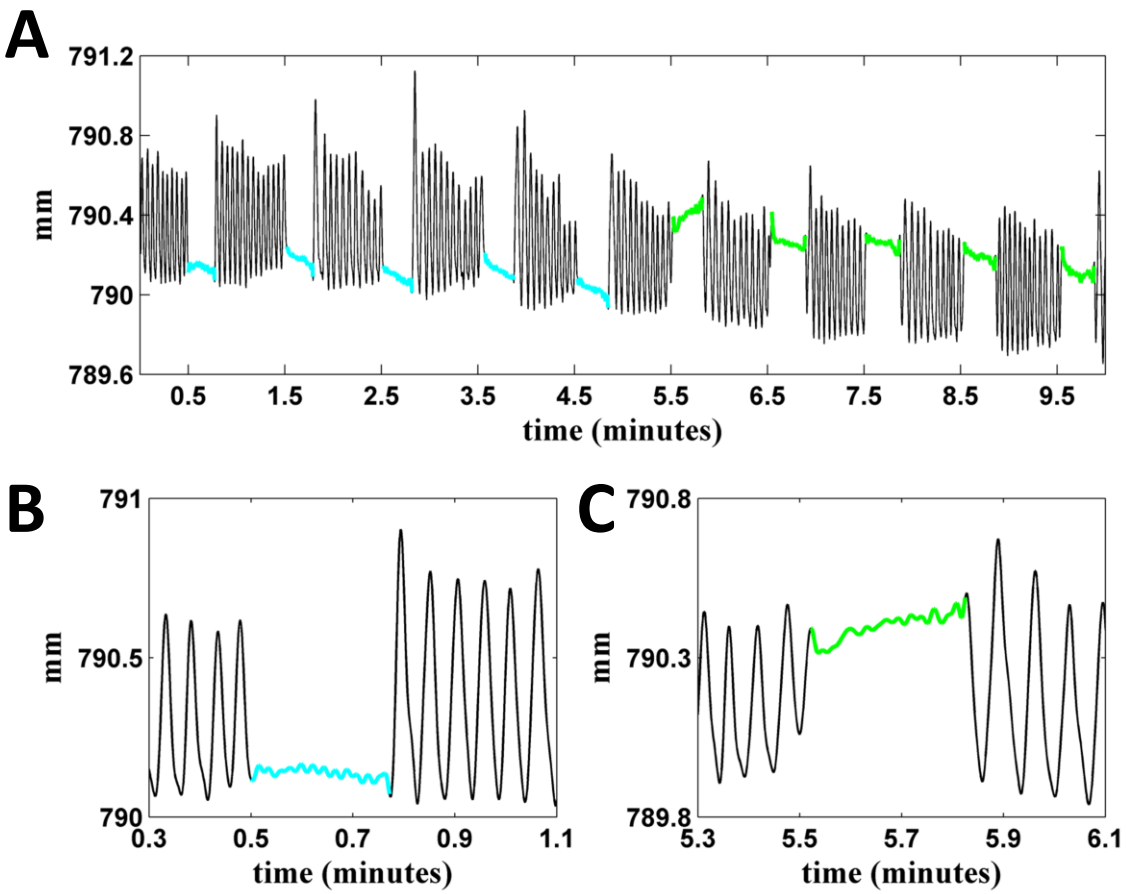

Figure 3-3. (**A**) Ten minutes of the CoP_y signal calculated from load cell data collected while a subject was lying on their back on the bed/mattress system. The subject held their breath 5 times at the end of expiration (marked in blue) and 5 times at the end of inspiration (marked in green). The CoP_y signal was low-pass filtered using a 4th order Chebyshev Type II filter that was monotonic in the pass-band, had a stop-band edge frequency of 1.6 Hz, and attenuated the stop band by 40 dB. (**B**) Close up view of the subject holding their breath after expiration. The CoP_y signal shows the mass holding near the lower values y indicating that the mass has been displaced towards the head of the bed as y = 0 was defined to be at the head of the bed when calculating CoP_y. (**C**) Close up view of the subject holding their breath after inspiration. The mass appears to remain around the higher values of y indicating that the mass was displaced towards the foot of the bed during inspiration.

for about 15 seconds at the end of expiration. Then, at approximately the 5.5, 6.5, 7.5 8.5, and 9.5 minute marks, the subject was instructed to hold their breath for about 15 seconds at the end of inspiration. Figure 3-3 contains the 10 minute filtered *CoP* signal calculated using the load cell data and equation 3.10 in the y-direction (i.e. the long axis of the bed).

When calculating the CoP_y signal, the Cartesian coordinate system was designed to have the origin at the upper right (UR) corner of the bed (in reference to the subject's right while lying on the bed/mattress system on their back) with the positive y axis extending towards the foot of the bed. This particular coordinate axis system was chosen so that inspiration would be represented as a positive deflection in the CoP_y signal (i.e. increasing values in the y-direction) and expiration would be seen as a negative deflection (i.e. decreasing values in the y-direction). The periods when the subject was holding their breath as seen in the CoP_y signal in figure 3-3 verify the model that during inspiration mass from the visceral organs is displaced towards the foot of the bed (i.e. increasing values in the y-direction), and that this mass is displaced towards the head of the bed (i.e. decreasing values in the y-direction) during expiration. Another example of the CoP_y load cell breathing signal collected from an individual lying on the bed is shown in figure 3-1 (C).

Chapter 4: Bed/Mattress System Characterization and Testing

Bed/Mattress System Characterization

Motivation

Empirical evidence suggests that the bed/mattress system has an effect on the load cell signals recorded when an individual lies on the bed. In particular, frequency analysis of the load cell signals reveals a significant amount of power in the respiration frequencies (i.e. < 1 Hz) and in the 2-5 Hz range (suspected to be the resonance response of the bed/mattress system to the heart beating) when an individual lies on the bed (see figure 4-1). Therefore, in order to better understand how the bed/mattress system may affect the ability of the load cell system to detect the breathing of an individual lying on the bed, I experimentally estimated the impulse response of the entire structure for several different mattress types. I specifically analyzed the mass dependent frequency of response and damping characteristic for each mattress's response to an impulse.

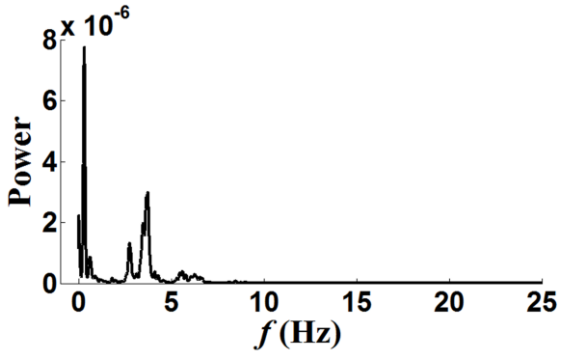

Figure 4-1. Power spectral density from one minute of data collected from a single load cell when an individual is lying on the bed.

Figure 4-2. Illustration of the setup used to characterize the effect of an impulse being applied to the bed/mattress system. The wooden platform is placed one the mattress in the approximate location of an individual lying in the middle of the bed. The platform has two locations for mass to be incrementally loaded onto the bed. The center of the platform has also been removed for the application of the impulse.

Setup

Load cells were placed under the supports of a standard metal full sized bed frame in the Point of Care Laboratory. A 1.8 cm piece of plywood with similar dimensions to the mattresses was placed on top of the metal frame and was used to support one of the four different mattresses used for the experiment. Four different mattress types were used for this experiment: 1.) a mattress with an air-filled bladder with adjustable air pressure encased in foam (similar to a Sleep Number® mattress), 2.) a mattress made of memory foam (similar to a Tempur-Pedic® mattress), 3.) a spring coil mattress with independent springs (i.e. springs that are not connected), and 4.) a coiled mattress with dependent springs (i.e. all the springs are connected). During the experiments, a wooden platform (91.4 cm x 40.3 cm x 1.9 cm) that was specially manufactured to be loaded with several masses was placed on top of the mattress. A round hole was cut out of the center of the platform (diameter ≈ 26 cm) allowing a small mass (0.77 kg) to be dropped onto the respective mattress acting as the applied impulse (see figure 4-2). The wooden platform was placed on each respective mattress so that the hole cut out for the impulse was approximately in the location of an individual's chest if they were to be lying on the mattress.

Methods

One minute of load cell data was collected for each mattress before they were loaded with the wooden platform and masses. The wooden platform was then placed on the bed and incrementally loaded with 8 various amounts of mass ranging from 0 kg to approximately 132 kg. At each loading of the wooden platform, one minute of load cell data was collected using a sampling rate of 500 Hz for each individual load cell. At about the 25 second mark during each data collection, an impulse was applied to the mattress by dropping an 'impulse' weight (0.77 kg) onto the mattress in the approximate center of the hole cut out of the wooden platform from a height of about 30 cm. The impulse mass was allowed to "bounce" only once on the mattress before being caught and removed. The exception being the experiments performed using the foam mattress where the impulse mass did not physically "bounce" off the mattress and was therefore simply dropped and left. Load cell data with the corresponding impulse was collected 4 separate times for each of the various mass loadings on the bed. This protocol was followed for each mattress. For a more detailed explanation of the experiment protocol, please refer to Appendix A.

Analysis

I theorized the bed/mattress system would respond to an impulse with decaying oscillations due to results from preliminary testing. Therefore, in order to analyze the response of the bed/mattress to an impulse, I modeled the response of each load cell independently as a damped sine wave,

$$z(t) = Ae^{-\lambda t}\sin\left(2\pi ft + \varphi\right) \tag{4.1}$$

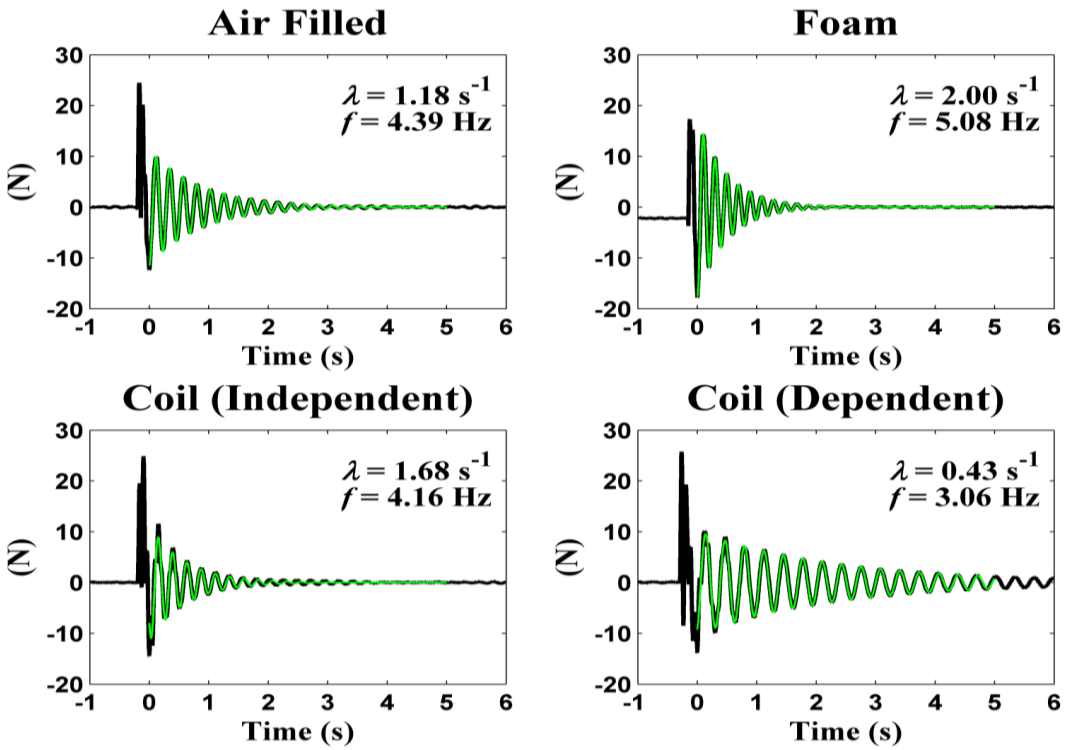

Figure 4-3. Load cell data collected from the UR load cell for each different mattress type after an impulse was applied with approximately 90 kg loaded on the bed/mattress system. The raw load cell signal is shown in black, and the results of fitting the load cell data to the damped spring model is shown in green. When fitting the load cell data to the model: the median was subtracted, t = 0 was chosen as the point of minimum value in the load cell signal, and the following 5 seconds of load cell data was used for the model. The amount of damping (λ) and frequency of response (f) are also displayed.

where A is the amplitude, λ represents the rate of decay, f is the frequency of oscillation in Hz, and φ is the initial phase of the sinusoid.

The amount of damping (i.e. λ) and the frequency of response (i.e. f) for each mattress at each loading condition was ascertained by fitting the load cell data resulting from each applied impulse to equation 4.1[1]. The data from each individual load cell was fit separately. Figure 4-3 shows an example of load cell data collected after an applied impulse and the corresponding results after the data has been fit to the model described in equation 4.1. In order to gain some insight into the relationship between the damping and frequency of response for each bed/mattress system and the amount of mass loaded on

[1] A and φ were also determined during the fitting process but are not reported herein.

the mattress, the average λ and f were estimated along with the corresponding mass loaded on the mattress for each loading condition. The averaged sum of data from all the load cells, collected for 10 seconds before each impulse was applied, minus the weight of the overall bed/mattress system was used to estimate the amount of mass on the mattress for each loading condition. This averaged sum was divided by the acceleration due to gravity ($g = 9.80665\ m/s^2$) so the mass would be in units of kg.

Fitting the impulse response collected by the load cell data to the previously described damped sinusoid should accurately represent the prevailing response of the bed immediately after the impulse. However, there also may be some residual effects of the impulse that are not as evident. In order to ascertain other possible responses to the impulse, the spectral content of the load cell signals was calculated. Specifically, Welch's method [62] was used to estimate the power spectral density for 30 seconds of load cell data (decimated to a sampling rate of 25 Hz) beginning 5 seconds after each impulse.

Results

Figure 4-4 contains 4 individual plots showing the mass dependent frequency of responses found for each load cell across all four mattress types. The load cells are designated as upper right (UR), upper left (UL), lower right (LR), and lower left (LL), where upper refers to the head of the bed, lower refers to the foot of the bed, and left-right is determined in reference to an individual lying on their back on the bed. The plots show that while each mattress type exhibits slightly different response frequencies, there is a similar trend of decreasing frequency of response across all mattress types as mass loading on the bed increases. It should be mentioned that when fitting the model to the

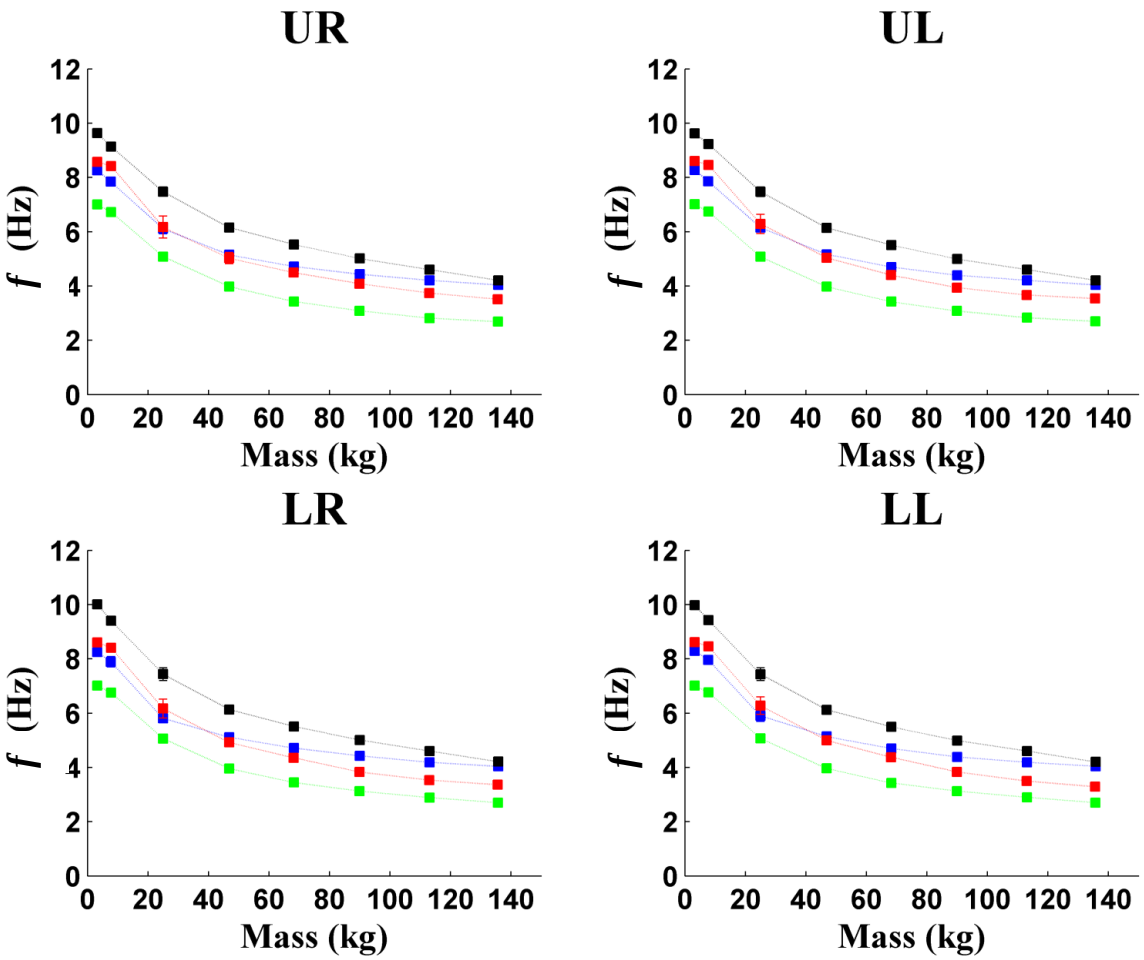

Figure 4-4. Mass dependent frequency response for each load cell across all mattress types. The different colors represent the different mattress types. The air-filled mattress results are shown in blue, the foam mattress results are shown in black, the independently coiled mattress results are shown in red, and the dependently coiled mattress results are shown in green. The squares represent the mean frequency response across the four trials, and the error bars signify one standard deviation. It should be noted that many of the error bars are not visible due to the relatively small nature of the represented standard deviations.

load cell data there were no constraints set for the model parameters which led to a few results with negative frequencies (f). All the results with negative frequencies had similar absolute values to the other non-negative frequencies estimated from the other trials with the same setup. Therefore, it may have been that the negative frequencies were a result of the final value chosen during the fitting process for φ. When calculating the mean frequency of response, shown in figure 4-4, any negative frequencies were simply ignored.

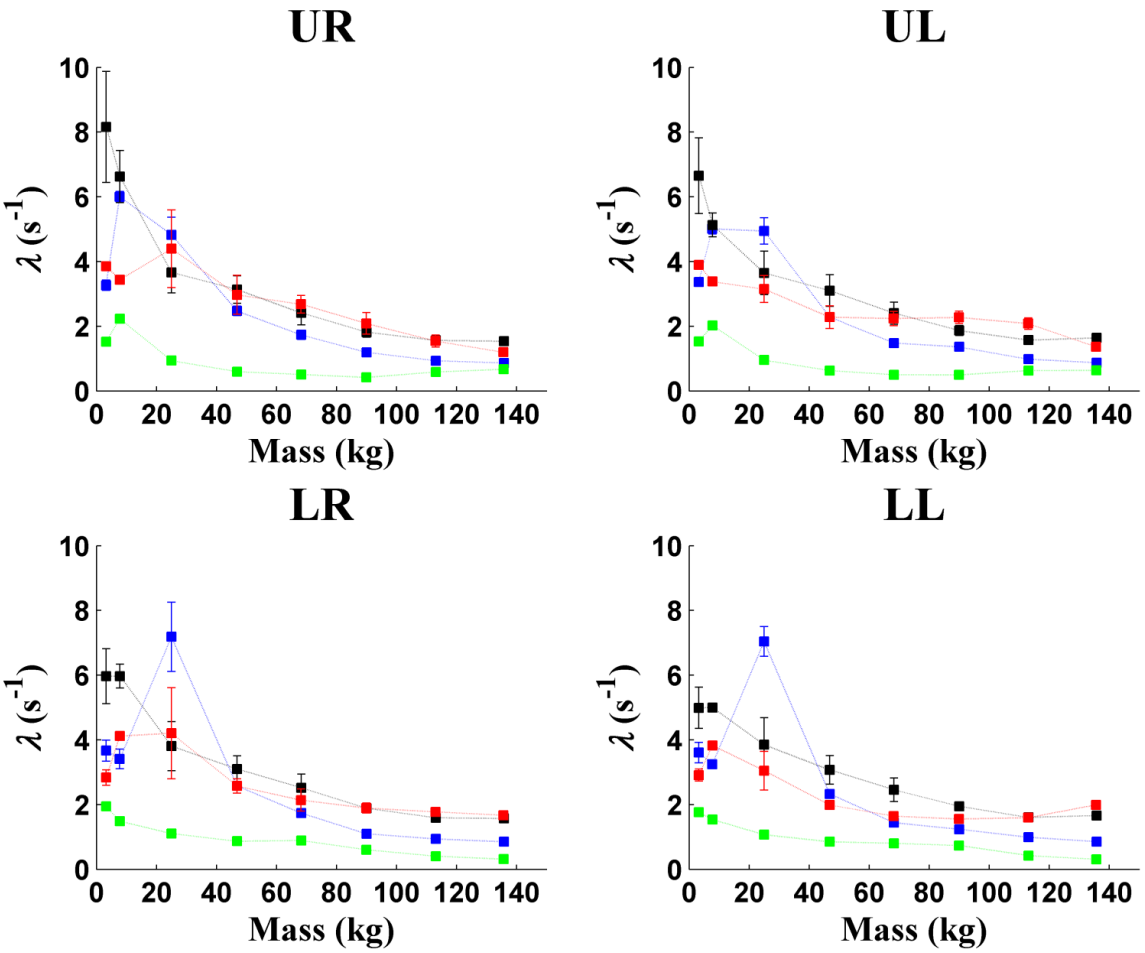

Figure 4-5. Mass dependent damping characteristic for each load cell across all mattress types. The different colors represent the different mattress types. The air-filled mattress results are shown in blue, the foam mattress results are shown in black, the independently coiled mattress results are shown in red, and the dependently coiled mattress results are shown in green. The squares represent the mean damping across the four trials, and the error bars signify one standard deviation. It should be noted that many of the error bars are not visible due to the relatively small nature of the represented standard deviations.

The mass dependent damping characteristic estimated for each load cell and mattress are shown in figure 4-5. Similar to the frequency of the responses for the different mattresses, the amount of damping for each mattress generally decreases with an increasing amount of mass on the bed. Interestingly, during the first few mass loadings on the bed mattress system, there are many instances where the amount of damping actually increases with more mass. This is especially evident for the air-filled

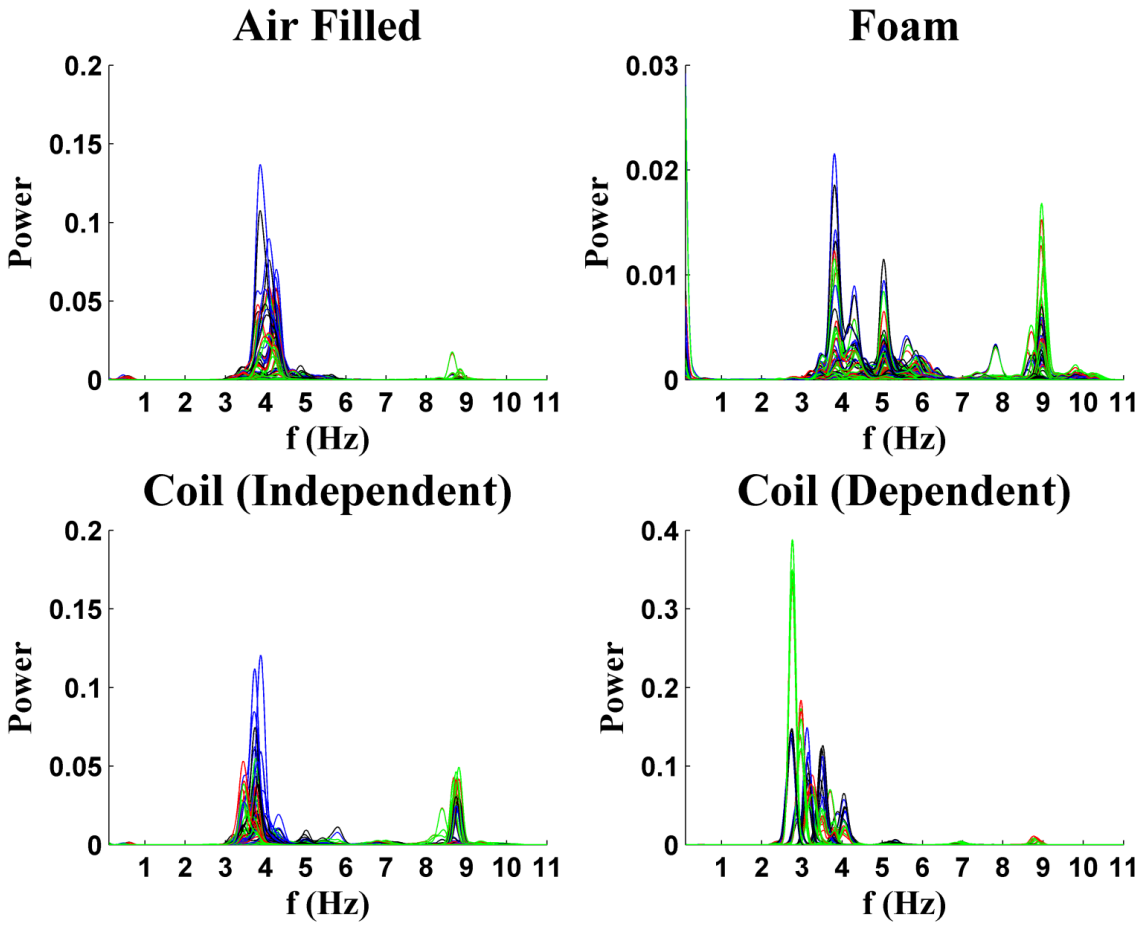

Figure 4-6. Power spectral density (PSD) for the 30 seconds of load cell data beginning 5 seconds after each application of the corresponding impulse. Each plot for the different mattress types contains the PSD for all trials across all mass loadings. PSD results for specific load cells are represented with different colors: UR results are in blue, UL results are in black, LR results are in red, and LL results are in green.

mattress (blue). Also noteworthy is the overall low amount of damping for the dependently coiled spring mattress (green).

The frequency components contained in the residual effects after an applied impulse for each mattress type are shown in figure 4-6. The power spectral densities between 0.1 Hz and 11 Hz are shown in the figure. The upper limit of 11 Hz was selected based on the results shown in figure 4-4, and the lower limit of 0.1 Hz was chosen to eliminate any power resulting from possible baseline shifts of the data from 0. The majority of the power for each mattress appears to reside in the range of frequencies

that were present immediately after the application of the impulses (see figure 4-4). However, there also seems to be some power below 1 Hz that is especially noticeable in the air-filled, foam, and independently coiled mattresses.

Discussion/Conclusion

Preliminary, unreported data collected using the spring coil mattress where the springs are all connected suggest that the bed/mattress system would 'resonate' at different frequencies depending on the amount of mass loaded on the bed. Results from the experiments described in this section indicate that the four mattress types tested herein exhibit similar overall trends in frequency of response and damping characteristics (see figures 4-4 and 4-5). The frequency of oscillation is dependent upon the mattress, but tends to decrease as the mass on the bed increases. While the amount of damping appears to be mattress dependent, for each mattress the damping decreased with mass loading on the bed suggesting that the effects (i.e. oscillations) caused by quick, impulsive movements on the bed will be longer for individuals of larger masses that are being monitored with the bed/mass system.

While the overall results from these experiments offer insight into the behavior of the bed/mattress system, some care must be used when interpreting the results. The response of the bed/mattress system to an applied impulse was assessed by fitting the damped sinusoid model (see equation 4.1) to each load cell separately. However, the load cells are all connected to the same bed/mattress system which will likely cause some interdependence between the data collected by each load cell. Also, the damped sinusoid model only accounted for a single frequency of oscillation. While this is an oversimplification of what is actually happening, there is a dominant frequency response

of each mattress to an impulse that the model is able to detect as seen in figure 4-3. However, spectral analysis of the load cell data collected from the 5 second mark to 35 second mark after the impulse was applied (see figure 4-6) indicates that there are some low frequency components (i.e. < 1 Hz) in the bed mattress system despite the majority of the spectral power residing in the 2-11 Hz ranges as predicted by the model. These lower frequency of responses are concerning since they correspond to normal range of respiration.

The range of breathing rates expected from individuals lying on the bed is between 8 and 24 breaths per minute, which corresponds to a range of frequency components in the load cell breathing signal (i.e. CoP_y) of about 0.13 to 0.4 Hz. The experiments outlined in the next section are designed to verify that the possible low frequency components seen in some of the impulse tests do not affect the load cell *CoP* signal's ability to track mass movement similar to that expected while an individual is lying on the bed. The higher frequency of responses (i.e. 2-11 Hz) for the bed/mattress systems can be removed using low pass filtering. Therefore, throughout this dissertation, analysis of the load cell *CoP* signals generally includes low pass filtering to attenuate any 'resonance' of the bed and leave behind only frequency components expected to be associated with breathing.

Bed/Mattress System Response to Low Speed Mass Movement

Motivation

According to the load cell breathing model outlined in chapter 3, the load cells should be able to detect respiration by tracking the time dependent *CoP* signal resulting from mass movements caused by breathing. In this experiment a mass is placed on the bed/mattress system and rotated in a known circular path in order to validate how well the load cell *CoP* signal (see equation 3.10) is able to recreate center of mass changes occurring on top of the bed/mattress system. In addition this experiment was designed to explore the effects of the bed/mattress system, as characterized in the previous section, when a mass is rotating on the bed at rates similar to respiration. This experiment is an effort to substantiate the use of the load cell *CoP* signal to recreate the breathing signal of an individual lying on the bed/mattress system by tracking the mass movements resulting from respiration.

Setup

Load cells were placed under the supports of a standard metal full sized bed frame in the Point of Care Laboratory (POCL). A box spring was placed on top of the metal frame that supported one of the four different mattresses used for the experiment. Four different mattress types were used for this experiment: 1.) a mattress with an air-filled bladder with adjustable air pressure encased in foam (similar to a Sleep Number® mattress), 2.) a mattress made of memory foam (similar to a Tempur-Pedic® mattress), 3.) a coil mattress with independent springs (i.e. springs that are not connected), and 4.) a coiled mattress with dependent springs (i.e. all the springs are connected). A 1.8 cm

piece of plywood with similar dimensions to the mattresses was placed on top of each mattress during the testing. The plywood was utilized to eliminate back and forth rocking noticed during preliminary tests of the device used to rotate the mass when placed directly on the mattress.

A wooden platform was placed on top of the plywood that was specially manufactured to be loaded with several masses of approximately 11 kg each[2]. A device used to rotate a 2.27 kg mass was placed on the plywood near the center and perpendicular to the wooden platform. The 2.27 kg mass represents the mass of the organs displaced during breathing. A 15V, 5A power supply (Heath Schlumberger, Model SP-2720) was used to regulate the speed of the motor used to rotate the mass, and a METEX® ME-22T digital multimeter (METEX Corporation, Seoul, Korea) was utilized to verify voltage supplied to the motor from the power supply.

In order to acquire independent confirmation of the frequency of rotation, video data was collected continuously during the entire experiment for each different mattress setup. A Flip MinoHD video camera (Cisco, Irvine, CA) was positioned over the bed using a microphone boom so that the device used to rotate the mass was in the video frame. A bubble level was used to verify that the video camera was level. A green dot with a diameter of 5 cm was positioned at the approximate center of the mass being rotated to allow for automatic tracking of the rotating mass in the video data. An example of the setup is shown in figure 4-7.

[2] When discussing the actual masses that are approximately 11 kg each, they are referred to as the ≈11 kg masses.

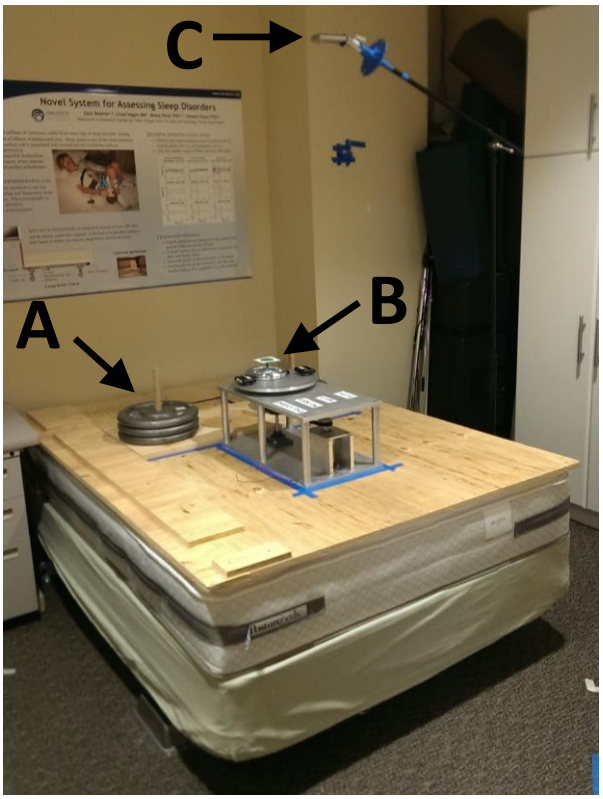

Figure 4-7. Image showing an example of the setup for the experiment. (**A**) Varying amounts of mass can be loaded on the bed/mattress system using a wooden platform. The wooden platform has two places where various masses can be loaded. One is visible in the image and the other is hidden by the device used to spin the 2.27 kg mass. (**B**) A 2.27 kg mass is rotated in a circular motion. A green dot is placed at the approximate center of the mass being rotated. (**C**) Video camera used to track the motion of the spinning 2.27 kg mass.

Methods

Experiment 1

The following protocol was used two times for each different mattress, one time with the center of the rotating mass placed approximately 6 cm from the center of the rotating platform and once with the center of the rotating mass placed at approximately 12 cm. The 6 cm and 12 cm tests for each different mattress were performed without altering the position of the video camera. With the camera at the same height, the absolute magnitudes of the mass' rotation for the 6 cm and 12 cm tests could be compared for each particular mattress. The video data was recorded at 30 frames per

second and load cell data was collected at 500 samples per second for each individual load cell.

The wooden platform and the mass rotation device were placed on the bed/mattress system. The DC power supply was either set at 0 V, 6 V, 9 V, or 12 V which corresponded to the 2.27 kg mass rotating at approximately 0, 9.3, 14.3, an 19.3 rotations per minute (rpm) respectively. These rotation speeds were chosen as they spanned the normal range of breathing. One minute of load cell data was collected for various amounts of mass loaded on the bed/mattress system for each of these rotation speeds (see table 4-1).

Table 4-1.
Table illustrating the setup for each individual one minute data collection. For each rotation speed, between 0 and 10 masses of approximately 11 kg each were loaded on the bed/mattress system.

	Trials					
RPM	1	2	3	4	5	6
0	0*11 kg	2*11 kg	4*11 kg	6*11 kg	8*11 kg	10*11 kg
9.3	0*11 kg	2*11 kg	4*11 kg	6*11 kg	8*11 kg	10*11 kg
14.3	0*11 kg	2*11 kg	4*11 kg	6*11 kg	8*11 kg	10*11 kg
19.3	0*11 kg	2*11 kg	4*11 kg	6*11 kg	8*11 kg	10*11 kg

Experiment 2

The same setup was then utilized to explore the load cell system's ability to track a mass rotating at increasingly smaller diameters. This experiment was conducted only with the foam mattress setup. The 2.27 kg mass was placed on the rotation device at several different radii of approximately 12 cm, 6 cm, 3 cm, 1 cm, and 0.5 cm leading to displacement diameters of approximately 24 cm, 12 cm, 6 cm, 2 cm, and 1 cm respectively. Load cell data was collected while the mass rotated at each diameter (DC power supply set to 9 V) when two different amounts of mass were loaded on the

bed/mattress system using the weight platform. One minute of load cell data was collected for each displacement diameter with approximately 21.6 kg loaded on the bed, and one minute of data was collected for each diameter while about 109.3 kg was loaded on the bed/mattress system.

Analysis

In chapter 3 it is hypothesized that the load cells can track the breathing of an individual lying on the bed/mattress system by using the *CoP* signal estimated using the load cells placed under the bed. The load cell data collected during these experiments were used to calculate the *CoP* signals for each specific data collection (see equation 3.10). To aid in the comparison of video and load cell data, the load cell *CoP* signals calculated in the experiments contained in this chapter were estimated using a Cartesian coordinate system that matched the axes of the camera. The load cell *CoP* signals used for qualitative analysis or visual inspection only (see figures 4-8, 4-9, 4-16 through 4-18, and 4-20 through 4-22) were low pass filtered in order to minimize the resonance of the bed using a 3rd order Chebyshev Type II filter that was monotonic in the pass-band, had a stop-band edge frequency of 3 Hz, and attenuated the stop band by 30 dB. Ground truth evidence of the rotating mass was extracted from the video data using a software program that was developed to isolate the green dot in the video files and calculate the *xy* location of its centroid on a frame by frame basis.

Experiment 1

Quantitative analysis of the results from the first experiment consisted of two parts. First, the amplitudes of *CoP* displacement for the 2.27 kg mass were calculated

from the load cell signals for each 1 minute segment of data. These estimated amplitudes were then compared to the expected amplitudes of *CoP* displacement. Second, the frequencies of rotations for the 2.27 kg mass were calculated using the load cell data. These estimated rates were then compared to the frequencies of rotation estimated using the ground truth video data.

CoP *Displacement Amplitude Comparisons*

It was assumed during the testing and data collection that, in reference to the entire bed/mattress system, the small 2.27 kg mass was the only non-symmetrical mass experiencing any movement over time. The calculation for estimating the CM can be expanded to show that when only a small portion of the overall mass of the bed/mattress system is changing its *xy* location, the general magnitude of the change to the *CM* is dependent upon size of the mass that is moving in relation to the overall mass of the system. This relationship is illustrated by:

$$\boldsymbol{CM}(t) = \frac{\left(\sum_{j=1}^{n} M_j \boldsymbol{r}_j(t)\right)}{\sum_{j=1}^{n} M_j} = \frac{M_S\left(\boldsymbol{r}_S^0 + \boldsymbol{r}_S(t)\right) + M_\Delta\left(\boldsymbol{r}_\Delta^0 + \boldsymbol{r}_\Delta(t)\right)}{M_S + M_\Delta} \tag{4.2}$$

where M_j is the j^{th} mass representing the bed, mattress, or individual masses on the bed, and $\boldsymbol{r}_j(t)$ is the time dependent location of the j^{th} mass. M_j and $\boldsymbol{r}(t)$ were expanded with M_Δ representing the small mass that is rotating, M_s representing the combined mass of everything else supported by the load cells (i.e. bed/mattress system etc. minus M_Δ), $\boldsymbol{r}_\Delta^0$ representing the center of mass location of M_Δ at t=0, $\boldsymbol{r}_\Delta(t)$ representing the time dependent displacements of M_Δ from $\boldsymbol{r}_\Delta^0$, $\boldsymbol{r}_S^0$ representing the center of mass location of

M_s at t=0, and $\boldsymbol{r}_s(t)$ representing the time dependent displacements of M_s from $\boldsymbol{r}_S^0$. By expanding equation 4.2

$$\boldsymbol{CM}(t) = \frac{M_S\boldsymbol{r}_S^0 + M_S\boldsymbol{r}_S(t) + M_\Delta\boldsymbol{r}_\Delta^0 + M_\Delta\boldsymbol{r}_\Delta(t)}{M_S + M_\Delta} \tag{4.3}$$

then combining the time dependent terms

$$\boldsymbol{CM}(t) = \frac{M_S\boldsymbol{r}_S^0 + M_\Delta\boldsymbol{r}_\Delta^0}{M_S + M_\Delta} + \frac{M_S\boldsymbol{r}_S(t) + M_\Delta\boldsymbol{r}_\Delta(t)}{M_S + M_\Delta} \tag{4.4}$$

and finally assuming that the overall center of mass location of M_s does not change with time

$$\boldsymbol{CM}(t) = \frac{M_S\boldsymbol{r}_S^0 + M_\Delta\boldsymbol{r}_\Delta^0}{M_S + M_\Delta} + \frac{M_\Delta\boldsymbol{r}_\Delta(t)}{M_S + M_\Delta} \tag{4.5}$$

we see that $\boldsymbol{CM}(t)$ has a constant offset of $\frac{M_S\boldsymbol{r}_S^0 + M_\Delta\boldsymbol{r}_\Delta^0}{M_S + M_\Delta}$. From the remaining terms $\frac{M_\Delta\boldsymbol{r}_\Delta(t)}{M_S + M_\Delta}$, we see that the effect of any $\boldsymbol{r}_\Delta(t)$ on the magnitude of change in $\boldsymbol{CM}(t)$ is less with increasing M_s (i.e. loading more mass on the bed/mattress system).

Equation 4.5 suggests that the amplitudes of *CoP* displacement that is detected for the 2.27 kg mass by load cell system should decrease as more ≈11 kg masses are placed on the bed. To verify this relationship, the amplitudes of *CoP* displacement for the *x* and *y* components of the load cell *CoP* signals for each data segment were calculated. The CoP_x and CoP_y signals were first decimated[3] to a sampling rate of 10 Hz and then low pass filtered using an 8^{th} order Chebyshev Type II filter that was monotonic in the pass-band, had a stop-band edge frequency of 0.75 Hz, and attenuated the stop band by 40 dB.

[3] References to decimation in this dissertation were implemented using the Matlab® routine "decimate". This routine uses a low pass filter before down sampling in order to avoid aliasing.

The local minimum and maximum values were then located in the filtered CoP_x and CoP_y signals. These peaks and troughs represented the minimum and maximum displacements of the respective CoP_x and CoP_y signals. Finally, the load cell estimated amplitudes of *CoP* displacement for each segment in both *x* and *y* directions were estimated by subtracting the median trough values for each data segment from the median peak values for the same segments.

For comparison, the expected amplitude of *CoP* displacement for each data segment was calculated mathematically using

$$CM(t_{\max}) - CM(t_{\min}) = \frac{M_S r_S^0 + M_\Delta r_\Delta^0}{M_S + M_\Delta} + \frac{M_\Delta r_\Delta(t_{\max})}{M_S + M_\Delta} - \left(\frac{M_S r_S^0 + M_\Delta r_\Delta^0}{M_S + M_\Delta} + \frac{M_\Delta r_\Delta(t_{\min})}{M_S + M_\Delta} \right) \quad (4.6)$$

where *CM* represents the center of mass and *r* is the location of the respective masses (either the *x* or *y* direction due to symmetry) at t_{max} and t_{min}. t_{max} is the time point when M_Δ is at its maximum displacement and t_{min} is the time when M_Δ is at its minimum displacements in either the *x* or *y* direction. Equation 4.6 can be simplified to

$$CM(t_{\max}) - CM(t_{\min}) = \frac{M_\Delta \left(r_\Delta(t_{\max}) - r_\Delta(t_{\min}) \right)}{M_S + M_\Delta}. \quad (4.7)$$

$M_s + M_\Delta$ was calculated for each loading condition by summing the mean output of each load cell during the data collection when the M_Δ was not spinning. Since the load cell output had been converted to Newtons, this sum was divided by the acceleration due to gravity (i.e. 9.80665 m/s^2). M_Δ was expected to be 2.27 kg, and $r_\Delta(t_{max})$-$r_\Delta(t_{min})$ was either set to 120 mm when M_Δ was placed at a radius of 6 cm or 240 mm when M_Δ was placed at a radius of 12 cm.

Rotation Frequency Comparisons

The frequency of rotation of the mass was estimated from the *xy* components of the *CoP* signals (CoP_x and CoP_y) and compared to the rotation frequencies calculated from the *xy* components of the green dot in the respective video files (VID_x and VID_y). The frequency content for each signal was calculated by first decimating each particular $CoP_{x,y}$ or $VID_{x,y}$ to a sampling rate of 10 Hz and then estimating the power spectral density using Welch's method for each one minute segment of data. The rotation frequency for each 1 minute segment for both load cell and video data was then determined to be the maximum frequency in the 0 Hz to 0.5 Hz band of the estimated power spectral density.

Bland-Altman plots [63] were used to visually compare the frequencies estimated for CoP_x to those calculated for VID_x and similarly to compare the frequencies estimated for CoP_y to the frequencies of rotation calculated for VID_y. Paired t-tests were used to test whether or not there was a significant difference between the rotation frequencies estimated using the load cells compared to those calculated using the video data. When calculating the paired t-tests, the data was combined across all experimental conditions (i.e. mattress type, displacement diameter, amount of mass loaded on the bed, and rotation speed). N-way analysis of variance was also utilized to explore the effects of mattress type, the location of the rotating mass (i.e. r = 6 cm or r = 12 cm), the amount of mass loaded onto the wooden platform, and the speed of rotation on the difference between the frequencies measured by the load cells and those measured using the video data. The four grouping variables were modeled as having fixed effects, and for analysis,

the main and two-factor interactions were used. The data segments collected when the mass was not rotating were not used for comparing rotation frequencies.

Experiment 2

Quantitative analysis was performed using the load cell data from experiment 2 to explore how well the load cell system could be used to discern different amplitudes of displacement for the 2.27 kg mass. In particular, the purpose of experiment 2 was to show that decreases in the displacement amplitudes of a mass on the bed were detected as decreases in amplitudes in the corresponding load cell *CoP* signal. The amplitudes of *CoP* displacement for each 1 minute data segment were estimated using the same method as described in experiment 1. The expected *CoP* displacement amplitudes were also calculated as previously described using equation 4.7. The $r_{\Delta}(t_{max})$-$r_{\Delta}(t_{min})$ values were set at 240 mm, 120 mm, 60 mm, 20 mm, and 10 mm when the mass displacement diameters were 24 cm, 12 cm, 6 cm, 2 cm, and 1 cm respectively.

Results

Experiment 1

Figure 4-8 shows and example of the load cell *CoP* signal for a single one minute data segment. The load cell data for the segment was collected using the coiled mattress where the springs are all connected, with the 2.27 kg mass placed at a radius of 12 cm from the center of the rotation platform, while the wooden weight platform was loaded with 6 masses of ≈11 kg each, and the platform was spinning at the highest setting used for the experiment (i.e. 19.3 rpm). The power seen in the 0-1 Hz is a result of the spinning 2.27 kg mass. Per the results of the previous section (i.e. Bed/Mattress System

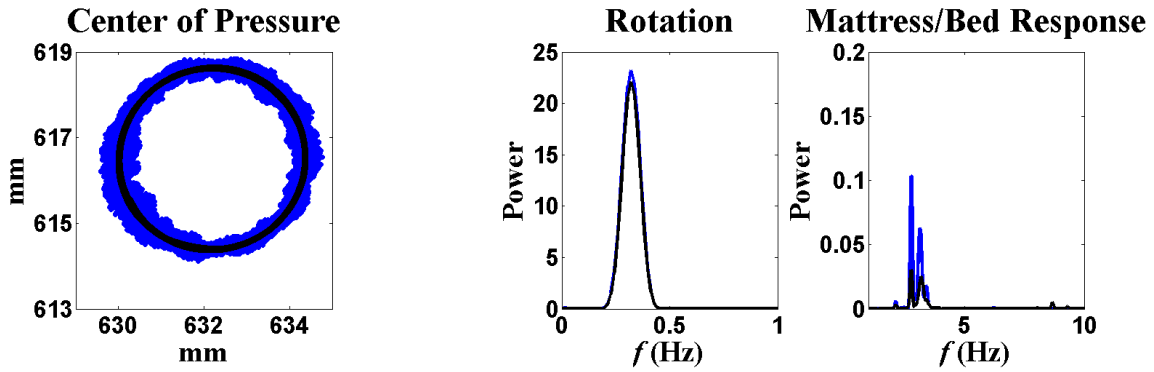

Figure 4-8. Example of the load cell *CoP* signal for a single one minute data segment. The raw *CoP* (blue) and low pass filtered *CoP* (black) is plotted in the left most image. The power spectral density for the CoP_x (blue) and CoP_y (black) are shown in the right two images for frequency ranges of 0-1 Hz and 1–10 Hz respectively.

Characterization), the power in the 1-10 Hz range is attributed to the residual 'resonant' response of the bed/mattress system to disturbances caused during the loading or unloading of the ≈11 kg masses on the mattress in between each data collection.

Figure 4-9 contains the low pass filtered load cell *CoP* signals collected during the first experiment using the memory foam mattress for each 2.27 kg mass location on the spinning platform, each rotation speed, and each number of ≈11 kg masses loaded onto the wooden platform. The subfigures show the low pass filtered *CoP* signals for each loading condition of the bed/mattress system (i.e. number of ≈11 kg masses loaded on the wooden platform). The results for both placements of the 2.27 kg mass (i.e. 6 cm or 12 cm from the center of the rotation platform) are shown in each subfigure. Low pass filtered *CoP* signals representing data collected when the 2.27 kg mass was not spinning are cyan, and those signals collected while the mass was spinning at "low" (9.3 rpm), "medium" (14.3 rpm), and "high" (19.3 rpm) speeds are plotted in green, red, and blue respectively. The black traces represent the expected amplitudes of *CoP* displacement calculated using equation 4.7. The *x* and *y* axes limits for all subplots were set to 10 mm

in order to allow comparison of *CoP* displacement amplitude across the different loading conditions of the bed/mattress system.

A similar figure that shows the ground truth movement of the 2.27 kg mass using the tracking results of the green dot in the video data is contained in figure 4-10. The main differences in this image is that the *xy* locations of the estimated centroid of the green dot are represented as pixels within the viewing frame of the video data, and the video data shown has not been low pass filtered. It is also evident that for the most part only the results from highest speed setting (shown in blue) are visible due to the almost identical results seen in the video data for each speed setting, loading condition, and placement of the 2.27 kg mass.

Figures showing low pass filtered load cell *CoP* signals and the corresponding video tracking results have been omitted for the remaining three mattress types as there is no significant difference between them and figures 4-9 and 4-10.

The *CoP* displacement amplitudes for CoP_x and CoP_y calculated across all iterations of the initial experiment are shown in figures 4-11 through 4-14. Each figure represents the results found for each different mattress. The amplitudes calculated while the 2.27 kg mass was spinning at “low” (9.3 rpm), “medium” (14.3 rpm), and “high” (19.3 rpm) speeds are plotted in green, red, and blue respectively. Results from data when the 2.27 kg mass was placed at 6 cm from the center of the rotation platform are plotted using ‘squares’ while ‘circles’ were used to represent results when the mass was placed at a radius of 12 cm. The black lines mark the expected amplitudes for each data collection as specified by equation 4.7.

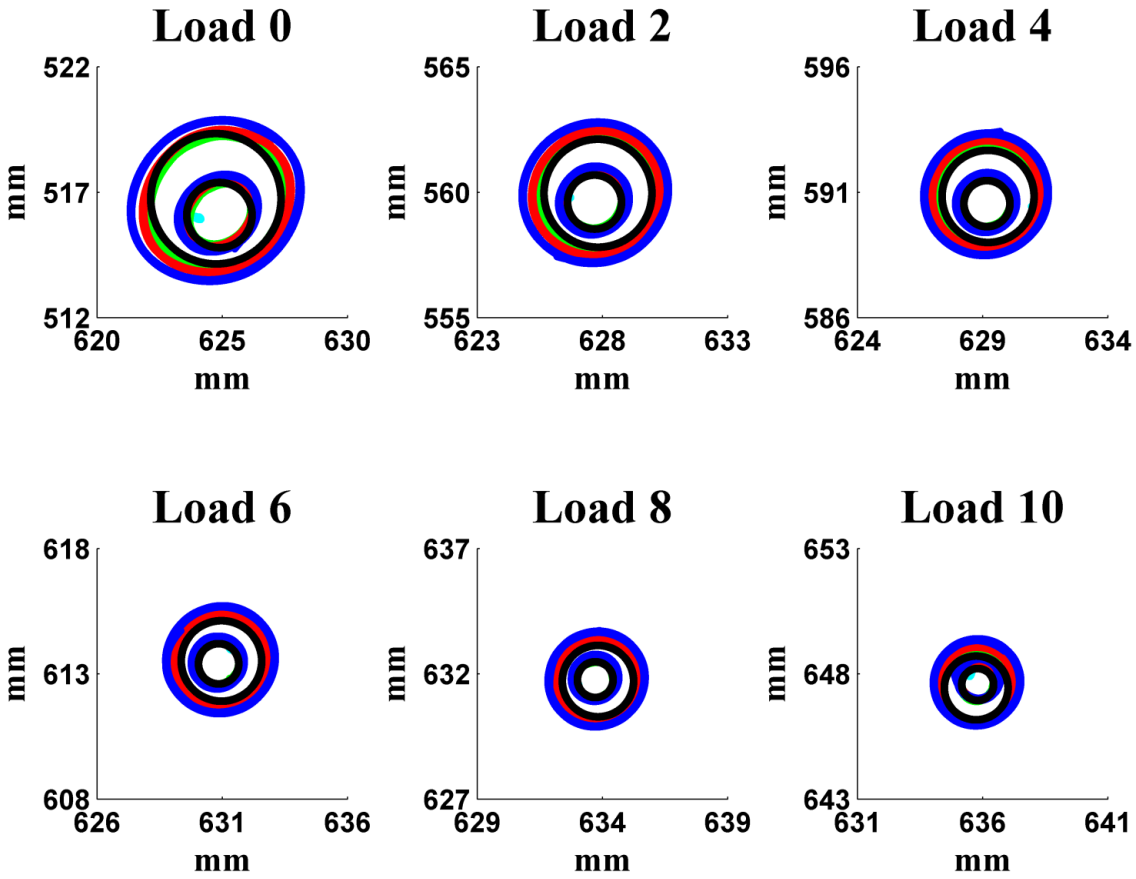

Figure 4-9. Load cell *CoP* signals calculated during experiments using the memory foam mattress. Each subfigure represents when the bed/mattress system was loaded with between 0 and 10 different masses of ≈11 kg each.

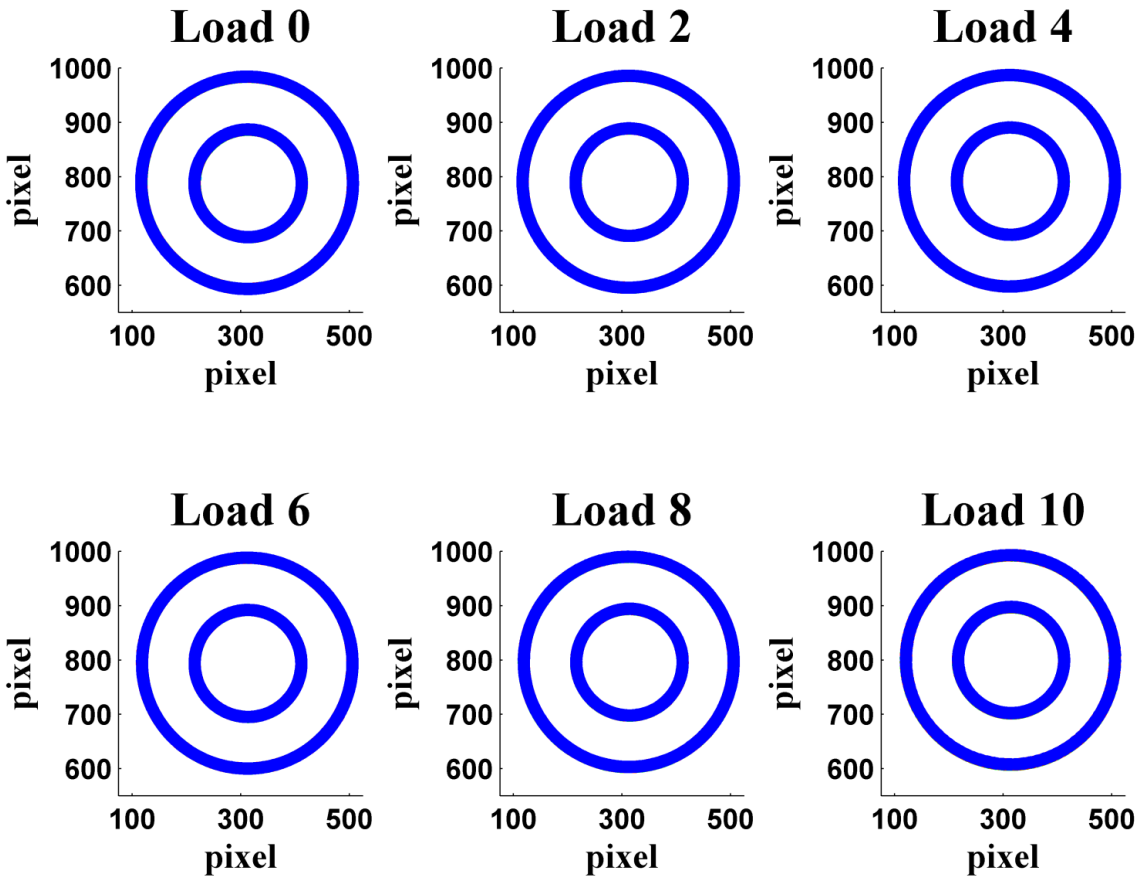

Figure 4-10. Video tracking results calculated during experiments using the memory foam mattress. Each subfigure represents when the bed/mattress system was loaded with between 0 and 10 different masses of ≈11 kg each.

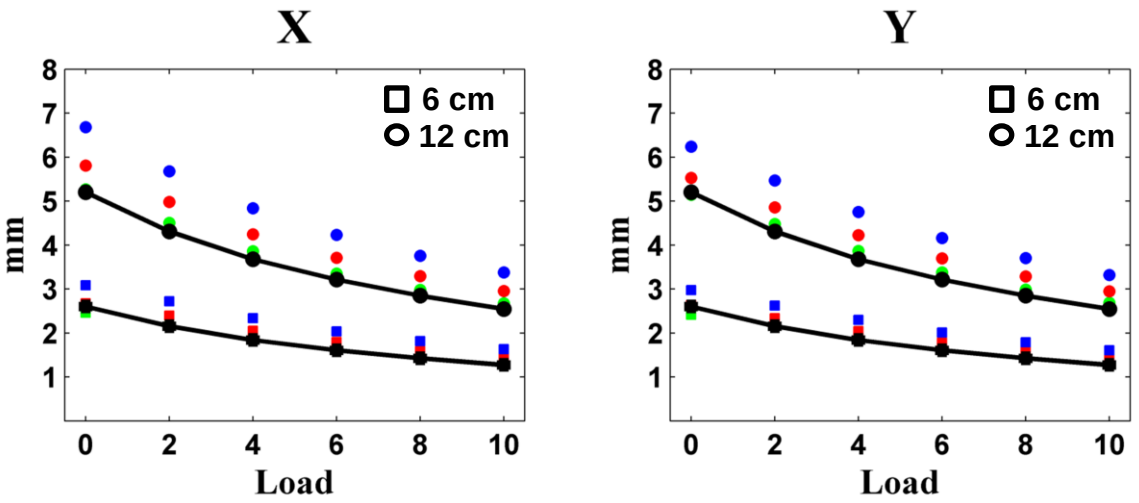

Figure 4-11. *CoP* displacement amplitudes (*y*-axis) estimated for CoP_x (left) and CoP_y (right) from experiments using the memory foam mattress. The solid black lines with black circles and squares designate expected amplitudes calculated using equation 4.7. The *x*-axis represents the number of ≈11 kg masses loaded on the bed/mattress system.

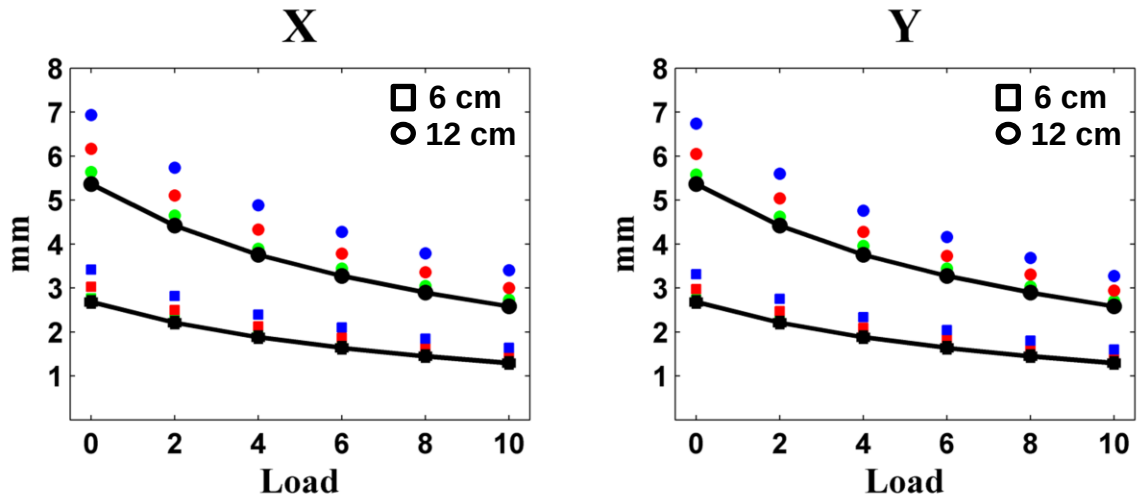

Figure 4-12. *CoP* displacement amplitudes (*y*-axis) estimated for CoP_x (left) and CoP_y (right) from experiments using the coiled mattress where the springs are all connected. The solid black lines with black circles and squares designate expected amplitudes calculated using equation 4.7. The *x*-axis represents the number of ≈11 kg masses loaded on the bed/mattress system.

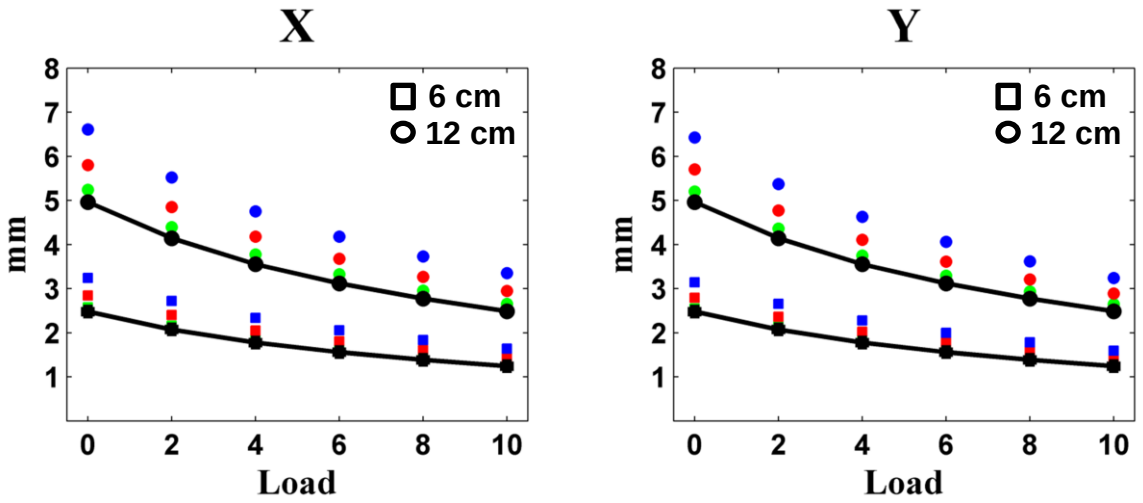

Figure 4-13. *CoP* displacement amplitudes (*y*-axis) estimated for CoP_x (left) and CoP_y (right) from experiments using the coiled mattress with independent springs (i.e. springs that are not connected). The solid black lines with black circles and squares designate expected amplitudes calculated using equation 4.7. The *x*-axis represents the number of ≈11 kg masses loaded on the bed/mattress system.

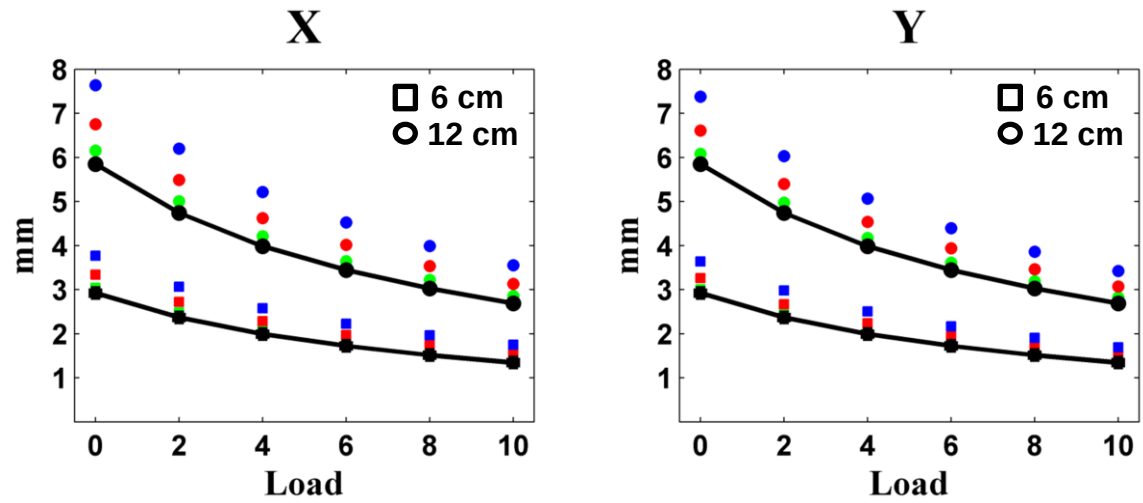

Figure 4-14. *CoP* displacement amplitudes (*y*-axis) estimated for CoP_x (left) and CoP_y (right) from experiments using the mattress with an air-filled bladder. The solid black lines with black circles and squares designate expected amplitudes calculated using equation 4.7. The *x*-axis represents the number of ≈11 kg masses loaded on the bed/mattress system.

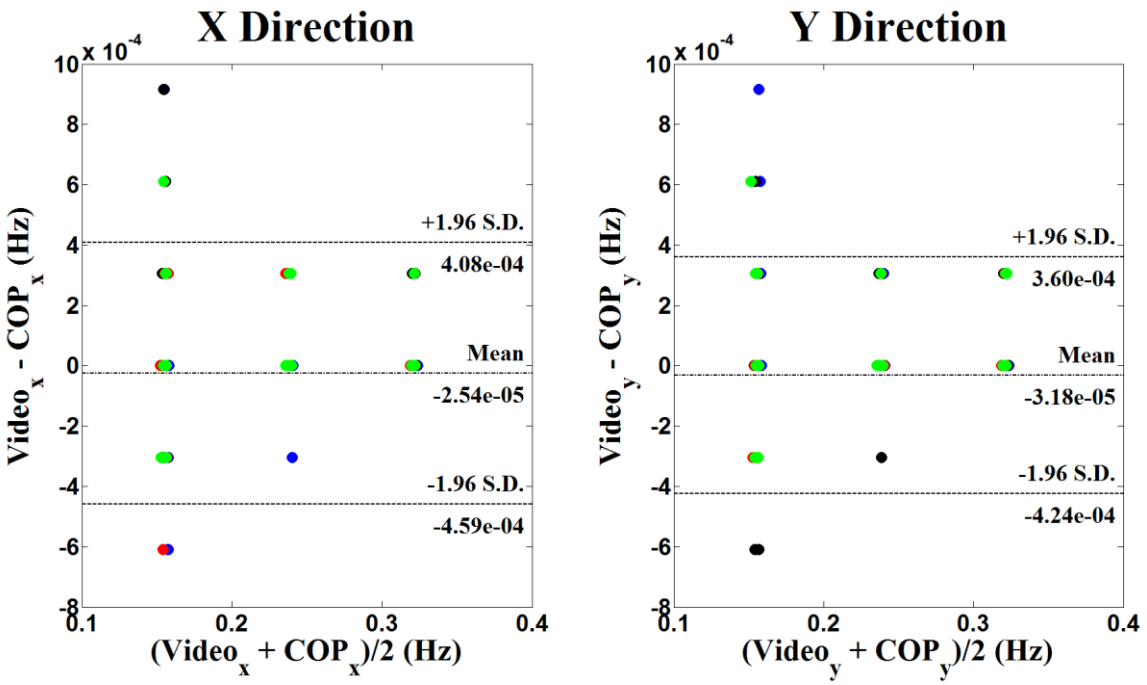

Figure 4-15. Bland-Altman plots showing the comparison of the rotation frequencies calculated using video and load cell data in the *x*-direction (left) and *y*-direction (right). Results for the four different mattress types are labeled using different colors. Green is used for the mattress with an air-filled bladder, blue is used for mattress made of memory foam, red is used for the coil mattress with independent springs, and black is used for the coiled mattress where the springs are all connected. The discrete nature of the difference between Video and *CoP* in the *y*-axis is due to the resolution of the power spectral density estimations (i.e. 3.0518 x 10^{-4} Hz per point). The discrete nature of the average results in the *x*-axis is due to the 3 different speeds of rotation.

The comparison of the rotation frequencies calculated for each separate data segment using the video data (VID_x and VID_y) to the frequencies of rotation calculated using the load cell data (CoP_x and CoP_y) are shown in the Bland-Altman plots in figure 4-15. The differences between frequencies calculated for each 1 minute segment from the video data and the load cell data are plotted on the *y*-axis, and the average of the calculated frequencies from both video and load cell estimates for each segment are plotted on the *x*-axis. Comparisons between results calculated in the *x*-direction are shown in the left plot and comparisons between results estimated in the *y*-direction are shown in the right plot. Results from the paired t-tests showed no significant difference between rotation frequencies estimated using load cell *CoP* signals and frequencies

estimated using the video data either in the x-direction (t_{143} = -1.38, p = 0.17) or in the y-direction (t_{143} = -1.91, p = 0.06).

Experiment 2

Overall results for the second experiment where a mass was rotated at increasingly smaller diameters are shown in figure 4-16. Results for when the mass was displaced at a 24 cm diameter are plotted in cyan, 12 cm diameter are plotted in black, 6 cm diameter are shown in red, 2 cm diameter results are plotted in green, and the 1 cm diameter results are blue. The *x* and *y* axes for the load cell *CoP* signals were kept at a constant 6 mm limit for both data collection setups (i.e. when approximately 21.6 kg was loaded on the bed and when about 109.3 kg was loaded on the bed/mattress system). In figures 4-17 and 4-18, the low pass filtered load cell CoP_x and CoP_y signals are plotted separately for both data collection setups. The overall offset for each data trace was arbitrarily set in order to easily visualize the decreasing amplitudes of the load cell signals. For ease of comparison, the plotting colors representing the data collection for each different diameter of CoP_x and CoP_y signal are the same as in figure 4-16. Finally, figure 4-19 contains data showing the expected diameter calculated for each 1 minute data segment using equation 4.7 as compared to the amplitudes calculated using the load cell *CoP* signals.

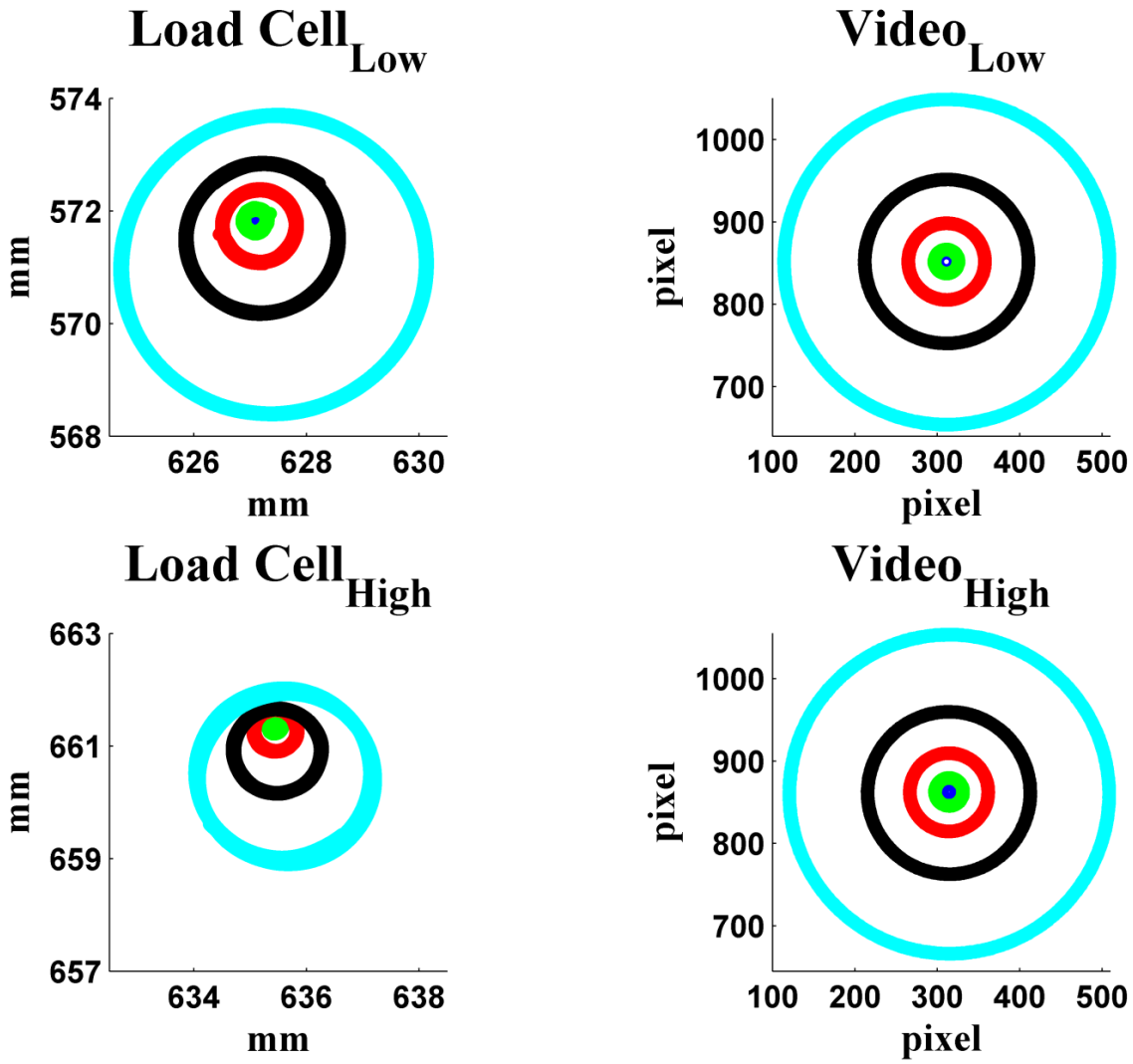

Figure 4-16. Load cell *CoP* signals (left column) and video tracking results (right column) calculated during the second experiment where the 2.27 kg mass was rotated at increasingly smaller diameters. Data collected when approximately 21.6 kg was loaded on the bed/mattress system are designated as "Low", and data collected when about 109.3 kg was loaded on the bed/mattress system are designated as "High". In the figures, the load cell data has been low passed filtered; however, the video data has not been low passed filtered.

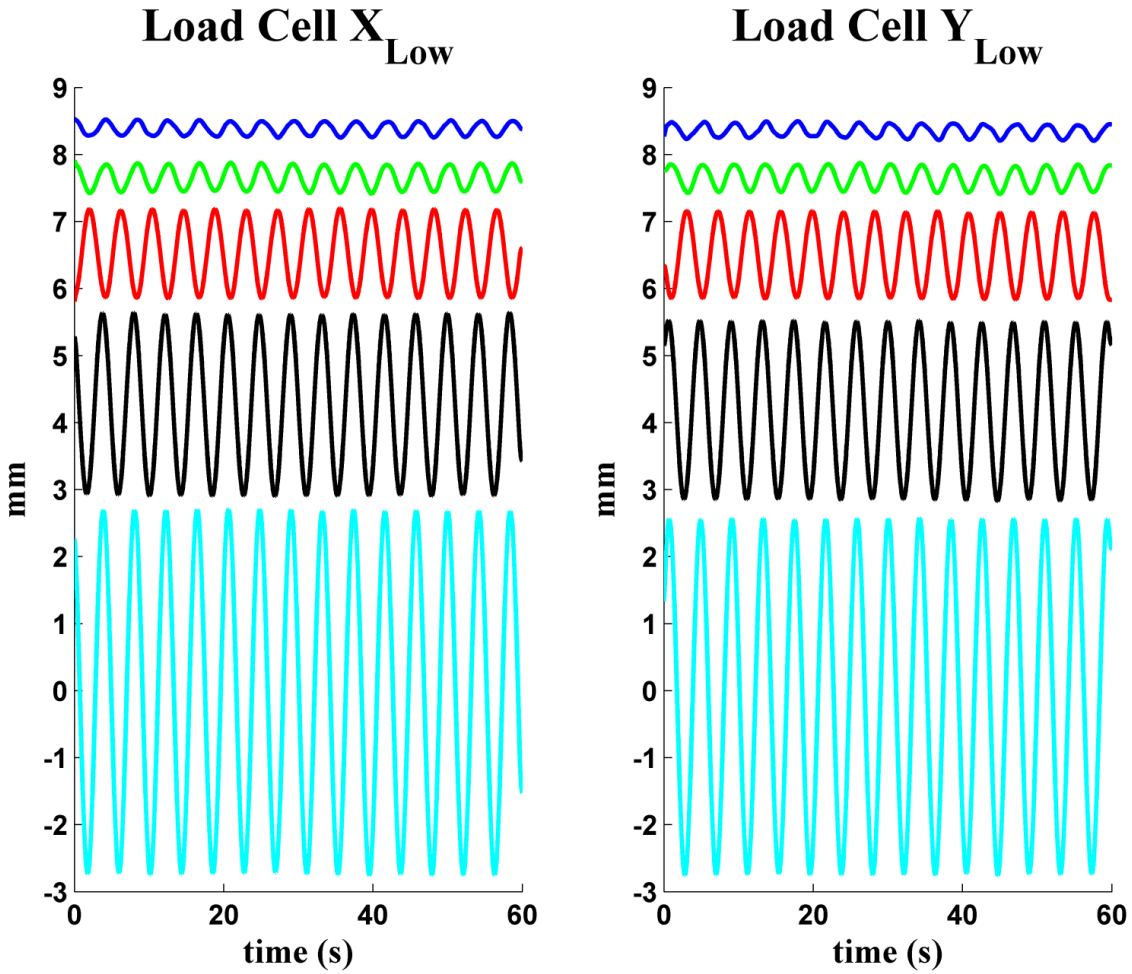

Figure 4-17. Low pass filtered load cell CoP_x (left) and CoP_y (right) signals calculated when approximately 21.6 kg was loaded on the bed/mattress system. Load cell signals calculated when the mass was displaced at a 24 cm diameter are plotted in cyan, results for a 12 cm diameter are plotted in black, results for the 6 cm diameter are shown in red, the 2 cm diameter results are plotted in green, and the 1 cm diameter results are blue.

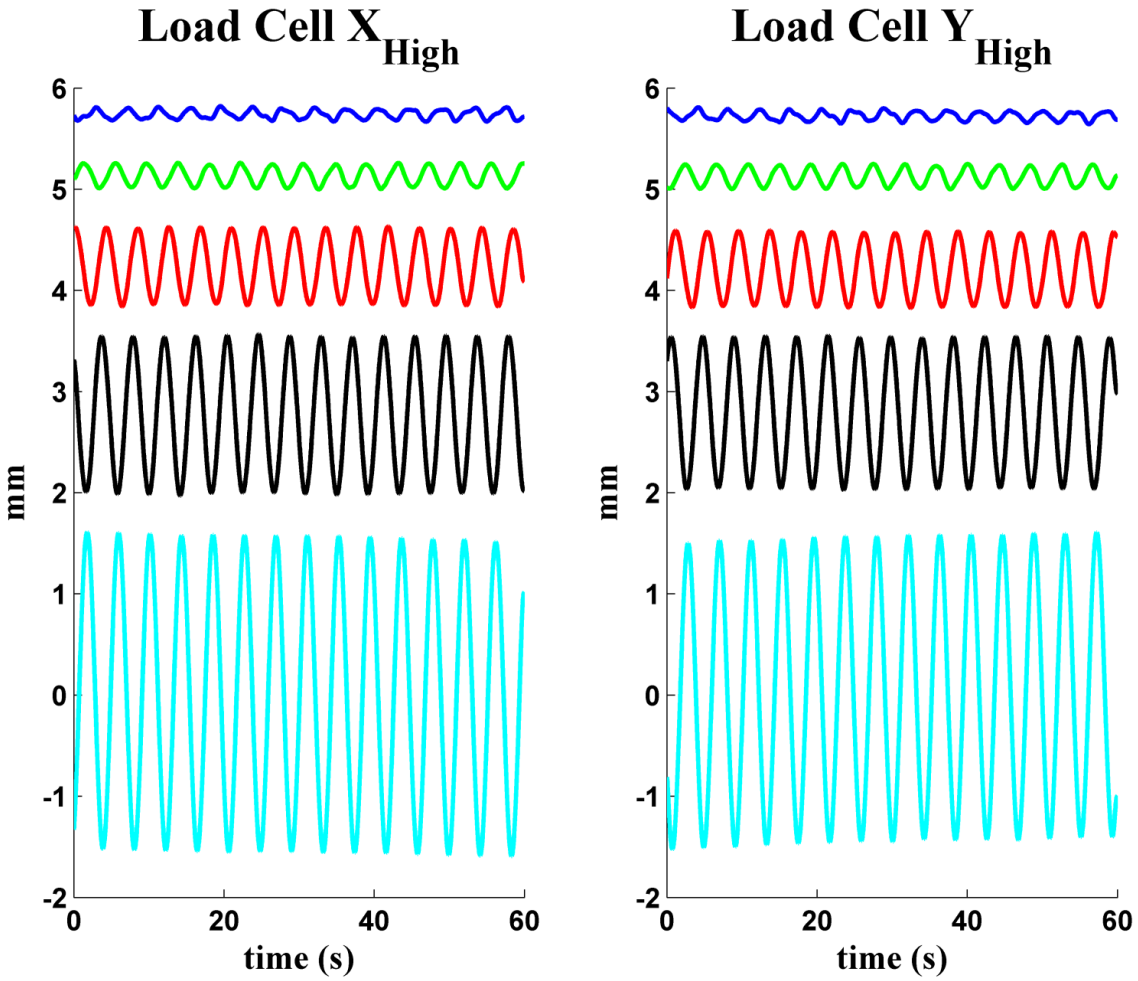

Figure 4-18. Low pass filtered load cell CoP_x (left) and CoP_y (right) signals calculated when approximately 109.3 kg was loaded on the bed/mattress system. Load cell signals calculated when the mass was displaced at a 24 cm diameter are plotted in cyan, results for a 12 cm diameter are plotted in black, results for the 6 cm diameter are shown in red, the 2 cm diameter results are plotted in green, and the 1 cm diameter results are blue.

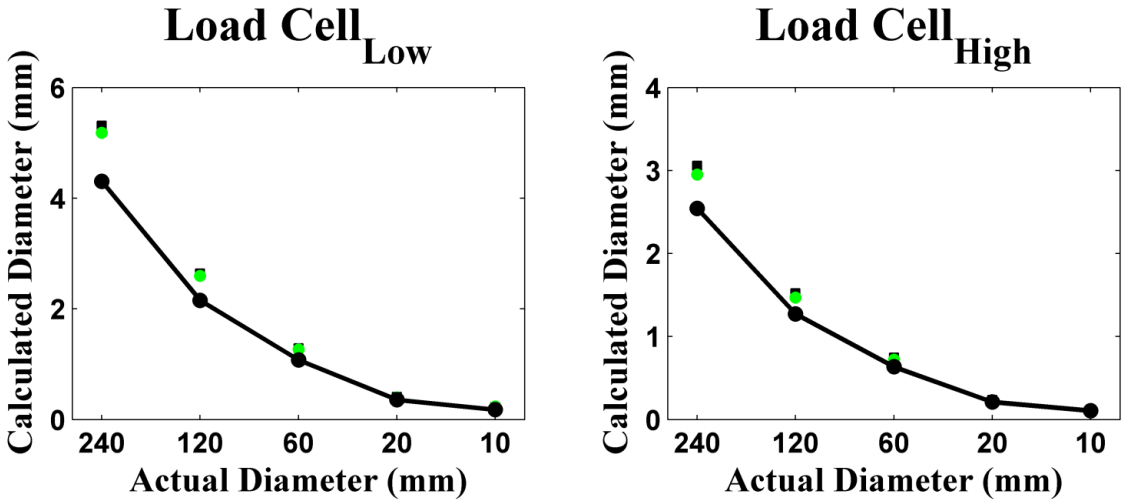

Figure 4-19. *CoP* displacement amplitudes calculated for CoP_x (black squares) and CoP_y (green circles) from data collected when approximately 21.6 kg was loaded on the bed/mattress system (left) and from data collected when about 109.3 kg was loaded on the bed/mattress system (right). The solid black lines with black circles designate expected amplitudes calculated using equation 4.7.

Discussion/Conclusion

Experiment 1

The load cell *CoP* signals (see figure 4-9 for an example) were able to generally recreate the circular motion of the 2.27 kg mass that was rotated on the bed/mattress system. However, the almost perfectly overlapping results seen in the video data (see figure 4-10) for each rotation speed were not recreated with the load cell *CoP* signal. This is likely due to the omission of centripetal forces that were not accounted for in the model described in equation 3.10. The load cells are obviously affected by reaction forces that are needed to keep the device used to rotate the 2.27 kg mass stationary. The overall sum of these forces (F_c) can be described using [64]:

$$\sum F_c = m_\Delta r\omega^2 \tag{4.8}$$

where m_Δ is the 2.27 kg mass, r is the distance of the mass from the center point that it is rotating about, and ω^2 is the angular speed. From equation 4.8 we see that with higher angular speeds (i.e. higher frequencies of rotation) the reaction forces would increase. This is consistent with the larger circular rotation paths predicted from the load cell *CoP* signals at higher angular speeds due to the increased forces detected by the load cells.

While the load cell *CoP* signals were mostly circular in nature as expected, there were a few instances when the detected motion was somewhat oval (i.e. results seen in the "Load 0" subfigure of figure 4-9). Since the corresponding video data does not exhibit a similar deviation, confirming the circular motion, it is assumed that either the angular speed that the 2.27 kg was rotating at was inconsistent during a single revolution, or that the bed/mattress system transferred the loading of the 2.27 kg mass to the load cells with different time delays for different load cells.

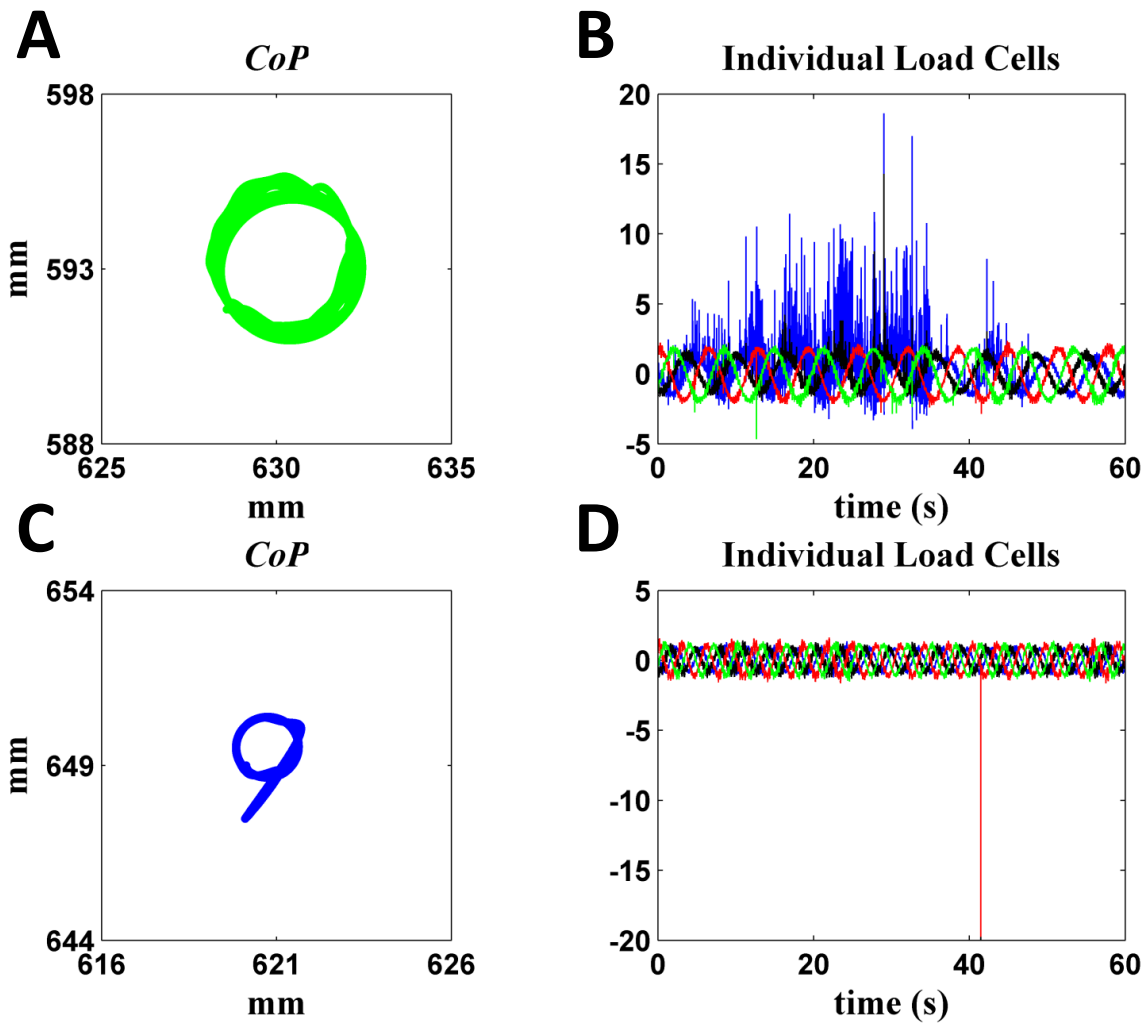

Figure 4-20. (**A**) Low pass filtered load cell *CoP* signal collected from the "low" speed experiment using the coiled mattress where the springs are all connected when the 2.27 kg mass was placed 12 cm from the center of the rotation platform and four ≈11 kg masses were placed on the bed/mattress system. (**B**) Individual load cell data collected during the same experiment shown in (**A**). The upper right (UR) load cell (in reference to an individual's right while lying on the bed/mattress system on their back) is shown in blue, the upper left (UL) load cell is shown in black, the lower right (LR) load cell is shown in red, and the lower left (LL) load cell is shown in green. (**C**) Low pass filtered load cell *CoP* signal collected from the "high" speed experiment using the mattress with an air-filled bladder when the 2.27 kg mass was placed 6 cm from the center of the rotation platform and ten ≈11 kg masses were placed on the bed/mattress system. (**D**) Individual load cell data collected during the same experiment shown in (**C**). The load cell traces are the same colors as mentioned in (**B**).

Two other specific irregularities in the load cell *CoP* signals were also found. Abnormalities were noticed in one data collection during the experiments with the coiled mattress where the springs are all connected (see figure 4-20 (A)) and in one iteration during the experiments using the mattress with an air-filled bladder (see figure 4-20 (C)).

The individual load cell data used to calculate the load cell *CoP* signal for each of these cases are shown in figure 4-20 (B) and 4-20 (D) respectively. In the case of the first anomaly (i.e. figure 4-20 (A-B)), there is a significant amount of high frequency "noise" seen for about 30 seconds in the data from the upper right load cell. During data collection this load cell was adjacent to a wall that separates our lab from a community walkway through several wet labs. It is possible that during data collection some kind of commotion on the other side of this wall could have led to high frequency vibrations transmitted to the upper right load cell. The second anomaly (i.e. figure 4-20 (C-D)) appears to be caused by a single erroneous data point with a significant larger absolute magnitude than the rest of the points which seems to have negatively affected the *CoP* signal calculation especially after the signal was low pass filtered.

Several of the low passed *CoP* signals appear to have small "tails" that do not fit the overall circular motion. It is suspected that these "tails" are the results of filter artifacts (see figure 4-21). When reversing the load cell data from the individual load

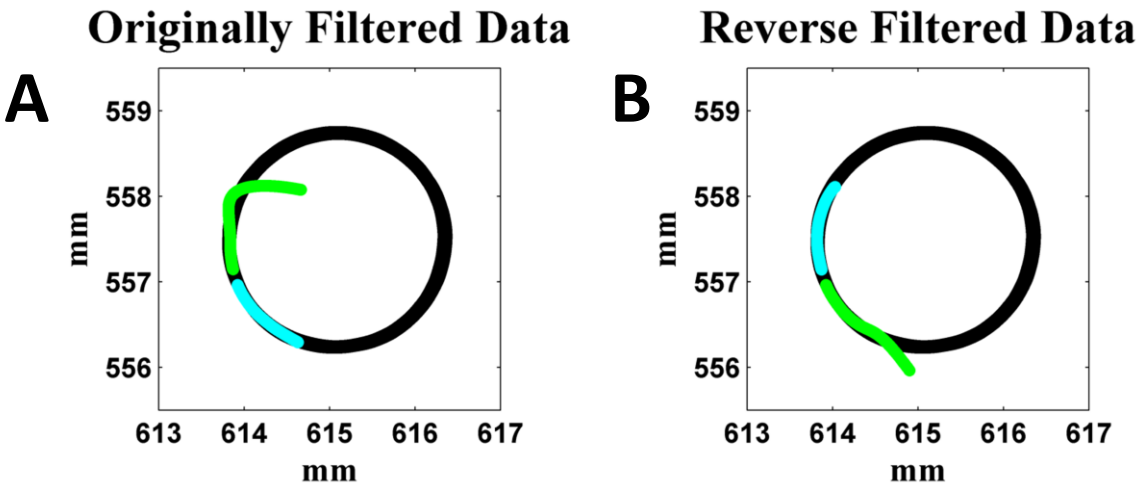

Figure 4-21. (**A**) Load cell *CoP* signal that has been low pass filtered. The first second worth of data is colored green and the last second worth of data is colored cyan. (**B**) The same load cell data as seen in (**A**); however, before estimating the *CoP* signal and low pass filtering, the load cell data was reversed (i.e. the first data point became the last and the last data point became the first). The data that now represents the first second is colored green and the data that now represents the last second is colored cyan.

cells and recalculating the *CoP* signal (figure 4-21 (B)), the "tail" appears once again at the beginning of the new *CoP* signal despite the fact that this same data was previously at the end of the *CoP* signal (figure 4-21 (A)) and was initially unaffected (i.e. fit the overall circular motion).

Amplitude calculations from the load cell *CoP* signals, while not the exact same as the expected amplitudes, exhibited similar decreasing trends with increasing loading on the bed mattress system (figures 4-11 through 4-14). Also, consistent with equation 4.8, increasingly larger amplitudes were estimated for increasing rotation speed. In fact, the amplitude estimations for the lowest rotation speed were typically very similar to those predicted by equation 4.7. It should be noted that when using equation 4.7 to predict the expected amplitudes, it was assumed that only the 2.27 kg mass was rotating (i.e. the only mass in the entire bed/mattress system that was changing its physical location). In fact, several different parts of the device used to spin the 2.27 kg mass were moving during the experiment such as the circular plate that the mass was attached to and the belt used to connect this plate to the motor. There were also two accelerometers attached to the plate during the experiment with unknown masses that were not accounted for. It is assumed that the plate and belt are of homogenous makeup (despite a groove in the plate used to attach the 2.27 kg mass); therefore, leading to negligible net changes in overall mass displacement due to their rotations. The mass of the two accelerometers are also assumed to be negligible compared to the 2.27 kg mass. These factors contribute to the discrepancies between the predicted and actual trajectories.

There was no significant difference detected between video data calculations and load cell calculations of the rotation frequencies in either the x or y direction. When

looking at the differences between load cell and video estimated rotation speeds, there was a small effect (F_{10} = 1.98, p = 0.04) found in the *y*-direction for the interaction between the number of ≈11 kg masses placed on the bed/mattress system and the speed of rotation. However, the overall accuracy of the load cell *CoP* signal's ability to estimate rotation speed of the 2.27 kg mass (as compared to video ground truth) did not appear to be affected by mattress type, rotation speed, diameter of displacement, or the amount of mass loaded on the bed/mattress system.

Experiment 2

In the second experimental setup where the 2.27 kg mass was placed at differing diameters, the load cell *CoP* signal performed very well at detecting and distinguishing between the different diameters of displacement when the mattress and speed of rotation were held constant. In particular, the amplitudes of *CoP* displacement calculated using the load cell *CoP* signals followed the expected amplitudes (see figure 4-19). The difference between load cell *CoP* estimated amplitudes and the expected amplitudes decreased when the 2.27 kg mass was rotated at smaller diameters. Per equation 4.8, extraneous forces - not accounted for in the load cell *CoP* signal calculations - should decrease with decreasing radial locations of the mass (*r*). Therefore, the load cell *CoP* representation of the 2.27 kg's rotation should become more accurate at smaller radii. The much lower diameters calculated when the bed/mattress system was loaded with the higher amount of mass (i.e. 109.3 kg) as compared to when the bed/mattress system was loaded with 21.6 kg are also consistent with equation 4.7.

One area of concern, however, is illustrated in figure 4-22. When 109.3 kg of mass is loaded on the bed/mattress system, the *CoP* signal in both the *x* and *y* direction

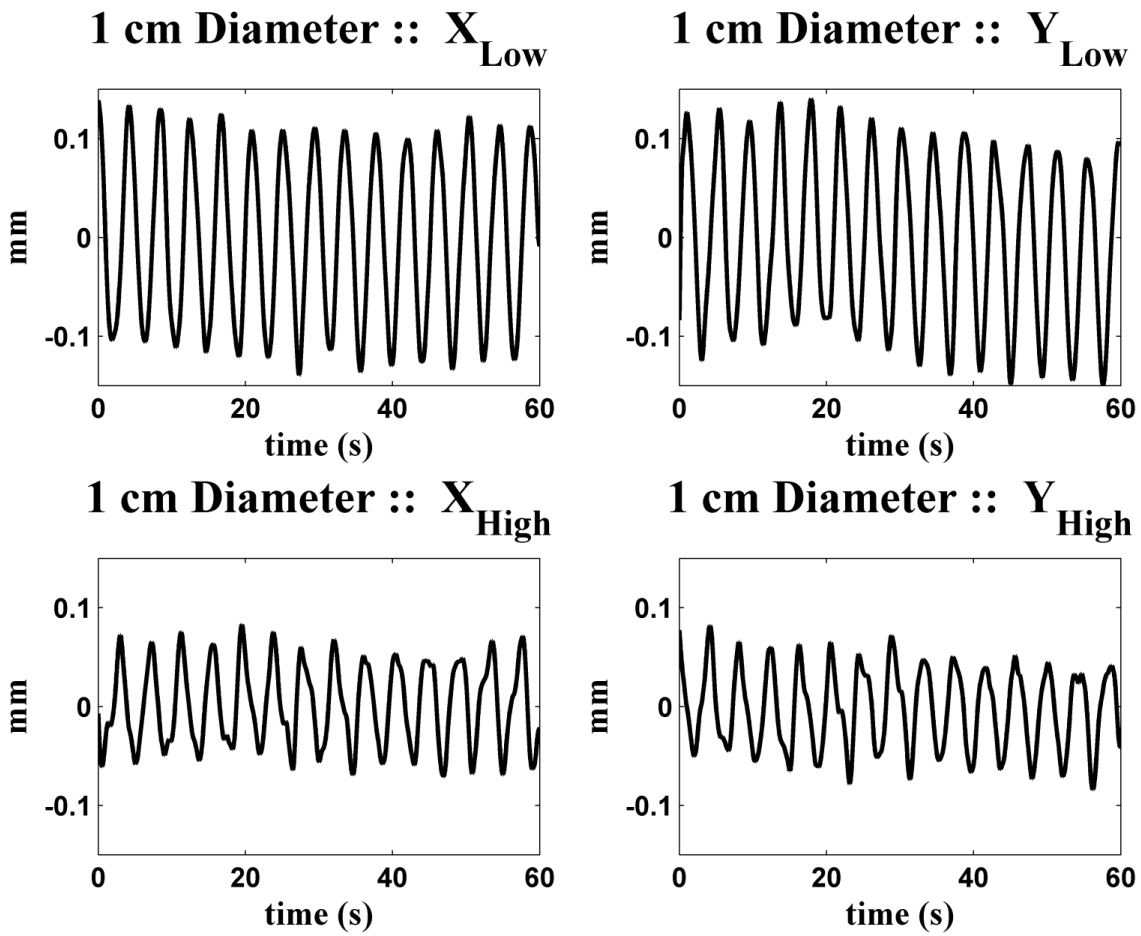

Figure 4-22. Load cell CoP_x (left column) and CoP_y (right column) signals collected when the 2.27 kg mass was placed at a 1 cm diameter on the rotation platform. The upper row contains data collected when approximately 21.6 kg was loaded on the bed/mattress system and the lower row contains data collected when about 109.3 kg was loaded on the bed/mattress system.

calculated for an actual diameter of 1 cm (bottom row) appears to have a less consistent amplitude of *CoP* displacement than those seen when only 21.6 kg was loaded on the bed/mattress system (top row). This could possibly limit the ability of load cells to detect apneas in larger individuals (i.e. looking for decreased amplitudes of breathing in the load cell *CoP* signal).

Another observation of note is the slight migration that is noticeable in the load cell *CoP* signals shown in figure 4-16. As the amplitude of *CoP* displacement decreases, the centroid of the *CoP* signal appears to move mostly in the positive *y* direction but also

slightly in the negative *x* direction. Data collection during the experiment started with the largest amplitude of displacement and proceeded to the smallest amplitude of displacement. Therefore, it is theorized that there was some settling of the mass loaded on the memory foam mattress over the time course of the entire data collection for the experiment. The migration of the *CoP* signals is mostly in the *y*-direction towards the location of the ≈11 kg masses loaded on the bed/mattress system indicating that the settling may have led to the load cells nearer the ≈11 kg masses supporting slightly more of the weight loaded on the system. This would lead to an absolute change in the location of the load cell *CoP* signal that changes slightly over the time course of the entire experiment while not being evident during the considerably short 1 minute data collections.

It is difficult to estimate the actual magnitude of displacement for the mass that is moved while an individual breathes. The results presented in this section show that the load cell *CoP* signal is able to recreate the motion of a mass comparable to the amount of mass that is expected to be displaced during respiration [65] when the bed/mattress system is loaded with several differing amounts of mass comparable to the mass of an individual lying on the bed. The amplitudes of *CoP* displacement estimated from the load cell *CoP* signals, especially those recorded in figure 4-22, are comparable to the respiration amplitudes found in the load cell *CoP* signals collected when actual individuals are lying on the bed mattress system (see figure 3-1 (C) and figure 3-3 (A-C)). Ultimately, these results suggest that the load cells could be utilized to track the mass displaced as an individual lying on the bed breathes and also used to detect changes in respiration amplitude which is critical in detecting apneic events.

Chapter 5: Breathing Detection

Breathing Detection Validation Experiment 1: Different Lying Positions

Motivation

In order to test and validate the load cell system's ability to detect the breathing of an individual lying on the bed, the respiration rates calculated using the load cell breathing signal for several healthy controls were compared to respiration rates found using clinically accepted signals and methods. Respiration rates were compared for various lying positions in order to ascertain the effect of lying position on the load cell system's ability to detect breathing.

Subjects

Twenty-four healthy subjects were recruited from a convenience sample to participate in the study. Eleven subjects were female and 13 were male. The average age was 30.5 ± 8.0 years, the average weight was 76.0 ± 16.8 kg, and the average BMI was 24.5 ± 4.7 kg/m^2.

Setup

Each participant was outfitted with several sensors connected to a portable PSG monitor: respiration belts around their chest and abdomen, a nasal pressure cannula placed in their nostrils, and a finger pulse oximeter attached to their right index finger. For this experiment two portable PSG monitors were utilized. Subjects were either outfitted with the Embletta® system (Embla, Ontario, Canada) or the Alice PDx system (Phillips Respironics, USA). The subjects also wore five different tri-axial accelerometers (PAM-RL, Phillips Respironics, OR, USA), one attached to each wrist and each ankle, and one placed around their abdomen. One load cell (V1) was installed under each of the 4 supports of a full sized bed for a total of 4 load cells. During the experiment load cell data was collected at 2000 Hz.

Methods

The study participants were instructed to lie on the bed and breathe normally without any extraneous movements except when explicitly instructed to move. The experiment lasted 32 minutes during which time the participants were instructed using a prerecorded message to lie in 4 different positions. The participants spent 8 minutes lying in each of the following positions: back, left side, right side, and stomach. The interpretation of how to lie in each of these positions was left up to the discretion of each participant. At the 2.5 and 5 minute mark after having assumed each of the 4 positions, the participants were prompted to shift the position of either their arm(s) or leg(s). Once again, the particular movement of the arm or leg was left to the participant's own interpretation. The study protocol was approved by the Oregon Health & Science University Institutional Review Board.

Analysis

Clinically Accepted Respiration Rate Calculation:

The several medical devices that are used to monitor respiration output a respiration rate estimate. The algorithms used to calculate the respiration rate are usually proprietary and the results vary in accuracy. Therefore, the clinical standard for estimating an individual's breathing rate is to simply count the number of breaths that occur during a specified amount of time such as 30 seconds or 1 minute. I developed an algorithm that would estimate the temporal location of each breath in the flow signal (i.e. the breathing signal measured using the nasal pressure cannula placed in the participants' nostrils). Then following clinical convention, the algorithm's estimate of each breath location was visually inspected by an independent investigator, and any detection errors were fixed manually.

The algorithm detected each breath by first decimating the flow signal to a sampling rate of 5 Hz. In order to attenuate any frequencies in the flow signal that were not associated with respiration, the decimated flow signal was then low pass filtered using an 8^{th} order Chebyshev Type II filter that was monotonic in the pass-band, had a stop-band edge frequency of 0.6 Hz, and attenuated the stop band by 40 dB. The temporal location of each breath was estimated by locating the peaks and troughs in the low pass filtered flow signal that represent the transitions between inspiration and expiration.

The trend of the decimated flow signal was estimated using a 4^{th} order low pass Chebyshev Type II filter that was monotonic in the pass-band, had a stop-band edge frequency of 0.05 Hz, and attenuated the stop band by 20 dB. Peaks were detected by

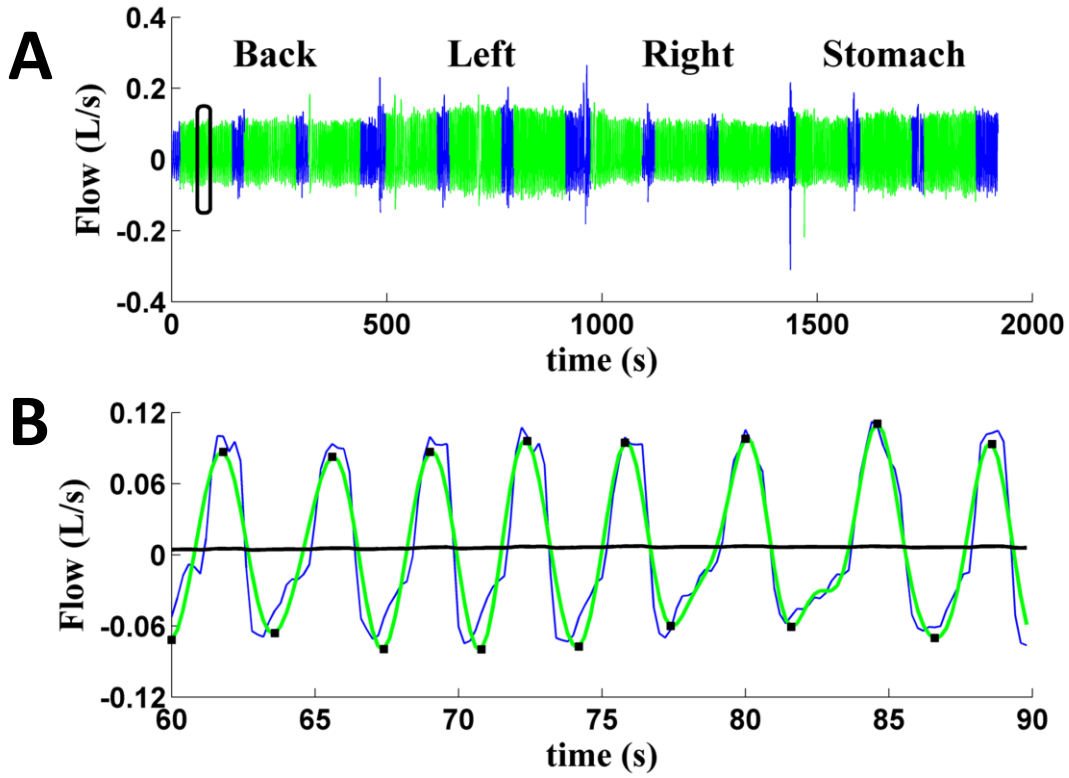

Figure 5-1. Illustration of the algorithm implemented to locate each breath in the flow signal from the nasal pressure cannula. (**A**) Flow signal (blue) recorded during the experiment for one subject. The 12 two minute segments of quiescence (3 for each lying position) that were used to estimate respiration rate are highlighted in green. (**B**) Close up visualization of the 30 seconds of data that are outlined with the black rectangle in '**A**'. The flow signal that has been decimated to 5 Hz is shown in blue. The green trace represents the decimated flow signal after being low passed filtered. The black line denotes the trend estimated for the decimated flow signal. Peaks and troughs (black squares) were calculated as the local maximums and minimums in the green trace above and below the trend respectively. The peaks and troughs represent points of transition between inspiration and expiration and vice versa for each breath. The time points of these detected peaks and troughs on the original flow signal would then be presented to the independent investigator for any needed corrections.

finding the point of maximum value during each period that the decimated flow signal was greater than the trend. Troughs were detected by finding the point of minimum value during each period that the decimated flow signal was less than the trend. The peak and trough times were then multiplied by the same factor used to decimate the flow signal to 5 Hz so that the locations of the each breath (i.e. the peaks and troughs) could be visualized on the original flow signal for inspection. An example of the implementation of the algorithm is shown in figure 5-1.

The corrected peaks and troughs from the flow signal were used to estimate the respiration rate for 12 predefined 2-minute segments. The 2-minute segments were chosen to include periods of quiescence between each movement. In all there were three 2-minute segments selected for each lying position (back, left side, right side, and stomach). The respiration rate measured in breaths per minute for each segment was calculated by first finding the average time in seconds between serial peaks and between serial troughs. This average time for each breath (seconds/breath) was then inverted (breaths/second) and multiplied by 60 (seconds/minute) in order to derive a respiration rate in breaths per minute.

Load Cell Respiration Rate Calculation:

An algorithm was developed to automatically detect peaks and troughs in the load cell breathing signal that represent the transitions between inspiration and expiration. While these peaks and troughs are utilized to calculate the respiration rate, such as is done in this chapter, peaks and troughs detected using this algorithm are also used to estimate breathing amplitude from the load cell breathing signal - an important part of the automatic sleep apnea detection algorithm described in chapter 7. There was some concern that a peak/trough detection method which found the maximums and minimums above or below a trend line would miss the peaks and troughs associated with breaths during an apnea or a hypopnea that had significantly attenuated amplitudes. Therefore, the developed algorithm detects all local maximums and minimums in the load cell breathing signal and eliminates any extraneous peaks and troughs that are not representative of inspiration/expiration transitions.

In the algorithm, the data from each load cell was used to calculate the center of pressure along the head-to-toe axis of the bed as described in chapter 3. The load cell center of pressure signal (CoP_y) was then decimated to a sampling rate of 10 Hz. Due to the nature of the experiment protocol, the temporal location of movements by the subject (e.g. arm movement, leg movement, rolling over, etc.) were known and subsequently removed. The linear trend was then subtracted from the remaining load cell data using data from periods when the subject was lying quiescently. With the significant movements and DC offset removed from CoP_y, the signal was low pass filtered in order to attenuate any frequencies not associated with breathing (i.e. 'resonant' response of the bed described in chapter 4). The filter used was a 6^{th} order low pass Chebyshev Type II filter that was monotonic in the pass-band, had a stop-band edge frequency of 0.76 Hz, and attenuated the stop band by 40 dB. Initial locations of each breath in the load cell signal were estimated by finding all the local peaks and troughs. Experience from working with the load cell breathing signals suggested that most extra peak and trough pairs were of considerable lower amplitude (measured as the distance between the peak and trough) than both the preceding and following peak/trough pairs. Therefore, any peak/trough pair found to be significantly less than the smaller of the preceding or following peak/trough pairs was eliminated. This procedure is illustrated in figure 5-2.

The respiration rate for each segment was estimated in the same manner as utilized for the reference flow signal, using the average time between subsequent peaks and subsequent troughs. Critical to the function of the algorithm for estimating the respiration rate for the load cell breathing signal was the determination of the threshold for deciding when to eliminate peak/trough pairs. In other words, a peak/trough pair

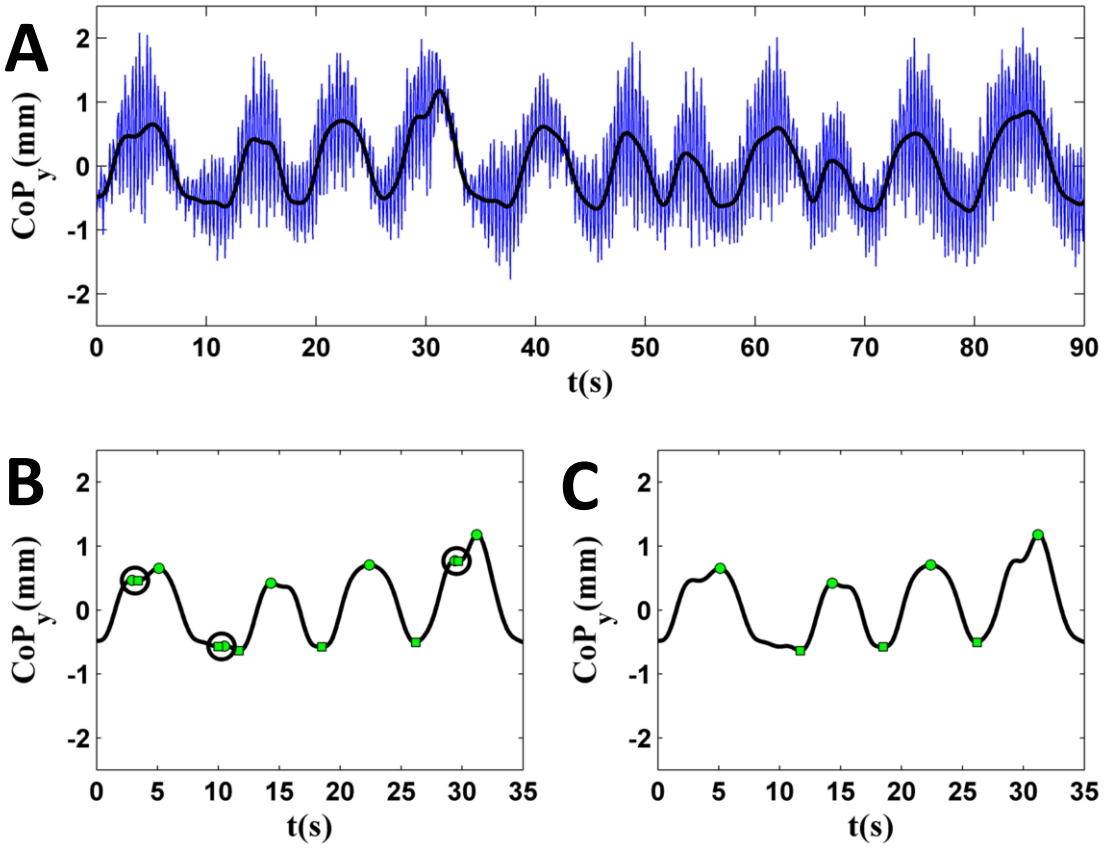

Figure 5-2. Illustration of the algorithm developed to detect individual breaths in the load cell breathing signal. (**A**) Ninety seconds of load cell data collected from one subject. The load cell center of pressure (CoP_y) signal that has been decimated to a sampling rate of 10 *Hz* is shown in blue. The black trace represents the CoP_y signal after having been low pass filtered. (**B**) The first 35 seconds of the low passed CoP_y signal shown in '**A**'. The local peaks and troughs detected in the CoP_y signal are displayed as green circles and squares respectively. The black circles mark extraneous peak/trough pairs that meet criteria for removal (i.e. significantly lower amplitude than the surrounding peak/trough pairs). (**C**) The final peaks and troughs detected in the load cell breathing signal denoting the points of transition between inspiration and expiration for each breath.

would be removed if their amplitude is less than a specified percentage of the amplitude of the smaller of the previous or following peak/trough pair. To do this, thresholds ranging from 0% to 95% were tested. The respiration rates using the load cell breathing signal were estimated for all twelve segments for each subject using each of the different thresholds. These results were compared to the corresponding respiration rates estimated

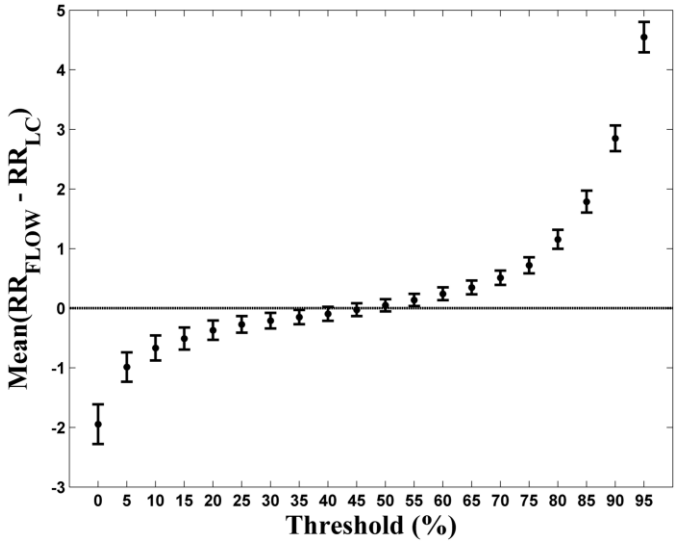

Figure 5-3. Average difference between RR_{FLOW} and RR_{LC} with corresponding 95% confidence intervals across all subjects and lying positions for various thresholds. The threshold represents the point at which a peak/trough pair will be eliminated because its estimated amplitude is less than this percent of the smallest amplitude estimated from the preceding and following peak/trough pairs.

using the reference flow signal (see figure 5-3). With the smallest average difference between the load cell and reference estimated respiration rates, a threshold of 45% was ultimately chosen.

Respiration Rate Comparisons:

Linear regression and R^2 values were used to compare the respiration rate estimated using the load cell breathing signal (RR_{LC}) to the respiration rates calculated from the flow signal (RR_{FLOW}). Agreement between the respiration rate measurements were also analyzed using Bland-Altman plots [63]. Finally, a 3-way repeated measures analysis of variance (ANOVA) was utilized to determine the effect of various factors on the agreement between the load cell measurement of respiration rate and the respiration rate estimated from the flow signal. The three factors were: (1) respiration measurement type (i.e. load cell vs. flow signal), (2) lying position (i.e. back vs. left side vs. right side vs. stomach), and (3) the three different 2 minute segments used for each lying position (i.e. trial 1 vs. trial 2 vs. trial 3). When analyzing the main effect of measurement type, the interaction of measurement type with lying position, and the interaction of

measurement type with lying position and trial, the Greenhouse-Geisser correction was used as these situations violated the assumption of sphericity.

Results

The linear regression and R^2 values for RR_{FLOW} vs. RR_{LC} separated out by lying position are shown in figure 5-4. The Bland-Altman plots showing the agreement between RR_{FLOW} and RR_{LC} for each different lying position are shown in figure 5-5. There was no significant main effect of respiration measurement type ($F_{1,23}$ = 0.043, p = 0.837). There were also no significant interactions found for respiration measurement type and trial ($F_{2,46}$ = 1.182, p = 0.316), respiration measurement type and lying position ($F_{1.566,36.012}$ = 3.486, p = 0.052), or respiration measurement type, lying position, and trial ($F_{3.258,74.937}$ = 0.653, p = 0.596).

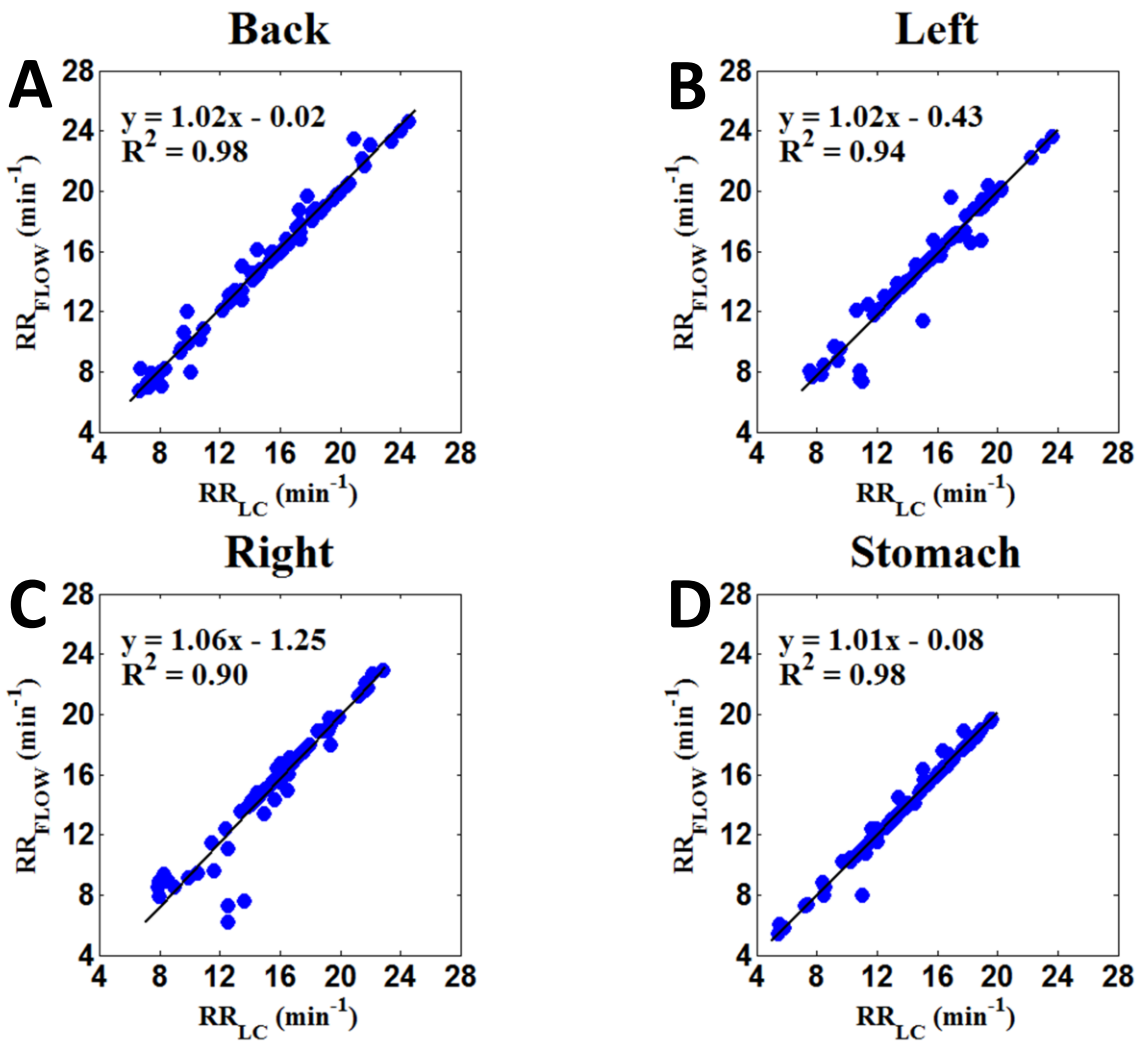

Figure 5-4. Linear regression plots including R^2 values for RR_{LC} vs. RR_{FLOW} while the subjects were lying on their (**A**) backs, (**B**) left sides, (**C**) right sides, and (**D**) stomachs.

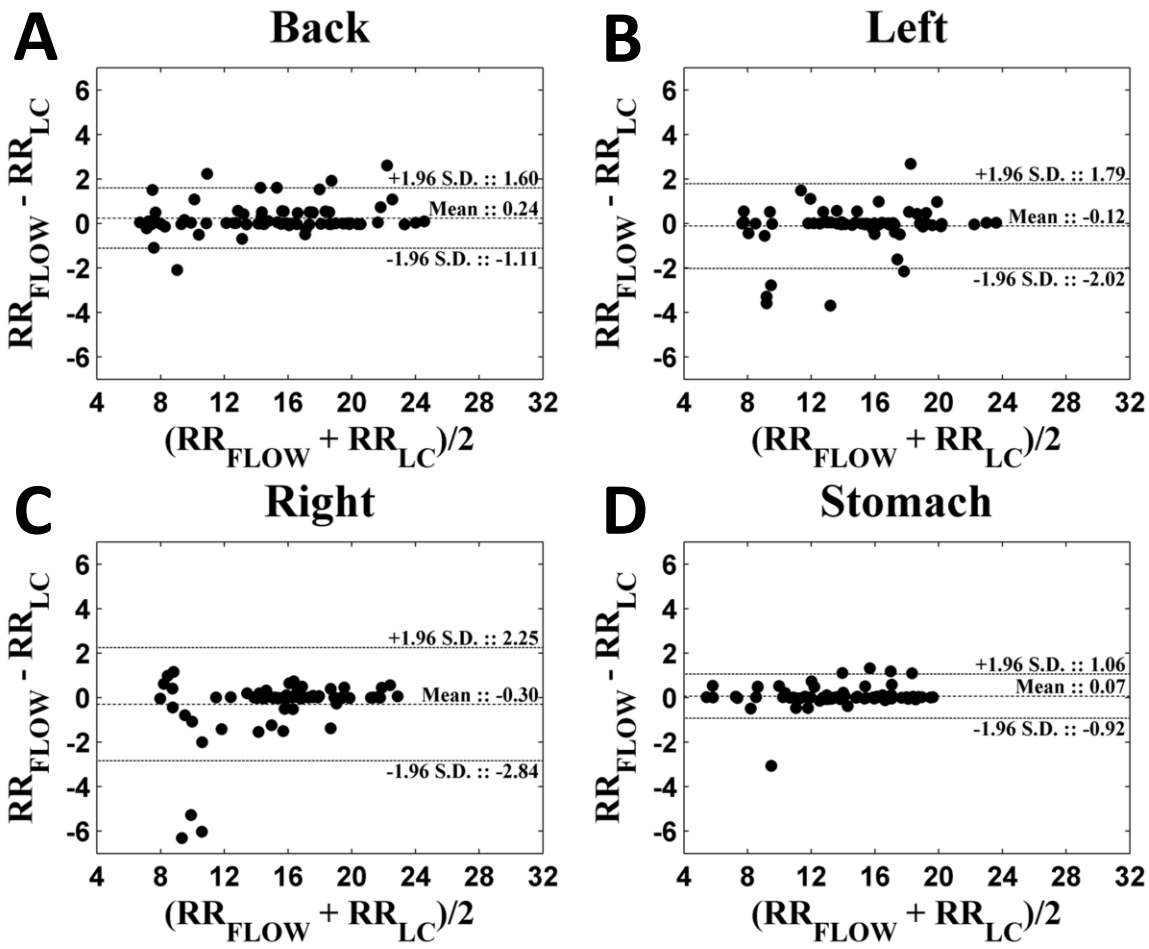

Figure 5-5. Bland-Altman plots for visualization of the agreement between the RR_{FLOW} and RR_{LC} while the subjects were lying on their (**A**) backs, (**B**) left sides, (**C**) right sides, and (**D**) stomachs.

Discussion/Conclusion

An accurate respiration rate was able to be estimated using the load cell breathing signal. This suggests that the load cell system can reliably detect the breathing of an individual lying on the bed. More importantly, these test results also suggest that the ability of the load cells to detect the breathing signal is independent of lying position. The respiration rate estimated by the load cell was consistently high for one individual especially while they were lying on their left and right sides ($RR_{LC} \approx$ 10-13 breaths per minute vs. $RR_{FLOW} \approx$ 6-8 breaths per minute). It is unclear whether the load cell system struggled with the somewhat low respiration rate or if there was something specific about this subject that caused the inaccuracies. The load cell breathing signal was used to accurately estimate respiration rate for other subjects/lying positions at similar low reference respiration rates so the issue may have been with some nuance on how the subject was breathing or possibly how they were lying on the bed. Overall, the load cell system did well at predicting respiration rate.

An important step in identifying individual breaths in the load cell breathing signal is low pass filtering. The higher frequencies in the load cell data associated with the heart beating and the resonance of the bed/mattress system need to be attenuated so that local peak/trough detection techniques can be utilized. With the typical breathing rate being between about 8 and 24 breaths per minute[4] or 0.13 and 0.4 Hz, setting the cutoff frequency for the low pass filter can be difficult. The filter must be designed so as not to attenuate higher breathing rates (e.g. 24 breathes per minute or 0.4 Hz); however,

[4] For reasons unknown, some subjects exhibited breathing rates below 8 breaths per minute during these experiments.

this often results in extra peaks/troughs showing up in the load cell data of individuals with lower breathing rates.

Paalasmaa et al. attempted to use several different low-pass filters with different cutoff frequencies to account for this issue when using load cells to estimate breathing rate [58]. Since the respiration rate of the individual is unknown in advance, their approach was based on filtering the load cell signal with all the different filters and then for various time segments choosing the filtered signal that resulted in the least variability in the breathing amplitude (measured using the detected peaks/troughs). Since the ultimate goal of this dissertation work is to detect sleep apnea where identifying periods of breathing amplitude change is critical, this approach is not ideal. Instead, I have developed an approach that uses a single low pass filter with a stop-band edge frequency of 0.76 Hz and a -3 dB point of 0.54 Hz. This filter effectively attenuates the 'resonance' response of the bed while not affecting any of the frequency content of the load cell *CoP* signal associated with the entire range of breathing rates expected from individuals lying on the bed/mattress system. Extra peaks and troughs are accounted for by eliminating extraneous peak/trough pairs that are 45% less than the immediately surrounding peak/trough pairs.

One area of concern for this approach is that during an apneic event the peaks/troughs associated with a single significantly attenuated breath could be eliminated. However, an analysis of over 38,000 apnea/hypopnea events associated with oxygen desaturations by Otero et al. found the average apnea or hypopnea event duration to be greater than 20 seconds for individuals without sleep apnea and greater than 23 seconds for patients with sleep apnea [66]. A breathing rate of approximately 3 breaths

per minute is unlikely; therefore, few apneic events that are a single breath in duration are expected. The outlined approach for eliminating extraneous peaks/troughs in the load cell breathing signal has been shown to accurately detect the breathing of an individual lying on the bed and is not expected to interfere with the overall goal of detecting sleep apnea.

Breathing Detection Validation Experiment 2: Different Mattress Types

Motivation

While the previous experiment demonstrated that the load cell system can reliably estimate the respiration signal independent of lying position, these tests were carried out using a single innerspring mattress. With the availability of several different mattress types for individuals to sleep on, it was also important to validate the ability of the load cell system to detect the breathing signal for several different commonly utilized mattress types. Therefore, the respiration rates calculated using the load cell breathing signal for several healthy controls lying on four different mattress types were compared to respiration rates found using clinically accepted signals and methods.

Subjects

Seventeen healthy subjects were recruited from a convenience sample to participate in the study. Eight subjects were female and 9 were male. The average age was 33.1 ± 13.1 years, the average weight was 76.9 ± 17.5 kg, and the average BMI was 26.4 ± 4.8 kg/m^2.

Setup

Each participant was outfitted with several sensors connected to the Embletta® portable PSG monitor (Embla, Ontario, Canada): respiration belts around their chest and abdomen and a nasal pressure cannula placed in their nostrils. A WristOx$_2$™ (Nonin Medical, Inc., MN, USA) pulse oximeter was placed on each participant's left wrist with the sensor attached to their left index finger. The subjects also wore five different tri-axial accelerometers (PAM-RL, Phillips Respironics, OR, USA), one attached to each

wrist and each ankle, and one placed around their abdomen. One load cell (V3) was installed under each of the 4 supports of a full sized metal bed frame for a total of 4 load cells. During the experiment load cell data was collected at 500 Hz. The different mattresses that were tested were: 1.) a mattress with an air-filled bladder with adjustable air pressure encased in foam (similar to a Sleep Number® mattress), 2.) a mattress made of memory foam (similar to a Tempur-Pedic® mattress), 3.) a coil mattress with independent springs (i.e. springs that are not connected), 4.) and a coiled mattress with dependent springs (i.e. all the springs are connected).

Methods

The following protocol was implemented for each study participant and repeated for each different mattress type. The study participants were instructed to lie on the bed and breathe normally without any extraneous movements except when explicitly instructed to move. The experiment for each mattress type lasted 10 minutes during which time the participants were instructed using a prerecorded message to lie in 4 different positions. The participants spent 2.5 minutes lying in each of the following positions: back, left side, right side, and stomach. The interpretation of how to lie in each of these positions was left up to the discretion of each participant. The study protocol was approved by the Oregon Health & Science University Institutional Review Board.

Analysis

Two minute segments of data were selected for each subject while they lay quiescently on their back, left side, right side, and stomach for each of the four mattress types. A total of 16 two minute segments were selected for each subject (i.e. 4 lying

position × 4 mattress types). The average respiration rate for each segment was estimated using the flow signal from the nasal pressure cannula (i.e. RR_{FLOW}) and the load cell breathing signal (i.e. RR_{LC}) following the same methods as described in the previous section (i.e. "Breathing Detection Validation Experiment 1: Different Lying Positions").

Similar to the last section agreement between RR_{LC} and RR_{FLOW} was analyzed using linear regression, R^2 values, and Bland-Altman plots [63]. A 3-way repeated measures ANOVA was again utilized to determine the effect of various factors on the agreement between RR_{LC} and RR_{FLOW}. The three factors for this experiment were: (1) respiration measurement type (i.e. load cell vs. flow signal), (2) lying position (i.e. back vs. left side vs. right side vs. stomach), and (3) the mattress type. When analyzing the main effect of measurement type and the interaction of measurement type with lying position and mattress type, the Greenhouse-Geisser correction was used as these situations violated the assumption of sphericity.

Results

The linear regression and R^2 values for RR_{LC} vs. RR_{FLOW} separated out by mattress type are shown in figure 5-6. The Bland-Altman plots showing the agreement between RR_{FLOW} and RR_{LC} for each different mattress type are contained in figure 5-7. There was a moderately significant main effect found for respiration measurement type ($F_{1,16}$ = 4.756, p = 0.044). There were also a significant interaction found for respiration measurement type and mattress type ($F_{3,48}$ = 5.338, p = 0.003). The interaction between respiration measurement type and lying position was not significant ($F_{3,48}$ = 1.395, p = 0.256). The interaction between all three factors was also found to not be significant ($F_{4.404,70.457}$ = 1.331, p = 0.265).

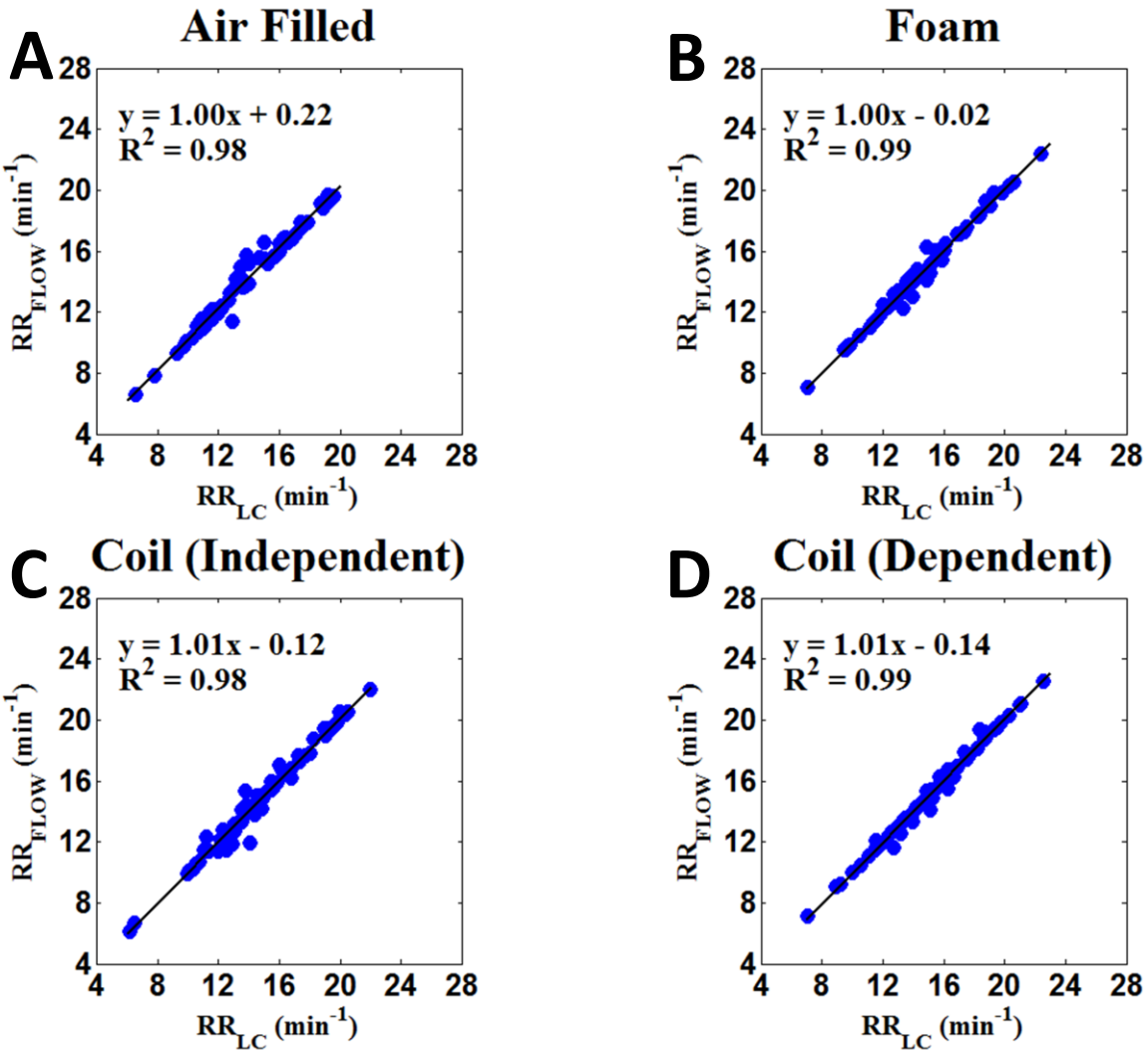

Figure 5-6. Linear regression plots including R^2 values for RR_{LC} vs. RR_{FLOW} while the subjects were lying on the four different mattress types: (**A**) the mattress with an air-filled bladder with adjustable air pressure encased in foam (similar to a Sleep Number® mattress), (**B**) the mattress made of memory foam (similar to a Tempur-Pedic® mattress), (**C**) the coil mattress with independent springs (i.e. springs that are not connected), and (**D**) the coiled mattress where the springs are all connected.

In order to explore the cause of the main effect found for the respiration measurement type and its interaction with mattress type, paired t-tests were used to test the difference between both measurement types for each mattress type. For the mattress with an air-filled bladder, it was found that on average RR_{FLOW} was 0.264 more than RR_{LC}, which was significant (t_{67} = 4.6286, $p << 0.001$ with a 95% confidence interval of [0.1503 0.3782]). The differences between RR_{FLOW} and RR_{LC} for the rest of the mattress

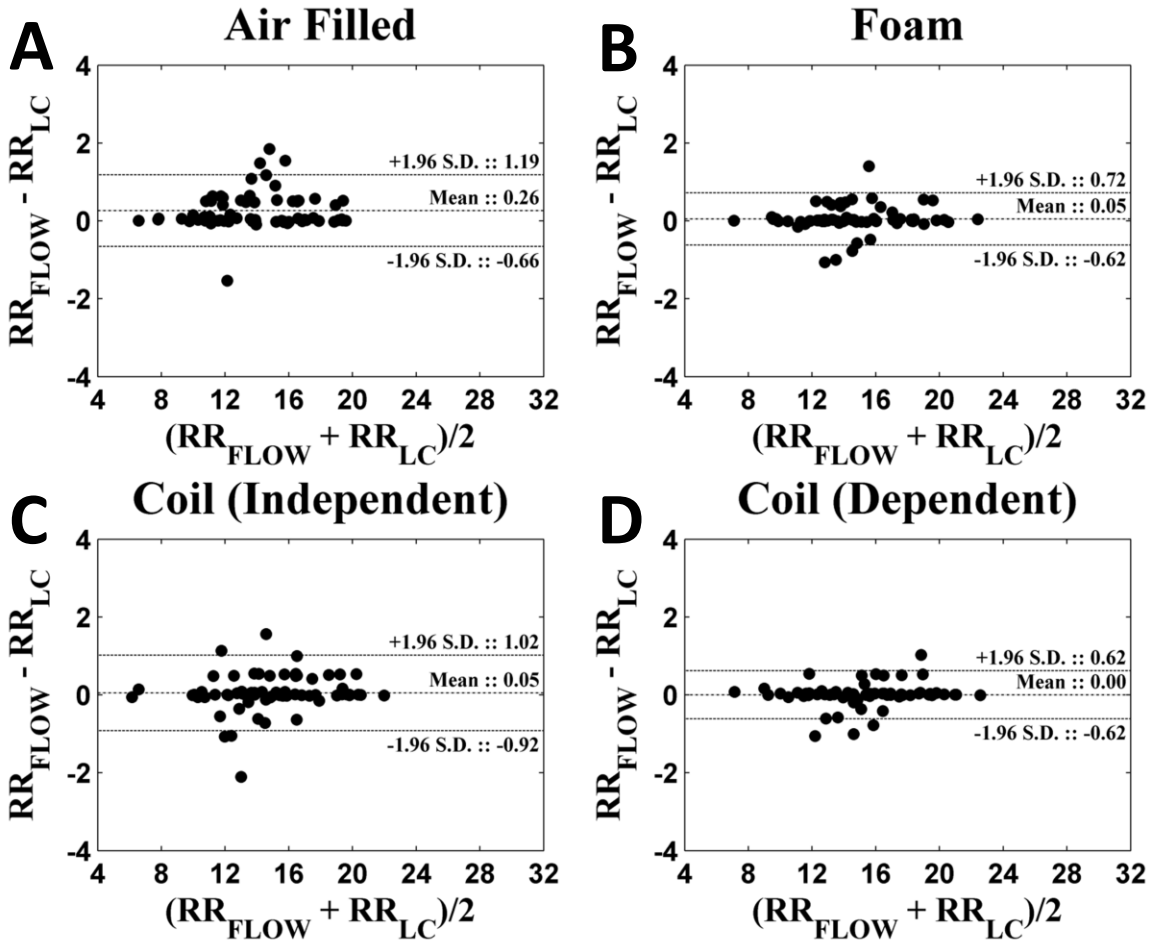

Figure 5-7. Bland-Altman plots for visualization of the agreement between the RR_{FLOW} and RR_{LC} while the subjects were lying on the four different mattress types: (**A**) the mattress with an air-filled bladder with adjustable air pressure encased in foam (similar to a Sleep Number® mattress), (**B**) the mattress made of memory foam (similar to a Tempur-Pedic® mattress), (**C**) the coil mattress with independent springs (i.e. springs that are not connected), and (**D**) the coiled mattress where the springs are all connected.

types were not significant. For the memory foam mattress RR_{FLOW} was on average 0.050 higher than RR_{LC} ((t_{67} = 1.1938, p = 0.2368) with a 95% confidence interval of [-0.0333 0.1323]). RR_{FLOW} from the data collected for the coil mattress with independent springs was on average 0.050 greater than RR_{LC} ((t_{67} = 0.8265, p = 0.4114) with a 95% confidence interval of [-0.0704 0.1699]). Finally, the results from the coiled mattress where the springs are all connected showed an average RR_{FLOW} that was 0.002 higher than RR_{LC} ((t_{67} = 0.0484, p = 0.9615) with a 95% confidence interval of [-0.0744 0.0781]).

Discussion/Conclusion

Overall data from the load cell system was able to be used to accurately estimate the breathing rate for individuals lying on the bed/mattress independent of mattress type. There was a small difference between RR_{FLOW} and RR_{LC} when using the mattress with an air-filled bladder with adjustable air pressure encased in foam. The Bland-Altman plot in figure 5-7 shows that for this mattress type RR_{FLOW} minus RR_{LC} is skewed in the positive direction. This, along with three possible outliers, likely led to the small bias between RR_{FLOW} and RR_{LC}. This difference of 0.264 represents only a 1.9% error when compared to the average breathing rate for all the subjects during the experiments for this mattress (14.05 breaths per minute). Furthermore, the high R^2 value and good agreement seen in figure 5-6 and figure 5-7 indicate that the load cell system is able to reliably detect the breathing signal for this mattress setup despite the slight offset between RR_{FLOW} and RR_{LC}.

Chapter 6: Movement Detection and Removal

Motivation

It has been shown that the load cell system installed under the supports of the bed is sensitive enough to detect small movements of mass such as those associated with an individual's respiration while lying on the bed/mattress system. From empirical evidence, I have observed that the movements associated with breathing that are detected by the load cell system are orders of magnitude smaller then movements such as the individual rolling over or changing lying position (see figure 6-1 (A)). These larger movements completely wash out the load cell breathing signal (i.e. *CoP*) and can affect analysis of the *CoP* signal near such large movements. For instance, low pass filters designed to remove the bed resonance (i.e. the 2-4 Hz impulse response believed to result from the heart beating) can result in significant artifact introduced into the *CoP* signal near large movements due to the impulse response of the filter, and any frequency analysis of the *CoP* signal will be altered in windowed regions that happen to include periods of significant movement. Therefore, in order to achieve the end goal of my dissertation which is to automatically analyze a complete night of load cell *CoP* data in order to automatically detect the presence of sleep apnea, a method to first remove any significant movements from the data is needed.

Brink et al. and Chung et al. have used load cells to detect movement [44, 45]; however, the ability of these approaches to detect individual movements was not systematically validated. Previous work in our lab has also focused on detecting movements of an individual lying on a bed/mattress system using the assumption that periods of movement would have much more variance than segments of non-movement [43, 46]. This work utilized the variance of windowed segments of data from each individual load cell weighted by their proximity to the estimated center of mass of the individual and then summed together in order to determine if movement was occurring or not. A supervised learning approach was used to determine which values of the weighted and summed load cell variance features were associated with movement and non-movement. Unfortunately, the generalizability of this supervised learning approach is uncertain.

I propose to sum all the outputs of the load cells before calculating the variance as opposed to calculating the variance from each individual load cell signal. This approach would reduce much of the variance due to the breathing signal detected by the individual load cells. The breathing signal detected by each load cell at the head of the bed is expected to be about 180° out phase with the load cells at the foot of the bed. Therefore, summing them all together would likely attenuate much of the breathing signal. In this chapter, I present a systematic approach to determining a generalizable (i.e. able to be used for load cell data collected while any individual sleeps on the bed/mattress system) threshold of variance in order to distinguish between periods of quiescence and movement using a slightly altered approach already developed in our lab [43, 46].

Subjects

The subjects recruited for this experiment were the same as those recruited for the "Breathing Detection Validation Experiment 1: Different Lying Positions" experiment in chapter 5.

Setup

The setup for this experiment was the same as the setup for the "Breathing Detection Validation Experiment 1: Different Lying Positions" experiment in chapter 5.

Methods

The methods for this experiment were the same as those used for the "Breathing Detection Validation Experiment 1: Different Lying Positions" experiment in chapter 5.

Analysis

Ground truth movement time periods were determined using data from the tri-axial accelerometers. The output from all 5 accelerometers was combined into a single signal (ACC_{sum}) by first combining the *xyz* components for each accelerometer and then summing these results across all 5 accelerometers. Cross-correlation analysis was then used to time align the accelerometer output to the load cell data. Finally, the ACC_{sum} signal was visually inspected and the beginning and ending points of all 11 movements from the experiment protocol (i.e. 3 roll overs and 8 arm and/or leg shifts) were annotated for each of the 24 subjects.

Periods of movement in the load cell data from each of the 24 subjects were detected by first summing together the output from each load cell (LC_{sum}). LC_{sum} was then decimated to a sampling rate of 40 Hz in order to match the sampling rate of the

accelerometers and the variance was calculated for N overlapping windows of length L (seconds) from this signal. Using a threshold specified as n times the median variance calculated from all the LC_{sum} segments of length L, the overlapping windowed segments containing movement were detected. Finally, overall movement periods in the load cell signal were determined by coalescing windows of data determined to be movement that either overlapped or were within 10 seconds of each other. The 10 second cutoff for the allowable time between movement windows was chosen because by definition an apnea must be at least 10 seconds in length [3].

In order to develop a generalizable solution for detecting movements in the load cell data based upon the approach previously used in our lab [43, 46], an optimal window length L and threshold n (i.e. n times the median variance) needed to be determined. Therefore, ROC curves were generated for each of the 24 subjects using several different thresholds (i.e. n) ranging from 1 to 5000 times the median variance. A separate ROC curve was generated for each subject for 10 different window lengths (i.e. L) ranging from 0.5 to 5 seconds. In order to produce the ROC curves, the sensitivity or true positive rate (TPR) for each threshold/window length combination was calculated using:

$$TPR = \frac{TP}{P} \tag{6.1}$$

where TP is the number of points determined as movement in LC_{sum} that correspond with points designated as movement from ACC_{sum} and P is the total number of movements labeled in ACC_{sum}. The false positive rate (FPR) or 1 – specificity was also calculated using:

$$FPR = \frac{FP}{(FP + TN)} \tag{6.2}$$

where *FP* is the number of non-movement points in ACC_{sum} detected as movement in LC_{sum}, and *TN* is the number of non-movement points in ACC_{sum} correctly deemed as non-movement in LC_{sum}.

The effectiveness of each window length (*L*) was assessed by estimating the area under each subjects' ROC curves (AUC) for each of the 10 different window lengths. The AUC values for each window length were then averaged across the 24 subjects, and analysis of variance was utilized to compare the mean AUC values in order to choose the window length *L*. Finally, the ROC curves for the chosen window length *L* were averaged across all the subjects, and the threshold for separating movement from non-movement windows was chosen as the value (i.e. *n* times the median variance) that was closest (Euclidean distance) to the FPR = 0 and TPR = 1 point.

Results

Figure 6-1 contains an example of how the variances calculated from LC_{sum} are utilized to detect movements in the load cell data. The AUCs estimated for each subject and window length *L* are shown in table 6-1 along the mean and standard deviation calculated for each window length. Window length did have an effect on the estimated AUCs ($F_{9,230} = 8.27$, $p << 0.01$). Further analysis using multiple comparison techniques revealed that the average AUC estimated for $L = 0.5$ seconds was significantly less than the other 9 window lengths. It was also found that only the mean AUCs for $L = 2.5$ seconds and $L = 3$ seconds were significantly higher than the mean AUC for $L = 1$ second which had the second lowest average. Ultimately, the window length chosen was $L = 2.5$ seconds as it had a slightly larger average AUC (0.9927 ± 0.0061). Consequently, the threshold chosen (i.e. *n* times the median variance) was 14 as shown in figure 6-2.

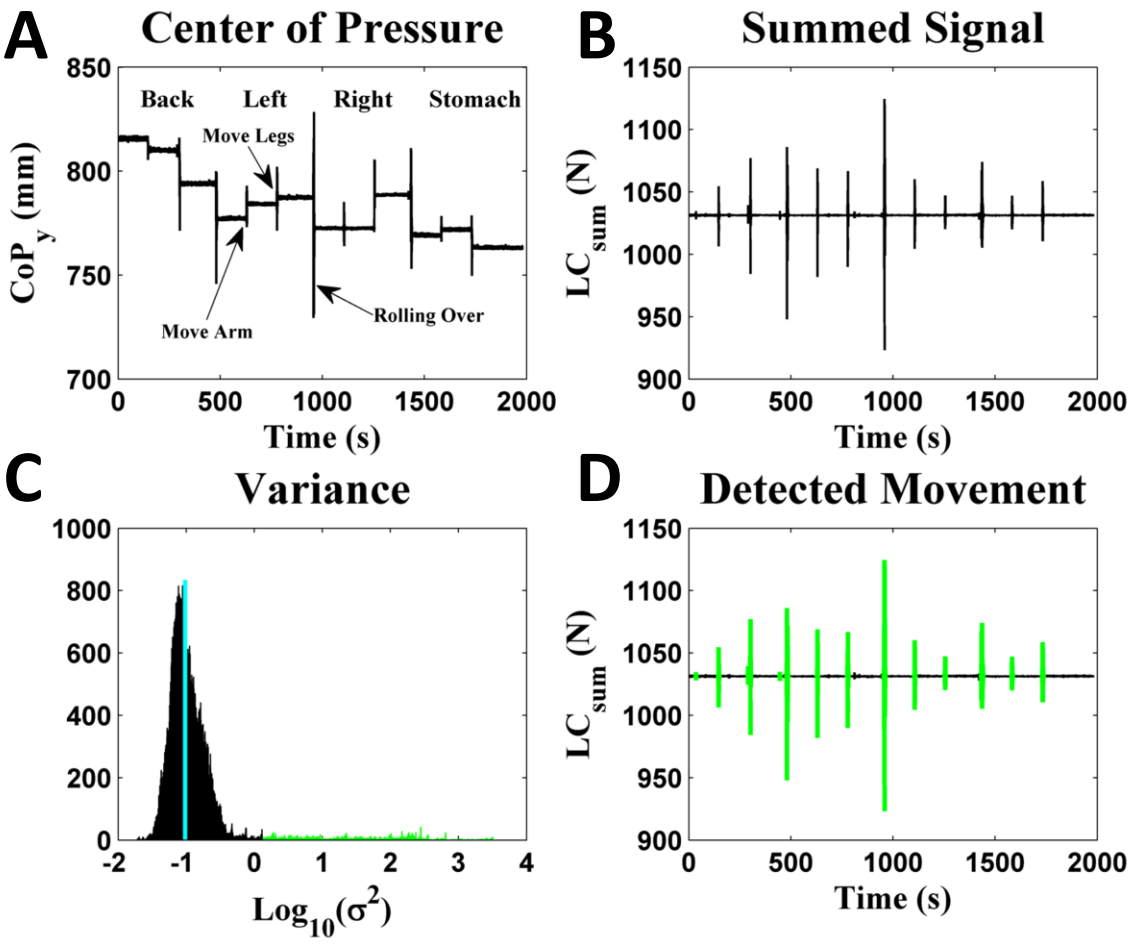

Figure 6-1. (**A**) Load cell *CoP* signal in the *y*-direction (head-to-foot axis of the bed) for one subject showing examples of large movements (i.e. rolling over) and smaller movements (i.e. moving an arm or a leg). (**B**) Load cell signal from the same subject where the data from all the load cells under the bed have been summed together. (**C**) Distribution of the variances calculated using the summed load cell data and a 2.5 second window. The median of all the variances is shown with the cyan line, and the variances considered to represent movement (i.e. 14 times the median variance) are shown in green. The data has been log transformed for visual purposes. (**D**) Summed load cell signal (black) with detected movements (green). Of note is the small movement detected at the very beginning of the signal that was not part of any prescribed movement and would therefore have been considered to be a false positive.

Table 6-1
Area Under Curve (AUC) calculated for each subject.

	Window Length									
Subject	**0.5 (s)**	**1 (s)**	**1.5 (s)**	**2 (s)**	**2.5 (s)**	**3 (s)**	**3.5 (s)**	**4 (s)**	**4.5 (s)**	**5 (s)**
1	0.9936	0.9939	0.9932	0.9929	0.9936	0.9939	0.9930	0.9919	0.9907	0.9890
2	0.9512	0.9776	0.9839	0.9862	0.9883	0.9888	0.9877	0.9857	0.9833	0.9811
3	0.9788	0.9978	0.9985	0.9977	0.9964	0.9945	0.9924	0.9901	0.9878	0.9855
4	0.8991	0.9476	0.9794	0.9902	0.9934	0.9933	0.9921	0.9900	0.9875	0.9846
5	0.8474	0.8870	0.9292	0.9703	0.9946	0.9958	0.9949	0.9936	0.9920	0.9903
6	0.9618	0.9604	0.9649	0.9672	0.9677	0.9686	0.9676	0.9674	0.9648	0.9637
7	0.9912	0.9969	0.9980	0.9982	0.9977	0.9966	0.9952	0.9936	0.9912	0.9887
8	0.9884	0.9982	0.9983	0.9975	0.9963	0.9947	0.9929	0.9909	0.9887	0.9865
9	0.9886	0.9954	0.9967	0.9964	0.9957	0.9949	0.9938	0.9926	0.9913	0.9894
10	0.9306	0.9533	0.9784	0.9924	0.9933	0.9933	0.9927	0.9915	0.9898	0.9878
11	0.9552	0.9759	0.9815	0.9853	0.9897	0.9927	0.9935	0.9923	0.9911	0.9897
12	0.9799	0.9926	0.9977	0.9978	0.9974	0.9968	0.9957	0.9944	0.9930	0.9917
13	0.9216	0.9467	0.9735	0.9869	0.9910	0.9918	0.9915	0.9900	0.9890	0.9863
14	0.9509	0.9670	0.9817	0.9942	0.9971	0.9963	0.9949	0.9934	0.9915	0.9896
15	0.9932	0.9990	0.9987	0.9980	0.9969	0.9956	0.9942	0.9923	0.9906	0.9884
16	0.9771	0.9843	0.9908	0.9921	0.9933	0.9934	0.9925	0.9912	0.9897	0.9880
17	0.9917	0.9944	0.9950	0.9944	0.9955	0.9947	0.9934	0.9919	0.9902	0.9885
18	0.9954	0.9963	0.9961	0.9958	0.9950	0.9942	0.9933	0.9920	0.9907	0.9884
19	0.9813	0.9886	0.9924	0.9933	0.9928	0.9930	0.9925	0.9915	0.9902	0.9886
20	0.9818	0.9953	0.9971	0.9973	0.9966	0.9955	0.9948	0.9939	0.9928	0.9916
21	0.9622	0.9747	0.9848	0.9929	0.9957	0.9947	0.9933	0.9919	0.9904	0.9882
22	0.9806	0.9885	0.9868	0.9866	0.9855	0.9840	0.9826	0.9812	0.9800	0.9785
23	0.9759	0.9854	0.9897	0.9925	0.9936	0.9937	0.9920	0.9901	0.9878	0.9857
24	0.9368	0.9706	0.9883	0.9889	0.9873	0.9858	0.9833	0.9815	0.9806	0.9801
	0.9631	**0.9778**	**0.9864**	**0.9910**	**0.9927**	**0.9924**	**0.9912**	**0.9898**	**0.9881**	**0.9862**
±	**0.0347**	**0.0249**	**0.0148**	**0.0078**	**0.0061**	**0.0058**	**0.0059**	**0.0057**	**0.0059**	**0.0057**

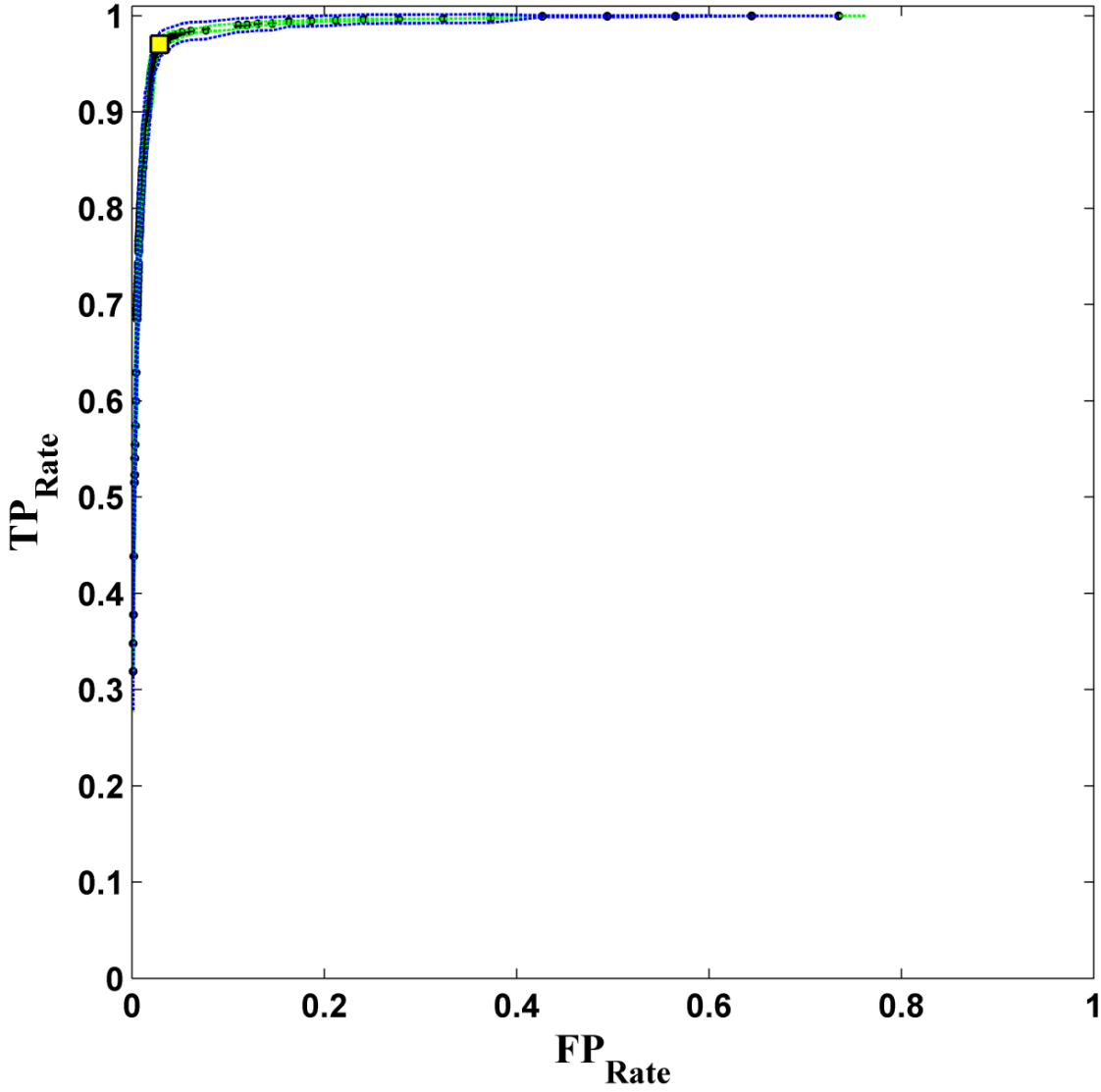

Figure 6-2. *ROC* curve for a window length of L = 2.5 seconds averaged across all 24 subjects (AUC = 0.9927 ± 0.0061). The *95%* confidence intervals for the FP_{Rate} values and TP_{Rate} values are shown in green and blue respectively. The chosen threshold (i.e. 14 times the median variance) is designated with a yellow square.

Discussion/Conclusion

Other groups, including researchers from our lab, have utilized load cells to detect the movement of individuals lying on the bed/mattress system [43-49]. However, the techniques used were either not clearly outlined or the eventual thresholds used for the parameters to distinguish movement from non-movement were not-expressly mentioned or are not generalizable. Therefore, building upon an approach previously designed in our lab, I developed a method for detecting movement based on the variance of the load cell data. I also systematically tested this method using a data set with known movement times in order to determine the optimal threshold (i.e. 14 times the median variance) and window length (i.e. L = 2.5 seconds) needed for the movement detection algorithm to function.

The development of the data set used to test the movement detection algorithm and determine the threshold and window length had a couple limitations. There was likely some error introduced by human bias when the ground truth movements were annotated. A concerted effort was also made to only annotate movements at the time periods when a movement was expected per the experiment protocol so there were some extraneous movements in the data set that were not annotated. It should also be mentioned that while the technique was tested using data sampled at 40 Hz, it is expected to function well for other sampling rates as the window length is dependent upon time duration in seconds and not the number of data points.

The developed movement detection algorithm did very well as is illustrated by the AUCs in table 6-1. In theory, since the threshold is individualized (i.e. 14 times the median variance estimated from each individual's own data) and not based upon an

absolute magnitude, the threshold should be generalizable across different individuals. However, this theory will need to be tested using a load cell data set with known movement time points that is separate from the data set used herein to determine the needed window length and threshold.

Chapter 7: Sleep Apnea Detection

Sleep Apnea Detection: Visual Scoring

Acknowledgement

The work presented in this section, with edits, was originally published in the *Journal of Sleep Research (2013)*.

Beattie, Z. T., Hayes, T. L., Guilleminault, C. and Hagen, C. C. (2013), Accurate scoring of the apnea–hypopnea index using a simple non-contact breathing sensor. Journal of Sleep Research, 22: 356–362. doi: 10.1111/jsr.12023

Motivation

The current clinical standard for diagnosing sleep apnea is an overnight sleep test or PSG test. During an overnight PSG test, several sensors are used to monitor the patient's respiration (e.g. nasal pressure, oral-nasal thermistor, chest belt, and abdominal belt) and blood oxygen levels (e.g. pulse oximeter). In order to ascertain the presence or severity of sleep apnea, a sleep technologist typically uses special software to view the signals collected during the PSG test. With 30 seconds to a couple of minutes worth of PSG signals displayed on the screen at a time, the technologist scrolls through the entire night of data and manually annotates each instance of an apneic event by looking for amplitude attenuations in the PSG breathing signals and blood oxygen desaturations.

This type of PSG analysis is frequently referred to as "visually scoring". The severity of sleep apnea is determined by the AHI[5] which is simply the number of apneic and hypopneic events divided by the total time in hours that the patient was asleep.

In order to initially test the efficacy of using the load cells to detect sleep apnea, I designed an experiment that yields comparable results as the standard test for sleep apnea. The following describes an experiment where I compared the traditional visual scoring of several overnight PSG tests to the visual scoring of the same data with replacement of all PSG breathing signals with load cell breathing signals.

Subjects

Forty-five patients from the Pacific Sleep Program sleep lab gave informed written consent to the study (OHSU Institutional Review Board eIRB 6308).

Setup

The load cell data for this study was collected from load cells that were placed under each of the 5 supports of a bed at the Pacific Sleep Program sleep lab (Portland, OR, USA). The load cell data was collected simultaneously with the overnight PSG data for each patient during their regularly scheduled sleep test.

Methods

PSG data was collected using Datalab, Rembrandt 9.0 (Embla 2008) and initially scored in accordance with current American Academy of Sleep Medicine (AASM) guidelines using Analysis Manager, Rembrandt 9.0 (Embla 2008). An experienced polysomnographic technologist used AASM rules for the scoring of AASM defined

[5] While typically not displayed, the units for index values such as the apnea-hypopnea index (AHI) or the respiratory disturbance index (RDI) are the number of events per hour.

Central apnea, Mixed apnea, Obstructive apnea, and Hypopnea [3]. The sum of scored apneas and hypopneas were divided by total sleep time to generate the *AHI-PSG*. Apneas (including central, mixed, obstructive) were scored when there was an amplitude reduction of 90% or greater for at least 10 seconds in the PSG breathing signals. Apneas were labeled as central when the amplitude reduction was associated with a lack of breathing effort as determined using the chest and abdomen belt and obstructive when effort was determined to still be present. Mixed apneas were scored when respiratory effort was initially absent but determined to be present at the end of the event. For determining hypopneas, an amplitude reduction of 30% in the PSG breathing signal that lasted at least 10 seconds and was associated with at least a 4% oxygen desaturation was required. In addition to scoring apneic events, the technologist also scored Respiratory Effort Related Arousals (RERA) defined by discernible reductions in airflow associated with arousal (i.e. patient awakenings) that did not meet criteria for other events. The total of these events were combined with the sum of apneas and hypopneas and divided by total sleep time to obtain the Respiratory Disturbance Index (*RDI-PSG*).

Apnea patients were then classified by their AHI as having negative ($AHI < 5$), mild ($5 \leq AHI < 15$), or moderate-severe ($AHI \geq 15$) apnea based on their PSG results. Fourteen records were selected for the negative group, 16 records were selected for the mild group, and 15 records were selected for the moderate-severe group (45 patients in total). The data for all 45 records were anonymized and converted to European Data Format (EDF). All PSG signal channels related to airflow or respiratory effort from each PSG record (nasal pressure, oral-nasal thermistor, chest belt, and abdominal belt) were replaced with load cell breathing signals. The load cell breathing signals were combined

with the usual PSG record (e.g. EEG, EKG, blood oxygenation, etc.) to create a load cell scoring montage (LC montage) (see figure 7-1 [59]). The load cell breathing signals included a band passed *CoP* signal in the *Y* direction (i.e. long axis if the bed) and an "all sum[6]" signal that consisted of the band pass filtered result of simply summing the output of all the load cells together. The band pass filter had a pass band of 0.077 Hz to 1 Hz.

The same scorer subsequently scored blindly the integrated load cell record at least 5 months after scoring the initial PSG, using Analysis Manager Rembrandt 9.0 (Embla 2008). Standard AASM respiratory event scoring rules for routine scoring were applied for duration of event and percentage reduction in the load cell (*LC*) tracing excursion. A 30% to 90% reduction in the *LC* excursion for greater than 10 seconds associated with a 4% desaturation was scored as obstructive hypopnea (*OH-LC*). A reduction of the *LC* excursion of 90% or greater for more than 10 seconds was scored as obstructive apnea (*OA-LC*). Absence of *LC* excursion for greater than 10 seconds duration was scored as central apnea (*CA-LC*). Load cell examples of actual respiratory events from each category (*OH-LC*, *OA-LC*, & *CA-LC*) scored by the technologist are shown in figure 7-2 (originally published in [59]). *AHI-LC* was determined from the number of events (*OH-LC*, *OA-LC*, and *CA-LC*) per hour of sleep. Discernible reductions in the load cell breathing signal excursion for 10 seconds or greater duration associated with an EEG arousal (i.e. awakening) that did not meet criteria for other events were scored as a RERA (*RERA-LC*). The number of *RERA-LC* was summed with the combined number of *OH-LC*, *OA-LC*, and *CA-LC*, and this overall total was divided by total sleep time in order to calculate the *RDI-LC*.

[6] The load cell "all sum" signal was included in the LC montage as a visual indication of gross movement picked up by the combined load cell signals.

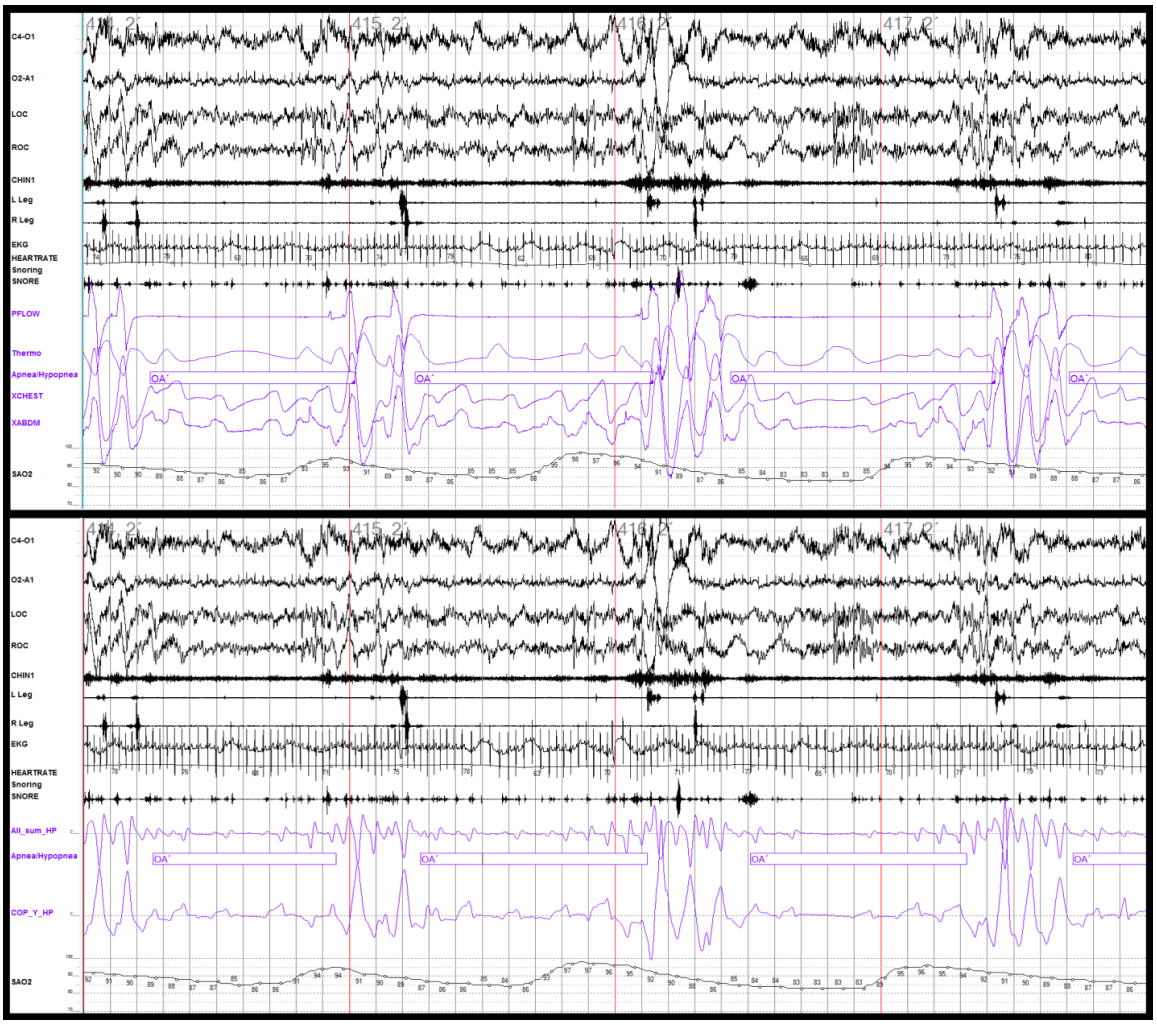

Figure 7-1. Screen shots comparing the scoring montages used for scoring with typical PSG signals (upper) and with load cell breathing signals (lower). The screen shots were taken from the same 120 seconds for both scoring results from one patient. The nasal pressure, oral-nasal thermistor, chest belt, and abdominal belt are colored purple in the PSG scoring montage (upper), and the load cell breathing signals are similarly colored purple in the load cell scoring montage (lower). The load cell tracing "*All_Sum_HP*" is the summation of all the load cells, and the "*COP_Y_HP*" is the center of pressure load cell signal. The purple, horizontal boxes in both cases indicate the locations of scored respiratory events.

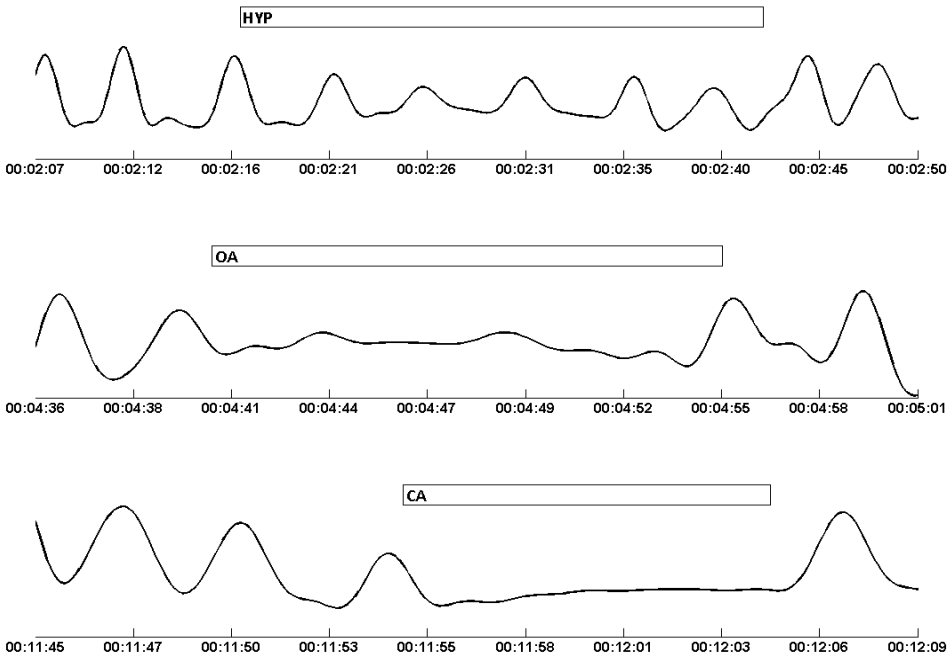

Figure 7-2. Segments of the load cell breathing signal from a single patient illustrating the scoring of respiratory events using the load cell trace. (Upper) A scored hypopnea showing a slight reduction in the excursion of the load cell signal. (Middle) A scored obstructive apnea showing a major reduction in the excursion of the load cells signal. However, some LC excursion appears to still be present suggesting breathing effort may still exist. (Lower) A scored central apnea showing a complete absence of excursion in the load cell signal.

Analysis

Differences between AHI severity group characteristics (specifically age, BMI, and sex) were examined using a multivariate analysis of variance (MANOVA) with the AHI group as the fixed effect. The dependence of the *LC* scoring accuracy on BMI was examined using linear regression and a *t* statistic to test whether resulting slope was different from 0. The log transformed absolute difference between PSG scoring and load cell scoring for both AHI and RDI (i.e. scoring error) was regressed against BMI for this analysis. Comparison of the traditional PSG to *LC* scoring was analyzed using linear correlation, a paired t-test, and 95% confidence intervals for the difference between the two scorings. Finally, the accuracy of scoring the AHI severity of patients using the load cell montage was assessed using sensitivity and specificity.

Results

The overall demographic information and the apnea class specific demographics are contained in table 7-1. There were significant differences in demographics between the groups (p = 0.02). Post-hoc tests revealed that this was due primarily to the younger age of the low AHI group compared to the high AHI group.

Table 7-1.
Demographic information for all patients. Values are reported as mean ± standard deviation.

	Gender (M/F)	Age (years)	BMI (kg/m^2)
AHI < 5	6/8	43.9 ± 13.6*	29.8 ± 7.1
5 ≤ AHI <15	10/6	52.4 ± 13.2	33.4 ± 6.5
AHI ≥ 15	11/4	56.1 ± 13.8*	33.7 ± 6.0
Overall	27/18	51.0 ± 14.2	32.3 ± 6.6

The intra-class correlation coefficient (ICC) for AHI was 0.97 with a 95% confidence interval of [0.95 0.98]; the ICC for RDI was 0.85 with a 95% confidence interval of [0.66 0.93]. The AHI estimated by PSG was on average only 0.4 larger than that estimated using load cells, which was not significant (t_{44} = 0.37, p = 0.71 with a 95% confidence interval of [-1.67 2.42]). In contrast, the RDI estimated from the *LC* montage was on average 7.7 greater than that obtained using the PSG montage; this difference was significant (t_{44} = -3.89, p <0.001) with a 95% confidence interval of [-11.7 -3.70]. Although there were differences in the absolute estimates of AHI and RDI, the PSG and *LC* scoring were strongly correlated for both AHI and RDI (Pearson's correlation coefficient 0.97 and 0.89 respectively). Least square linear fits for AHI and RDI comparing PSG and *LC* scoring are shown in figure 7-3. Agreement between the two scoring modalities is shown using Bland-Altman plots in figure 7-4. Both figures were originally published in [59].

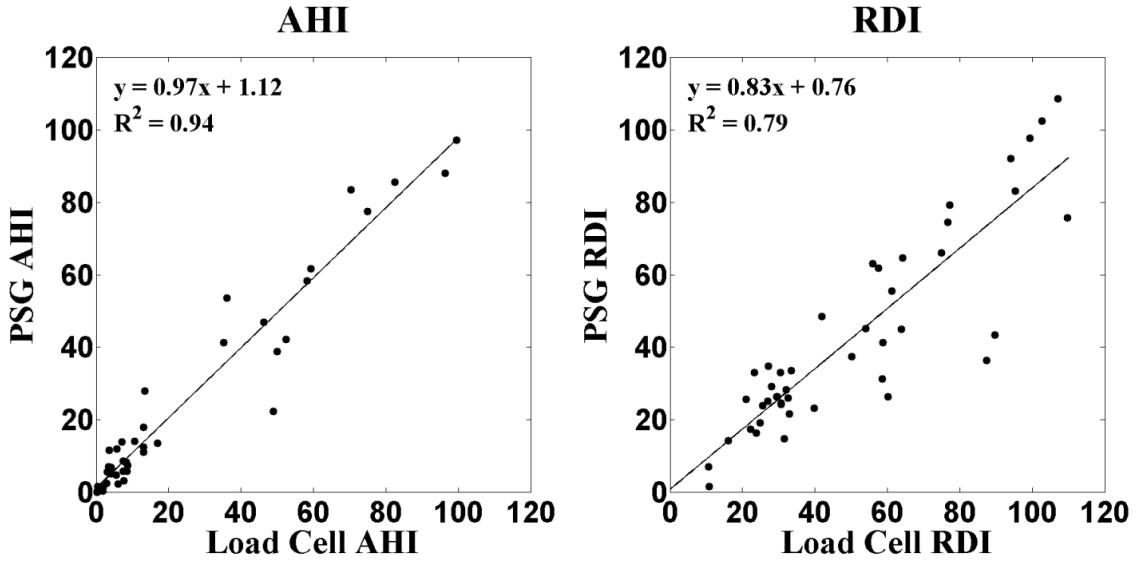

Figure 7-3. Linear least squares regression plots for *AHI-LC* vs. *AHI-PSG* and *RDI-LC* vs. *RDI-PSG*.

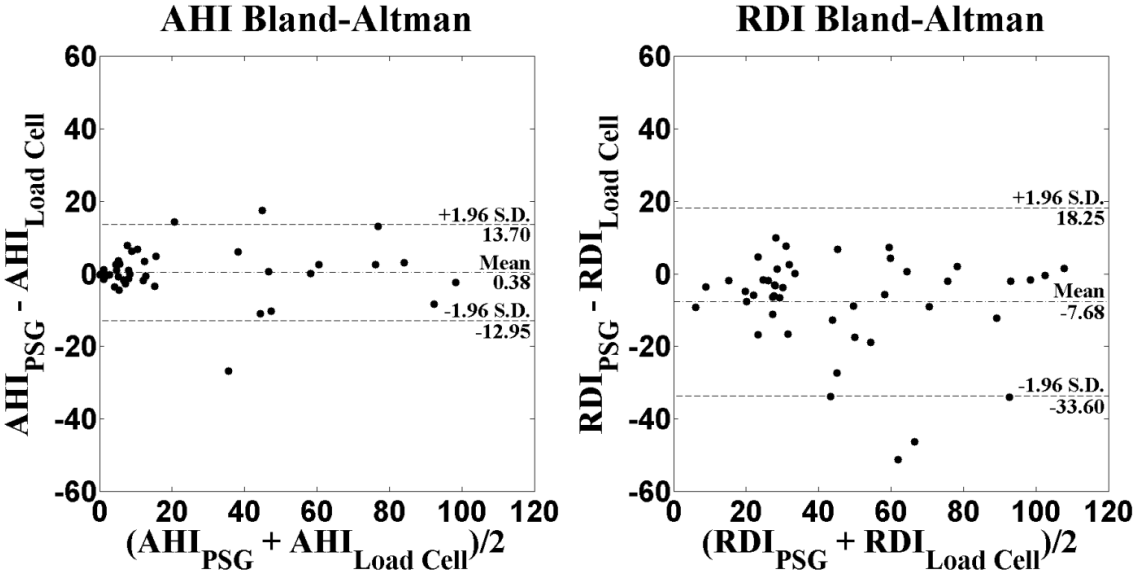

Figure 7-4. Bland-Altman plots for visualization of the agreement between the PSG and load cell scoring of AHI and RDI.

Table 7-2.
Sensitivities, specificities, and positive likelihood ratios (LR+) of using *AHI-LC* to detect sleep apnea for several AHI cutoffs.

	Sensitivity	Specificity	LR+
AHI ≥ 5	0.84	0.79	4
AHI ≥ 15	0.87	0.97	29
AHI ≥ 30	1.00	0.97	33

The sensitivities and specificities of *AHI-LC* to detect sleep apnea for various AHI cutoffs are contained in table 7-2. The positive likelihood ratios for each AHI cutoff are also presented in table 7-2. Our ability to detect severe apnea in particular was very high, with 100% sensitivity and 97% specificity, and with a positive likelihood ratio of 33.

Discussion/Conclusion

This study showed that using unobtrusive load cells under the bed to replace the four standard respiratory leads for polysomnography provides an accurate measure of AHI. The AHI using load cell respiration tracings was highly correlated with the standard montage. Finally, the load cell AHI was also highly predictive of the presence of sleep apnea particularly for AHIs greater than 15. Our success at detecting mild apnea is encouraging, and we believe load cell performance will improve with our future work to clarify how specific features in the load cell excursion correlate with various types of respiratory events.

In order to control for inter-rater variability, we chose to have both the standard PSG records and the *LC* montages scored by the same registered polysomnographic technologist. Thus, each PSG record was scored twice by the same individual. At least five months elapsed between the original scoring of the standard PSG record and the anonymized scoring of the *LC* montage. Consequently, between the 1st and 2nd scoring of each record the technologist scored over 300 PSG records, and prior to scoring the LC

montage the records were anonymized, further mitigating any chance that the technologist would be influenced by recollection of the 1st scoring. Thus, there could be no recall of raw data appearance or blinded record labels.

As expected, *AHI-LC* did very well compared to *AHI-PSG*. We were not surprised to find that load cell scoring tended to be less specific when scoring RERA compared to hypopnea and apnea. RERA scoring has been shown to have lower inter-scorer reliability, to be less sensitive when based on nasal pressure and respiratory inductance plethysmography [5], and is best performed with esophageal manometry, which was not used in this protocol. We are encouraged by our success at detecting respiratory effort related arousal. Though improvement is needed, our further work analyzing feature changes specific to flow reductions with arousal and RERA may permit a non-invasive method for detecting patients with upper airway resistance syndrome that have historically required more invasive tests with esophageal manometry [67]. There has been great interest in finding non-invasive ways to measure RERAs and flow limitations. Other groups have worked on novel methods for identifying respiratory effort [68]. Flow limitation during total sleep time is also of interest as flow limitation may impair sleep during each breath rather than with distinct scorable events [67, 69].

The load cell breathing signal comes from mass movement; therefore it may actually be more indicative of respiratory effort. However, it could also be argued that the load cells susceptibility to non-respiratory related movement could have contributed to more RERAs being scored. Similarly, since the load cells are detecting mass movements, we were concerned that higher BMI might make changes in the load cell breathing signal less apparent. In fact, the AHI scoring error (i.e. the difference between *AHI-PSG* and

AHI-LC) increased significantly with increasing BMI (t_{43} = 2.06, p = 0.05), although only 9% of the variance in the AHI scoring error was accounted for by BMI. There was no dependence (t_{43} = 1.09, p = 0.28) on BMI found for RDI scoring error.

The rules used in this study to identify apneic events were adapted from AASM standards for scoring events using flow and thermistor tracings. As the load cell signal originates from visceral mass movements caused by breathing as opposed to actually measuring air flow, it seems obvious that different standards fine tuned to the nuances of the load cell signals themselves would improve the accuracy of using the load cell tracings. Future work can isolate morphologic changes that improve event type specificity and should include an event by event analysis to develop load cell specific scoring features. We have previously reported successful discrimination of obstructive apnea from central apnea [70]. Discriminating central hypopnea from obstructive hypopnea may be aided by observation of retention of the normal rounded nasal pressure excursion, absence of paradoxical respiratory effort, absence of snoring, decreased intercostal EMG activity and/or less negative pressure swings on esophageal manometry when available. While we demonstrated that central apnea is reliably identified with load cells in previous work, we believe our future work at isolating the unique morphologic changes within the load cell signal will help identify reduced effort in more subtle events like central hypopnea and help discriminate these from obstructive hypopnea or RERA. In the future, we also plan to refine our ability to detect RERAs with the load cell signals, to explore the use of load cells to identify respiratory effort.

We have demonstrated the feasibility of using load cells installed under the bed to detect sleep apnea. Other unobtrusive devices have been proposed for monitoring sleep

apnea. Thermal infrared imaging [71], the static charge sensitive bed [72], a sheet array of pressure sensors [73], and a pressure sensitive pad [74] have all been studied. However, all of these devices have their limitations and are not as versatile as the load cell system. The infrared camera in [71] must have a clear view of the patients face to detect respiration and likely will not work if the subject turns away from the camera or covers their mouth/nostrils in some manner. The static charge sensitive bed [72] is placed under the mattress and the pressure sensitive sheet and pad [73, 74] are placed on top of the mattress. These all alter the sleeping environment and run the risk of undesirable interaction with the patient (e.g. sensor movement, becoming unplugged, etc.) which would make long-term, in-home monitoring difficult. The load cell system is completely out of the way and can detect the breathing from the patient lying anywhere on the bed. Calibrated load cells can also be used to monitor a patient's weight as well as the lying position of an individual lying on the bed [41]. Monitoring a patient's weight and lying position is important because sudden weight changes may indicate fluid retention due to heart issues [75] and many individuals with sleep apnea have more apneic events when lying on their back as opposed to their side [76-78]. The pressure sensitive [73] sheet may be able to detect lying position but not the patient's weight and the other sensors [71, 72, 74] are likely incapable of either.

Load cell data is easy to collect and does not require any sensors in contact with the patient. Current flow and effort leads during attended PSG are obtrusive and disruptive to sleep. Unlike standard polysomnography leads, the load cells do not become displaced during the night, resulting in more reliable signals and far superior signal integrity for serial night collections such as might be seen during unattended home

monitoring. While the study presented herein was performed in a sleep lab, we will soon be placing similar devices in patients' own homes for long-term, unobtrusive monitoring while they sleep in a familiar environment.

Sleep Apnea Detection: Automatic Scoring

Motivation

Using the load cell breathing signal to detect sleep apnea shows great promise in the sleep lab setting. I have shown that replacing several obtrusive breathing sensors with the load cell system is feasible during overnight sleep studies in the lab. Nonetheless, with the amount of individuals suspected of having sleep apnea in the United States alone [4], the often long wait times or limited access to overnight sleep studies [10], and the high cost of such sleep studies, a deployable solution to test/monitor individuals while they sleep in their own homes would be beneficial. The load cell system could be fitted to patient's beds permitting them to be monitored while they sleep in their own homes. This could allow for the triage of patients into the sleep lab, the possible diagnosis of individuals with severe sleep apnea, and/or track the progress of patients over time after the initial diagnosis of sleep apnea. However, it would be unreasonable to assume that each night of load cell breathing signal data collected could be visually scored by a sleep technologist due to the sheer amount of data that would be produced.

I have previously shown that load cell data can be used to differentiate between manually selected segments of normal breathing and apneic breathing [70]. Since then I have developed more reliable techniques to estimate the load cell breathing signal (*CoP*) and detect individual breaths allowing for more accurate breathing amplitude calculations. I have used these techniques to test the feasibility of detecting sleep apnea from continuous load cell recordings across the entire night that do not rely on predefined segments of data. In this section, I describe an algorithm that I developed as a first pass

attempt to automatically process the load cell data collected while an individual sleeps on the bed and produce an AHI representing the severity of sleep apnea exhibited by the patient. The predicted AHIs from this initial algorithm that uses only load cell data were compared to the corresponding clinical AHIs scored by sleep technologists utilizing standard PSG signals.

Subjects

The subjects for this study were recruited from the Oregon Health & Science University (OHSU) sleep lab and the Pacific Sleep Program (PSP) sleep lab. Fifteen patients from the OHSU sleep lab participated in this study (an IRB was deemed unnecessary by the OHSU Institutional Review Board). Eighty-nine patients from the Pacific Sleep Program sleep lab gave informed written consent to the study (OHSU Institutional Review Board eIRB 6308). Forty-five subjects were female and 59 were male. The average age was 49.3 ± 14.0 years and the average BMI was 32.8 ± 7.1 kg/m^2.

Setup

The load cell data from the OHSU sleep lab was collected from load cells placed under each of the 6 supports of a king sized bed. At the PSP sleep lab, load cell data for this study was collected from load cells that were placed under each of the 5 supports of a queen sized bed. At each sleep lab the load cell data was collected simultaneously with the overnight PSG data for each patient during their regularly scheduled sleep test.

Methods

Clinical AHI

For overnight sleep studies at both the OHSU and PSP sleep labs, the PSG data was scored by an experienced polysomnographic technologist employed at the corresponding sleep lab. In both cases, apneic events were scored in accordance with current AASM guidelines. Apneas were scored when there was an amplitude reduction of 90% or greater for at least 10 seconds in the PSG breathing signals, and hypopneas were scored when there was an amplitude reduction of 30% in the PSG breathing signal that lasted for at least 10 seconds and was associated with at least a 4% oxygen desaturation as measured by a pulse oximeter during the PSG test. The severity of sleep apnea presented by each patient was gauged using the AHI. The sum of scored apneas and hypopneas were divided by total sleep time to generate the *AHI-PSG*. In addition to scoring apneic events, the technologist also scored RERAs defined by discernible reductions in airflow associated with arousal (i.e. patient awakenings) that did not meet criteria for other events. The total number of these events were combined with the sum of apneas and hypopneas and divided by total sleep time to obtain the *RDI-PSG*.

Load Cell AHI

Several steps were involved to develop the algorithm used to automatically calculate the severity of sleep apnea (i.e. $AHI\text{-}LC_{AUTO}$ and $RDI\text{-}LC_{AUTO}$) using only the load cell data collected as a patient slept overnight on a bed with load cells placed under each support. First, the load cell data had to be conditioned or prepared so that relevant information about the load cell breathing signal could be extracted. Then features from

the load cell breathing signal were estimated. Finally, a linear model used to combine the various load cell features into a prediction of sleep apnea severity (i.e. $AHI\text{-}LC_{AUTO}$ and $RDI\text{-}LC_{AUTO}$) was trained and tested using the corresponding clinically estimated *AHI-PSG* and *RDI-PSG*.

Signal Conditioning

The load cell data collected from each overnight sleep test were first trimmed to only include the period from the time the patient fell asleep to the time when the lights were turned on indicating the end of the sleep test. The low pass filtered center of pressure (CoP_y) signal along with the corresponding peaks and troughs of CoP_y representing the transitions from inspiration to expiration were then derived from the load cell data following the procedures described in the analysis section of chapter 5. The only difference was that movements from the overnight load cell data were automatically detected by summing together the output from each load cell (LC_{sum}) and utilizing the protocol developed in chapter 6 with the exception that the load cell sampling rate was 10 Hz and not 40 Hz. Periods when the patient was estimated to be out of the bed (e.g. visiting the restroom) were grouped with the segments estimated to be movement and were subsequently removed. Out-of-bed segments were calculated using the K-means unsupervised clustering technique [79]. The details of this approach are described in [42] which outlines how differences in the total weight on the bed – as estimated using the summed output from all the load cells (LC_{sum}) - are used to predict periods when the patient is either in or out-of bed. Ultimately, assuming that the peaks and troughs of the CoP_y breathing signal represent the maximum (peaks) and minimum (troughs)

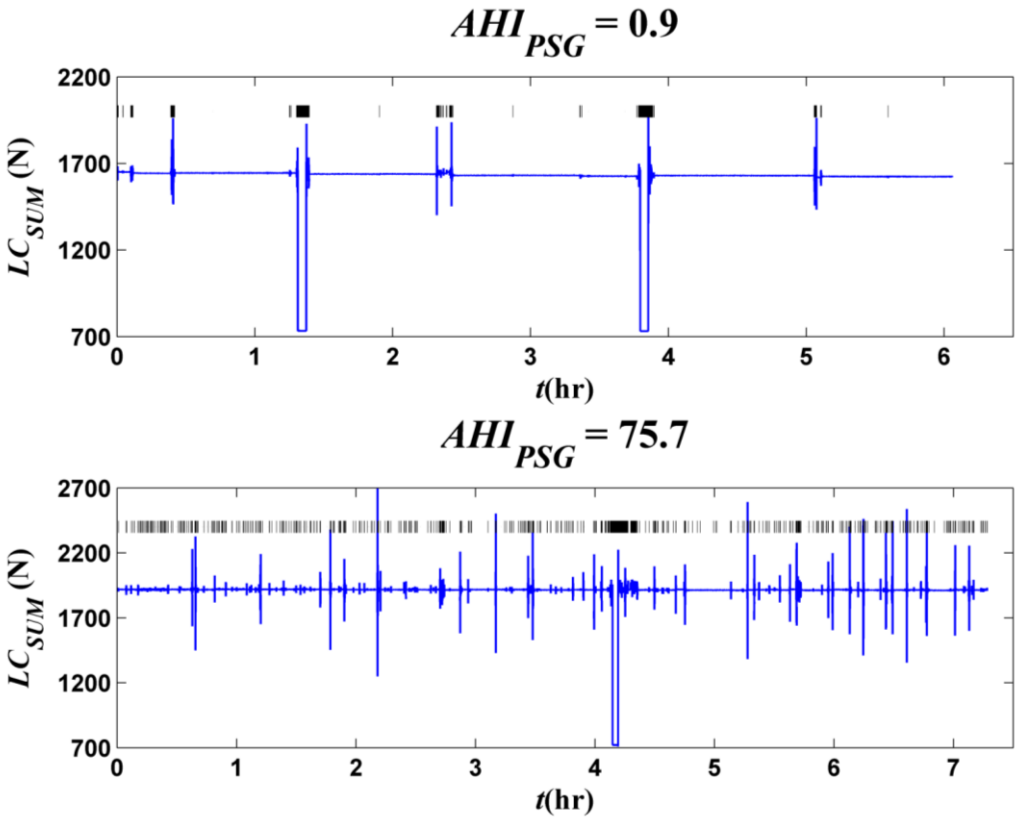

Figure 7-5. Load cell data collected during an overnight sleep test for a patient without sleep apnea (upper) and a patient with severe sleep apnea (lower). The summed output from each load cell placed under the bed (LC_{SUM}) is shown in blue. Movements detected using LC_{SUM} are illustrated in black above the load cell data. Significantly more movement was present for the patient with sleep apnea.

displacement of the mass moved during a breathing cycle, the breathing amplitude was estimated by calculating the difference between the peaks and troughs in the CoP_y signal.

Feature Extraction

Three features were calculated from each night of load cell data. The first feature was selected to represent the overall amount of patient movement detected during the night. Experience has shown that individuals with sleep apnea tend to have restless sleep (see figure 7-5) which is likely caused by small awakenings that frequently follow apneic events [80]. This first feature or movement index (*MI*) was calculated using:

$$MI = \frac{\#\,Movements}{T_{LC}} \tag{7.1}$$

where *#Movements* is the number of detected movement and/or out of bed segments and T_{LC} is the number of hours of load cell data collection.

Additional features were selected based on the fact that the load cell breathing signal is tracking the movement mass caused by the diaphragm during breathing. The theory is that when the airway into the lungs is occluded during an apneic event, the diaphragm is now pulling against a more negative pressure inside the lungs and subsequently will move less. This should lead to a gradual or sudden decrease in the amplitude of the load cell breathing signal. Eventually, as the patient increases their breathing effort during the apneic event, the diaphragm will increasingly begin to displace the mass tracked by the load cells more until the apneic event is terminated. It is also possible that once the airway is open there could be an increase in breathing amplitude above normal due to the recently heightened breathing effort. The second and third features were designed to capture these constant breathing amplitude changes that are hypothesized to frequently occur in individuals with sleep apnea.

The second feature was selected to capture variance in the breathing amplitude. The exact method used for estimating the breathing amplitude on a sample-by-sample basis from the load cell CoP_y signal for this feature is outlined in figure 7-6. The variance in the load cell breathing amplitude across the entire night was estimated using the coefficient of variation (*cV*) for non-overlapping windows:

$$cV(j) = \frac{\sqrt{\frac{1}{n-1}\sum_{i=1}^{n}\left(LC_{AMP}^{i} - \overline{LC}_{AMP}\right)^2}}{\frac{1}{n}\sum_{i=1}^{n} LC_{AMP}^{i}} \tag{7.2}$$

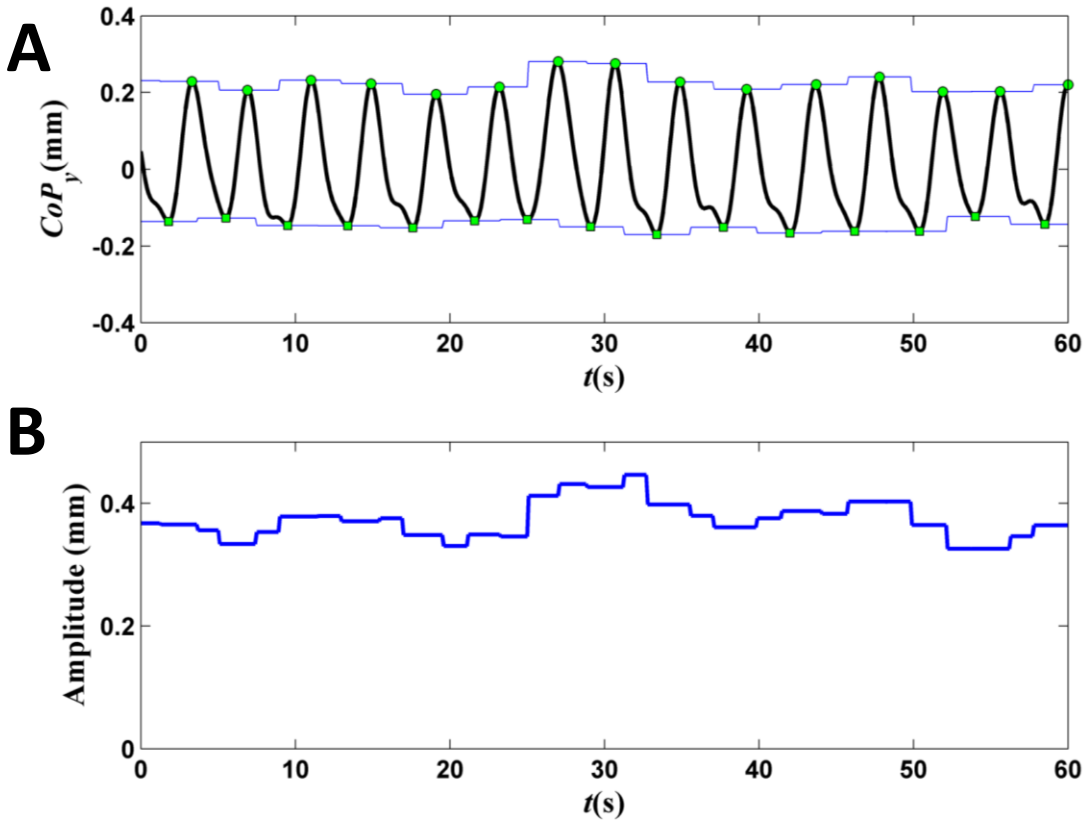

Figure 7-6. (**A**) The load cell breathing signal (CoP_y) is shown as the black trace with detected peaks (green circles) and detected troughs (green squares). A peak and trough value was estimated for each individual data point in the CoP_y signal (light blue traces) using nearest neighbor interpolation from the actually detected peaks and troughs (green circles and squares). (**B**) The breathing amplitude (dark blue trace) was estimated for every sample or data point in the CoP_y breathing signal by subtracting the interpolated trough values from the interpolated peak values.

where *cV(j)* is the coefficient of variation for the j^{th} window, LC_{AMP} is the amplitude of the load cell breathing signal, and *n* is the number of amplitude estimates contained in the j^{th} window. It was theorized that the cV would be higher in individuals with sleep apnea (see figure 7-7), and the second feature (*cV%*) is defined as the ratio of time that the *cV* of the load cell signal is above a defined threshold (thr_{cV}):

$$cV\% = \frac{\left(\#cV(j) > thr_{cV}\right) wn_{cV}}{t_{LC}} \tag{7.3}$$

where wn_{cV} is the window size is seconds used to calculate each *cV(j)* and t_{LC} is the total recording time in seconds.

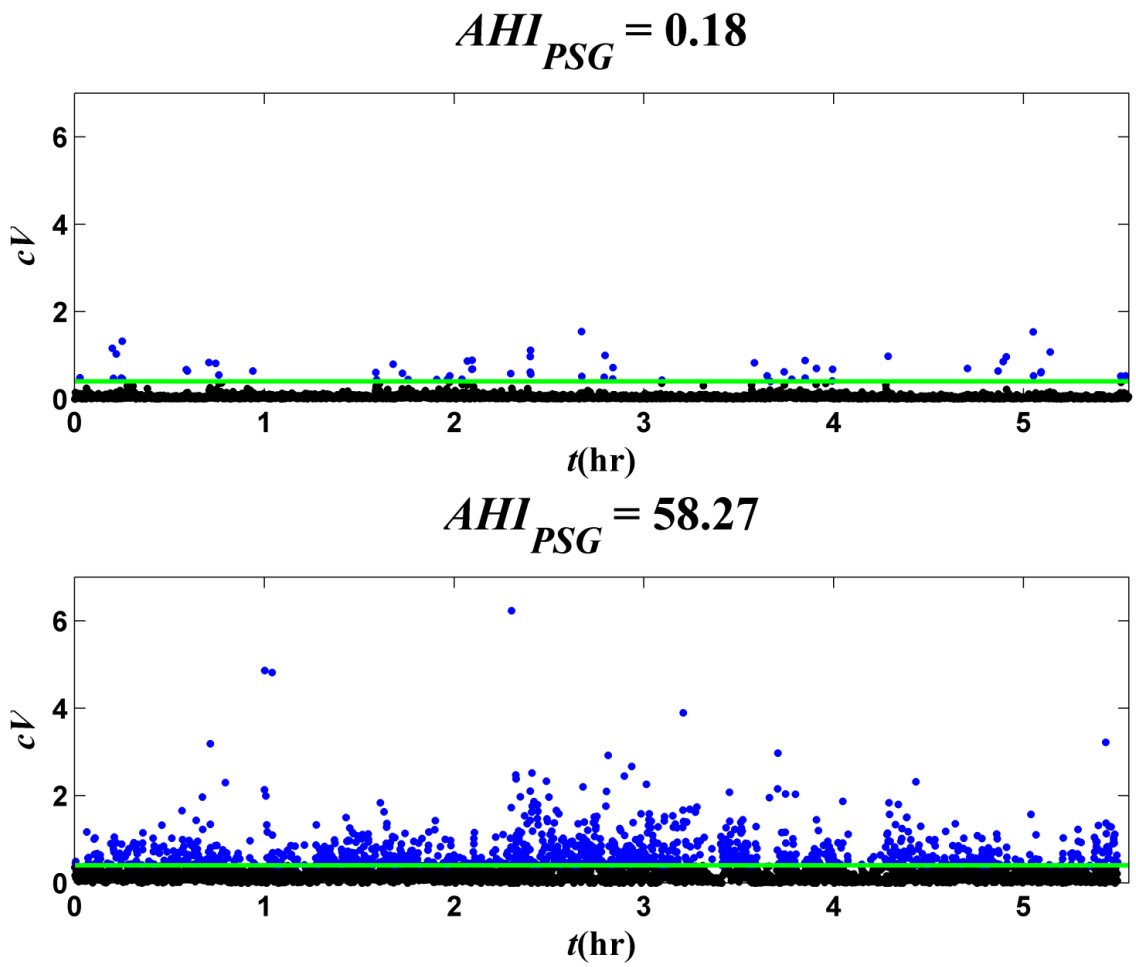

Figure 7-7. The coefficient of variation (*cV*) calculated from non-overlapping five second windows of load cell derived breathing amplitude. The load cell data was collected during an overnight sleep study for an individual without sleep apnea (upper) and a patient with sleep apnea (lower). The green horizontal line represents a threshold of 0.4. The *cV* data points below this threshold are shown in black and *cV* data points above the threshold are shown in blue. The patient with sleep apnea exhibits many more segments of high breathing amplitude variability than the patient without sleep apnea.

The third feature was developed to estimate the number of times per hour that the amplitude of the load cell breathing signal (i.e. CoP_y) decreased significantly during the course of the overnight sleep study. This feature was also used to capture the continual decreasing and increasing of load cell breathing amplitude that is often observed during apneic events (see figure 7-8). In order to calculate the third feature, the amplitude of the load cell breathing signal was estimated on a breath-by-breath basis using the difference

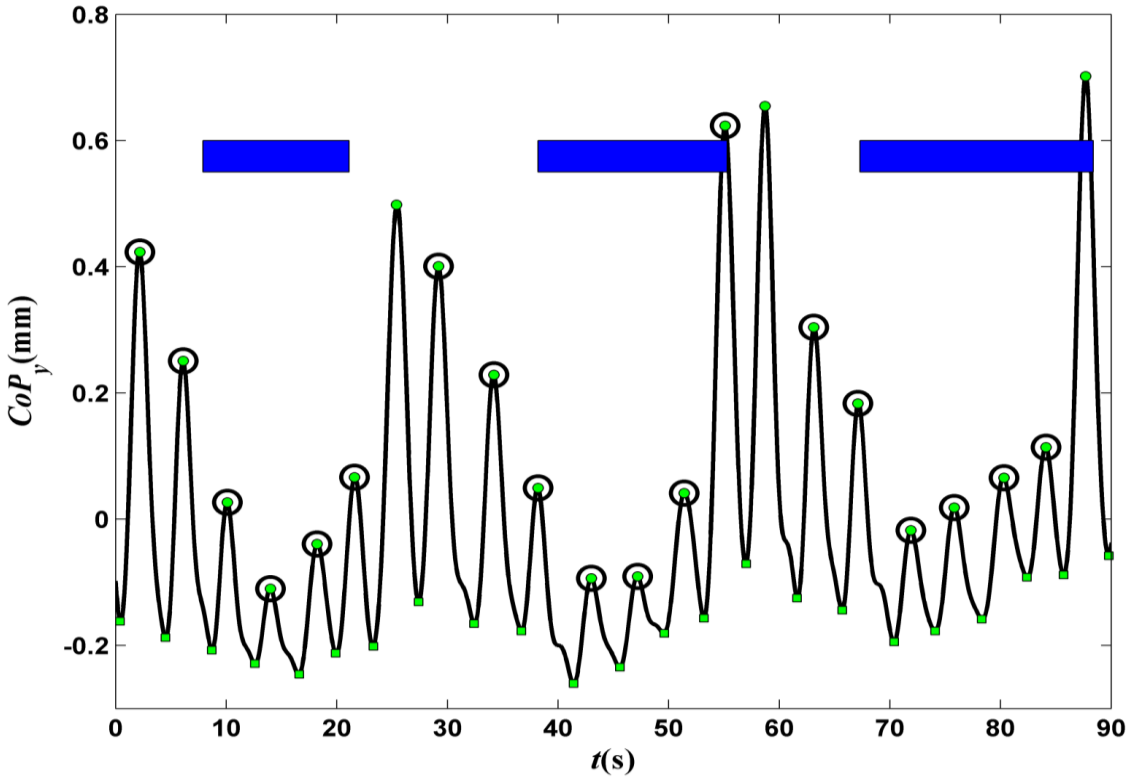

Figure 7-8. Ninety seconds of load cell breathing signal (black trace) collected from a patient during an overnight sleep study illustrating the decreasing followed by increasing breathing amplitude often observed in the load cell data during apneic/hypopneic events. Automatically detected peaks and troughs used for estimating the breathing amplitude on a breath-by-breath basis are displayed as green circles and green squares respectively. The peaks of breaths automatically determined to be part of a disordered breathing event are encased in black circles. Of note, is the peak at about 55 seconds which appears to represent a breath of significant amplitude. This peak was considered a continuation of the crescendo effect at the end of the disordered breathing event due to its amplitude - estimated as the difference between the peak value and the following trough value - being less than the following breath's amplitude at about 60 seconds estimated the same way. As a reference, time periods that were visually scored as apneas/hypopneas by a sleep technologist using the LC montage (see the "Sleep Apnea Detection: Visual Scoring" section) are presented as horizontal blue lines.

between peak/trough pairs in the load cell CoP_y signal. The amplitude of each breath was calculated twice. Once using the difference between the peak value of the breath and the following trough value and once using the difference between the same peak value of the breath and the previous trough value. The following methodology utilized both amplitude estimates independently to detect disordered breathing events and then combined the resulting disordered breathing events found using both estimates.

Disordered breathing events (i.e. apneas or hypopneas) were identified by first locating and marking individual breaths that had amplitudes that were less than a defined percentage (*AMP%)* of the median breathing amplitude that was estimated over the previous *N* seconds. Second, the breathing amplitudes of the individual breaths directly before any of these marked breaths were searched for a decrescendo effect in the breathing amplitudes. In other words, any breath that immediately preceded the originally marked breath that had a breathing amplitude less than the breath directly before it was marked as part of the disordered breathing event. Then, in a similar manner, the breathing amplitudes of the individual breaths directly after any of the originally marked breaths were searched for a crescendo effect in the breathing amplitudes (i.e. any breath with an amplitude larger than the breath directly after it was included in the disordered breathing event.). Finally, the third feature or disordered breathing index (*DBI*) was calculated using

$$DBI = \frac{\#Breath_{Disordered}}{T_{LC}} \tag{7.4}$$

where $\#Breath_{Disordered}$ is the number of disordered breathing events identified that met a minimum time duration constraint (t_{apnea}) and T_{LC} is the number of hours of collected load cell data after movement and/or out of bed periods have been removed.

Model Training/Testing

The three features defined were utilized to automatically estimate sleep apnea severity (i.e. $AHI\text{-}LC_{AUTO}$) using a linear model with constant coefficients.

$$AHI_{LC\ AUTO} = \beta_1 + \beta_2\left(MI\right) + \beta_3\left(cV\%\right) + \beta_4\left(DBI\right) \tag{7.5}$$

A leave one out method was used to iteratively train and test the model [79]. For each iteration, features calculated from the load cell data for one patient were held out. Then linear regression was used to estimate the model coefficients ($\beta_{1\text{-}4}$) by fitting the features from the remaining 103 patients to their corresponding *AHI-PSG* in a least-squares sense. The *AHI-LC*$_{AUTO}$ was estimated for the patient whose data was held out using these model coefficients and the features estimated for this patient. The whole process was repeated to estimate an *AHI-LC*$_{AUTO}$ for each of the 104 patients. An *RDI-LC*$_{AUTO}$ was also predicted for each of the 104 patients in the same manner with the exception that the model coefficients ($\beta_{1\text{-}4}$) were estimated utilizing *RDI-PSG*.

For the *cV%* and *DBI* features various thresholds and window sizes were initially unknown. In order to maximize the effectiveness of the *cV%* feature, the threshold (thr_{cV}) for distinguishing high variability from low variability and the size (in seconds) of the non-overlapping windows (wn_{cV}) needed to be chosen. For the *DBI* feature, the *N* previous seconds used to calculate the median breathing amplitude reference and the percentage of this reference amplitude (*AMP*%) that indicated a significant breathing amplitude attenuation needed to be found. Also, the minimum time duration (in seconds) of disordered breathing segments (t_{apnea}) needed for the segment to be considered an apnea or hypopnea had to be chosen. Therefore, a range of values for each parameter was investigated:

$$thr_{cV} = [0.1, 0.2, 0.3, 0.4, 0.5, 0.6, 0.7, 0.8, 0.9, 1]$$
$$wn_{cV} = [5, 10, 20, 30, 40, 50, 60, 70, 80, 90, 120]$$
$$N = [30, 60, 90, 120]$$
$$AMP\% = [10, 30, 50, 70, 90]$$
$$t_{apnea} = [5, 10,15, 20]$$

and an exhaustive search was carried out across every possible combination of these parameters in order to discover the combination that optimized the estimation of *AHI-LC$_{AUTO}$* and *RDI-LC$_{AUTO}$*.

Analysis

The combination of parameters (i.e. *thr$_{cV}$*, *wn$_{cV}$*, *N*, *AMP%*, and *t$_{apnea}$*) that resulted in the highest coefficient of determination (R^2) and lowest mean squared error (*mse*) were chosen when using *AHI-PSG* as the ground truth reference. R^2 was calculated using:

$$R^2 = \frac{\sum\left(AHI_{PSG} - AHI_{LC_{AUTO}}\right)^2}{\sum\left(AHI_{PSG} - \overline{AHI}_{PSG}\right)^2} \tag{7.6}$$

where $\overline{AHI}_{PSG}$ is the mean of *AHI-PSG*, and *mse* was calculated using:

$$mse = \frac{1}{n-4}\sum\left(AHI_{LC_{AUTO}} - AHI_{PSG}\right)^2 \tag{7.7}$$

where (*n* - 4) is the number of *AHI-LC$_{AUTO}$* minus the number of coefficients in the linear model shown in 7.5. The same method for choosing optimal parameters was utilized when using *RDI-PSG* as the ground truth method.

Comparison of *AHI-PSG* and *RDI-PSG* to *AHI-LC$_{AUTO}$* and *RDI-LC$_{AUTO}$* respectively was analyzed using paired t-tests with 95% confidence intervals for the difference between the two scorings. Bland-Altman plots were used to visually compare the results. Finally, the ability of the automatic scoring algorithm using the load cell data to detect sleep apnea was assessed using ROC curves. The sensitivities and specificities for detecting sleep apnea using *AHI-LC$_{AUTO}$* at various thresholds were calculated. Three *AHI* cutoff levels were considered for defining overnight sleep tests as being positive for sleep apnea: (*AHI-PSG* $\geq$ 5, *AHI-PSG* $\geq$ 15, and *AHI-PSG* $\geq$ 30). The sensitivities and

specificities for detecting sleep apnea using $RDI\text{-}PSG_{AUTO}$ were also calculated using three RDI cutoff levels for positive sleep apnea tests ($RDI\text{-}PSG \geq 15$, $RDI\text{-}PSG \geq 30$, and $RDI\text{-}PSG \geq 60$).

Results

The optimal combination of parameters when comparing the automatic scoring algorithm to *AHI-PSG* was ($thr_{cV} = 0.4$, $wn_{cV} = 5$ *s*, $N = 30$ *s*, $AMP\% = 50\%$, and $t_{apnea} = 10$ *s*). The optimal combination when comparing to *RDI-PSG* was ($thr_{cV} = 0.7$, $wn_{cV} = 5$ *s*, $N = 120$ *s*, $AMP\% = 50\%$, and $t_{apnea} = 10$ *s*). Tables 7-3 and 7-4 contain the average linear model coefficients with corresponding 95% confidence intervals used to estimate $AHI\text{-}LC_{AUTO}$ and $RDI\text{-}LC_{AUTO}$ respectively.

Table 7-3
Linear model coefficients used to estimate $AHI\text{-}LC_{AUTO}$.

Model Coefficients	Mean	Confidence Interval (95%)
β_1	-12.746	[-12.799 -12.692]
β_2	0.389	[0.387 0.392]
β_3	-195.198	[-196.121 -194.276]
β_4	2.159	[2.154 2.164]

Table 7-4
Linear model coefficients used to estimate $RDI\text{-}LC_{AUTO}$.

Model Coefficients	Mean	Confidence Interval (95%)
β_1	3.133	[3.080 3.187]
β_2	0.565	[0.563 0.567]
β_3	-276.584	[-277.461 -275.706]
β_4	1.743	[1.739 1.747]

Direct comparison of $AHI\text{-}LC_{AUTO}$ vs. *AHI-PSG* and $RDI\text{-}LC_{AUTO}$ vs. *RDI-PSG* are shown in figure 7-9 with the corresponding R^2 values. Comparison of the difference between the automatic scoring of the load cell data and the PSG scoring are shown in the Bland-Altman plots contained in figure 7-10.

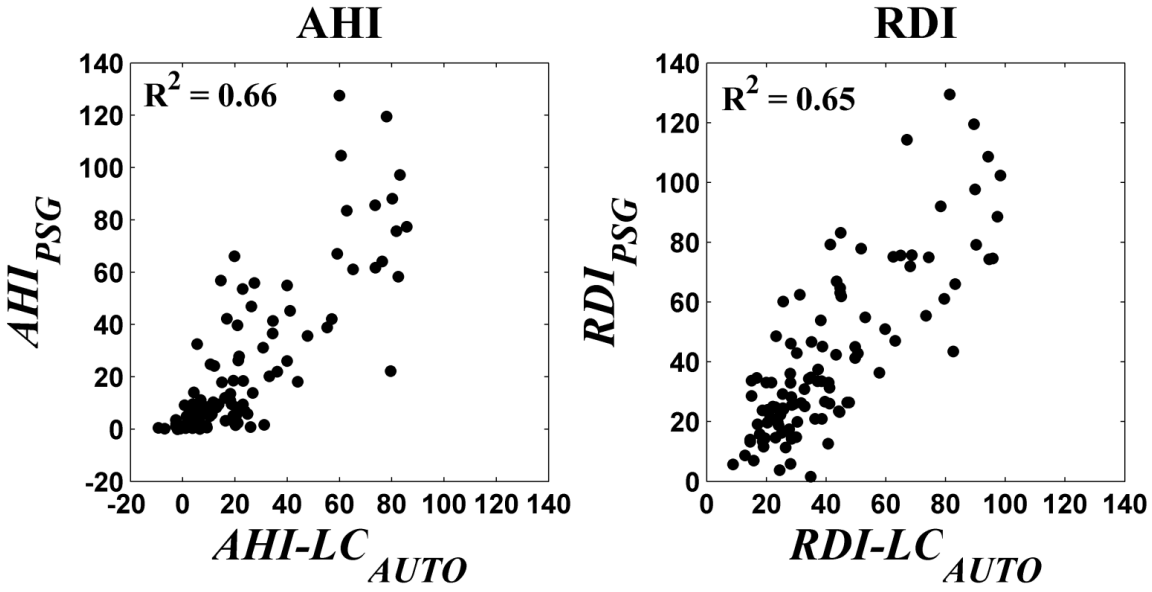

Figure 7-9. Comparison of *AHI-LC*$_{AUTO}$ vs. *AHI-PSG* (left) and *RDI-LC*$_{AUTO}$ vs. *RDI-PSG* with corresponding R^2 values. Due to the regression analysis utilized to predict *AHI-LC*$_{AUTO}$, some predicted values ended up being negative. While a negative *AHI* is not traditionally logical, the negative *AHI-LC*$_{AUTO}$ values only occurred for *AHI-PSG* values less than 5 suggesting that they are clinically equivalent to the absence of sleep apnea.

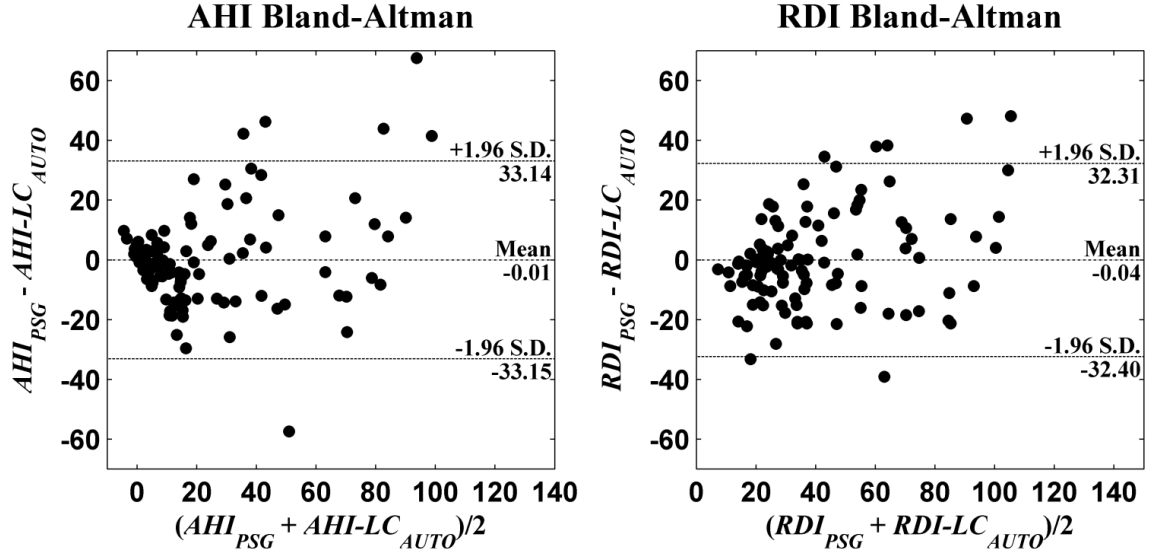

Figure 7-10. Bland-Altman plots showing the agreement between the *AHI-PSG* and *AHI-LC*$_{AUTO}$ (left) and *RDI-PSG* and *RDI-LC*$_{AUTO}$ (right).

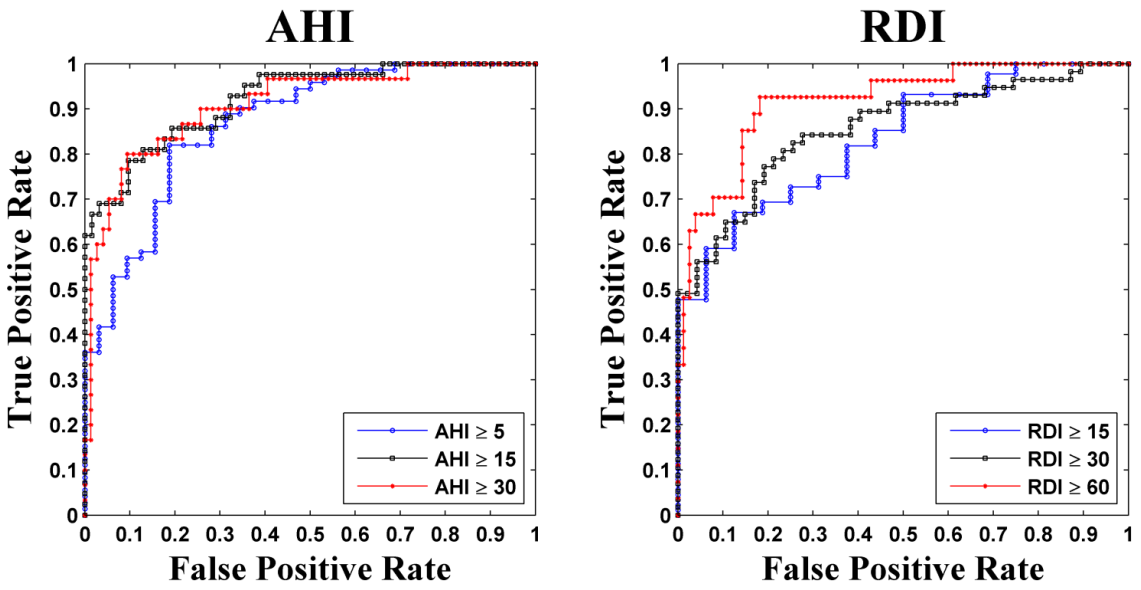

Figure 7-11. *ROC* curves showing the ability of the load cell data to predict overnight sleep studies positive for sleep apnea. The left plot displays the results for detecting sleep apnea at various thresholds of *AHI-LC*$_{AUTO}$ when positive tests are defined as *AHI-PSG* ≥ 5 (blue), *AHI-PSG* ≥ 15 (black), and *AHI-PSG* ≥ 30 (red). The right plot displays the results for detecting sleep apnea at various thresholds of *RDI-LC*$_{AUTO}$ when positive tests are defined as *RDI-PSG* ≥ 15 (blue), *RDI-PSG* ≥ 30 (black), and *RDI-PSG* ≥ 60 (red).

AHI-PSG was on average only 0.0058 less than *AHI-LC*$_{AUTO}$, which was not significant (t_{103} = -0.0035, p = 0.9972 with a 95% confidence interval of [-3.2947 3.2830]). *RDI-PSG* was on average 0.0449 less than that of *RDI-LC*$_{AUTO}$; this difference was also not significant (t_{103} = -0.0277, p = 0.9780) with a 95% confidence interval of [-3.2556 3.1659].

The *ROC* curves showing the ability of the automatically scored load cell data to determine the presence of sleep apnea are contained in figure 7-11. The Area Under Curve (AUC) for each cutoff level of AHI is 0.8698 for *AHI-PSG* ≥ 5, 0.9220 for *AHI-PSG* ≥ 15, and 0.9095 for *AHI-PSG* ≥ 30. The AUC for each cutoff level of RDI are 0.8345 for *RDI-PSG* ≥ 15, 0.8548 for *RDI-PSG* ≥ 30, and 0.9173 for *RDI-PSG* ≥ 60.

Discussion/Conclusion

The algorithm presented herein was a first-pass attempt to explore the feasibility of using only load cell data to automatically detect sleep apnea. High AUC values from the ROC analysis (see figure 7-11) indicate that the load cell system has promise as a prescreening tool where high sensitivity is desired to confirm the suspicion of sleep apnea. There was some variability in the results; however, this is not surprising due to the high inconsistency that is seen in the visual scoring of PSG between different sleep technologists [5, 81]. Therefore, exact agreement between the *AHI-LC*$_{AUTO}$ and *RDI-LC*$_{AUTO}$ with *AHI-PSG* and *RDI-PSG* was not expected. The results of the automatic algorithm are especially encouraging considering that the load cell data was collected at two different sleep labs (OHSU vs. PSP). Good agreement despite the variability introduced by different sleep technologists scoring the overnight sleep tests and despite slightly different load cell setups (i.e. different beds with differing numbers of load cells under each bed) suggests robustness and generalizability in the system and the automatic algorithm.

The negative coefficient for the *cV%* was also perplexing. It is counterintuitive that estimates for *AHI-LC*$_{AUTO}$ or *RDI-LC*$_{AUTO}$ would decrease with increasing variability in breathing amplitude as perceived by the *cV%* feature. The *cV%* feature was initially intended to capture the constant changes in breathing amplitude associated with recurring apneas and hypopneas. It may be that there is some complex interaction between the *cV%* feature and the *DBI* feature. It is possible that the *DBI* feature overestimates the presence of apneic and hypopneic events in individuals with high variability in their breathing amplitudes as detected in the CoP_y signal. In such a case, the *cV%* feature

could act as some sort of compensation for this overestimation. Further study is needed to determine whether this is the case or if there is some other cause. Future work should also include using a gradient descent method to search across a larger space for the optimal combination of parameters (i.e. $thr_{cV,}$ $wn_{cV,}$ N, $AMP\%$, and t_{apnea}) that maximize the ability of $cV\%$ and DBI to help estimate $AHI\text{-}LC_{AUTO}$ or $RDI\text{-}LC_{AUTO}$. It is likely that values for these parameters could be found that enhance the ability – measured using some combination of R^2 and mse – of the linear models used to estimate $AHI\text{-}LC_{AUTO}$ or $RDI\text{-}LC_{AUTO}$. Parameter values could also be discovered that lead to accurate linear models with more intuitive coefficients.

Other attempts to automatically detect sleep apnea using non-contact sensors have been made. In particular, Zaffaroni et al. used a radio-frequency sensor placed on a night table near the bed [82] and Agatsuma et al. used a sheet with an array of pressure sensors placed on top of the mattress [83] achieving good agreement between their estimates of AHI for several patients and the AHI calculated using traditionally scored PSG data. Zaffaroni et al. reported AUC values for detecting sleep apnea at several different AHI cutoff levels of 0.858 for $AHI\text{-}PSG \geq 5$, 0.940 for $AHI\text{-}PSG \geq 10$, 0.971 for $AHI\text{-}PSG \geq 15$, and 0.948 for $AHI\text{-}PSG \geq 20$ [82]. Agatsuma et al. reported AUC values for detecting sleep apnea at two different AHI cutoff levels of 0.96 for $AHI\text{-}PSG \geq 5$, and 0.97 for $AHI\text{-}PSG \geq 15$ [83]. However, both sensor modalities have their limitations. It is unknown how well the radio-frequency sensor will work if it's "view" of the patient is occluded by items placed on the night stand or by the patient sleeping under various layers of blankets and bedding. The sheet of pressure sensors is placed between the patient and their mattress which may lead to discomfort especially if several nights of

data are to be collected for long term monitoring. In contrast, once the load cells are placed under the supports of the bed, they are able to collect data without needing to alter the sleeping environment and have a minimal risk of being altered by patients during common practices such as changing bedding or placing items on their nightstand.

In 2007 the American Academy of Sleep Medicine (AASM) outlined rules for sleep technologists to follow when scoring sleep studies for sleep apnea. In an attempt to improve inter-rater reliability between scorers, the AASM advised that hypopneas (i.e. breathing amplitude reduction of 30% or more) must be accompanied by an oxygen desaturation [5]. This was the rule followed when defining *AHI-PSG* for comparison to the automatic load cell algorithm (i.e. $AHI\text{-}LC_{AUTO}$). Recently, in order to improve the overall detection of sleep apnea, the AASM has changed their recommendations for hypopnea detection. Hypopneas are now defined as discernible reductions in airflow ($\geq$30%) associated with an oxygen desaturation or arousal (i.e. patient awakenings) [84]. This new hypopnea definition corresponds to the rules followed for scoring *RDI-PSG*, the ground truth used for obtaining $RDI\text{-}LC_{AUTO}$. The results from the pressure sensor sheet were only compared to AHIs scored using a hypopnea rule requiring an oxygen desaturation. Therefore agreement between their results and AHIs scored following scoring rules similar to the improved recommendations by the AASM are unknown. The scoring rules followed for the radio-frequency sensor for manually scoring AHIs from the PSG data were unspecified. In contrast, the automatic scoring algorithm developed for the load cell data performed well when developed and compared to both *AHI-PSG* and *RDI-PSG*, and future improvements to the algorithm are expected to further enhance its

ability to automatically detect sleep apnea (i.e. increase AUC values for *AHI-PSG* cutoff levels of 5, 15, & 30 and *RDI-PSG* cutoff levels of 15, 30 & 60).

Chapter 8: Summary and Conclusions

Summary

Millions of Americans suffer from some sort of sleep disorder [1]. It is estimated that 9% of middle aged women and 24% of middle aged men have some degree of sleep apnea [4]. Several serious health risks, such as cardiovascular disease, are associated with sleep apnea [5]. The current clinical standard for diagnosing and monitoring sleep apnea (PSG) requires individuals who are already experiencing problems sleeping to sleep in a foreign environment while wired up to several uncomfortable sensors. The obtrusive nature and sometimes limited access [10] to PSG has led to a heightened interest in unobtrusive methods to monitor an individual's breathing while they are sleeping in a bed.

Previously in our lab, load cells placed under the supports of a bed were used to detect and classify movements while an individual was lying in the bed [43, 46-49] and to extract parameters of overall sleep hygiene [40]. The ability of load cells to detect breathing has also been shown [44, 58]. In order to build upon our earlier work to monitor individuals while they sleep with load cells placed under the supports of the bed and to enhance the ability of these load cells to detect the respiration of an individual lying on the bed so as to allow sleep apnea detection, I developed a functional and robust load cell system. With the exception of a commercial A/D converter, the electronics used

for conditioning (i.e amplifying and filtering) the load cell signals were designed and assembled in house with assistance of John Hunt M.S.E.E. Originally, the load cells were attached to steel bars housed in wood footings with cedar blocks attached to the top of the load cells fabricated to contain the supports of the bed (see figure 2-3). Eventually, this load cell setup was deemed unstable and new footings and connections to the bed frame were developed for the load cells. In the new setup, the load cells were bolted to aluminum bases and metal fittings were designed that could be attached to the top of the load cells and connect them to a conventional metal bed frame in the same manner as the traditional wheel castor (see figure 2-4). The voltage output from all the load cells was shown to be linearly dependent upon the amount of force placed on the load cells.

It is theorized that the load cell system is able to detect the breathing of an individual lying on the bed due to the displacement of visceral organs in the abdominal cavity caused by the movement of the diaphragm as the lungs are inflated and deflated. I was able to mathematically demonstrate that with reasonable assumptions the load cells placed under the supports of the bed could be used to track these center of mass changes caused by calculating the *CoP* (see equation 3.10). Using the *CoP*, I was able to confirm the theory behind the origin of the load cell breathing signal (see figure 3-3).

Several experiments were designed to determine what effect the bed/mattress system would have on the data collected from load cells placed under the supports of the bed. By applying an impulse to the bed/mattress system, I was able to show the frequency of response and damping characteristics of the system was dependent upon amount of mass loaded on the bed. Independent of mattress type, the resonant frequency of the bed/mattress system decreased with increasing load placed on the bed (see figure

4-4). Similarly, the amount of damping (i.e. the rate at which the impulse response amplitude was attenuated) generally decreased with increasing amount of mass loaded on the bed (see figure 4-5).

It was encouraging that the observed frequency responses of the bed/mattress systems ranging from approximately 2-10 *Hz* were not in the range of respiration rate that is expected to be below 0.5 *Hz*. Tests were performed to see how well the *CoP* signal could track the known motion of a mass rotating on the bed/mattress system and gauge the effects of the bed/mattress system on mass movements in the frequency range of respiration. Overall the load cell *CoP* signal was able to reliably recreate the movement of the mass on the bed despite some distortion caused by the bed/mattress system and centripetal forces not accounted for when calculating *CoP* (equation 4.8). I was also able to show that the load cell *CoP* signal could detect changes in the amplitude of mass movement on the bed which is an important function of the load cell system in order to detect sleep apnea as apnea are mainly defined as changes in breathing amplitude.

An algorithm was developed to detect individual breaths in the load cell *CoP* signal that tracked mass movements due to breathing. Each breath in the load cell *CoP* signal is detected by detecting local peaks and troughs found in the low pass filtered version of the *CoP* signal. These peaks and troughs represent the transitions between the direction of mass movement during inspiration and expiration. Extraneous peaks and troughs that frequently appear in the low passed *CoP* signal and that do not signify inspiration/expiration transitions were eliminated by discarding any peak/trough pairs that had significantly smaller amplitude than the preceding and following peak/trough pairs.

In order to test how well the load cell *CoP* signal could detect the breathing of an individual lying on the bed, two experiments were designed to compare the respiration rate derived from the peaks and troughs in the load cell *CoP* signal to the breathing rate estimated using the flow signal from a nasal pressure cannula. There were no differences between the respiration rates estimated using the load cell *CoP* and the respiration rates estimated from the flow signal for lying position or three mattress types (memory foam mattress and the two coiled spring mattresses). There was a significant difference between the two methods of respiration rate estimation found using the mattress with an air-filled bladder encased in foam. This difference of 0.264 breaths/minute is not clinically significant. Overall, the results from two experiments revealed that the peaks and troughs in the load cell *CoP* signal could be used to accurately and reliably estimate the respiration rate of individuals lying quiescently on the bed regardless of lying position or mattress type.

Large movements by an individual lying in the bed (i.e. rolling over or moving an arm or leg) result in excursions of the load cell signal that are orders of magnitude greater than the load cell breathing signal. These large movements completely "washout" the ability of the load cell system to detect breathing during the movement and can significantly alter the effects of the low pass filter on the load cell data in the immediately surrounding regions. Previous work in our lab focused on detecting such large movements [43, 46]. I was able to build upon this research and develop an approach to automatically remove all significantly large movements from the load cell data. With the large movements detected and removed, the remaining load cell data representing periods

of quiescence could be analyzed for the presence of apneic events which is the ultimate goal of this dissertation.

The load cell system has been shown to have great capacity to be used to detect sleep apnea. A sleep technologist was able to score overnight sleep studies for sleep apnea using modified PSG data (i.e. traditional respiration tracings replaced with load cell breathing signals) with similar accuracy to the scoring of the PSG data with the original breathing signals. I was also able to develop an algorithm that could automatically detect the presence of sleep apnea using only load cell data. These results suggest that the load cell system could be beneficially used in both the sleep lab and in patients' homes. In the sleep lab, the load cell breathing signal could be utilized for all patients or targeted to those who have a difficult time tolerating the currently used obtrusive breathing sensors (e.g. belts placed snuggly around the chest and abdomen along with thermistors and nasal pressure cannulas positioned inside the nostrils) such as those with insomnia, allergies to adhesives, children, and the elderly. The load cell system could also be outfitted to patients' beds in order to prescreen patients suspected of having sleep apnea or monitor patients with known sleep apnea for extended periods of time while they sleep in their own unaltered sleeping environments.

Future Work

The natural progression of this research is to collect data from load cell systems deployed into patients' homes. Individuals suspected of have sleep apnea could have load cells attached to the supports of their own beds and load cell data could be collected each night for the week before they are scheduled to have an overnight test at the sleep

lab. Load cell data would be collected along with traditional PSG data during their stay at the sleep lab. Comparison of the load cell system's prediction of sleep apnea severity while the patients sleep in their own homes versus the severity of sleep apnea detected by the load cells and PSG during the overnight sleep study would be very useful. This has substantial clinical utility given the known night-to-night variability of sleep apnea [85-88]. It is also widely believe that individuals sleep differently in the sleep lab and this may affect the results of their sleep test [7, 8].

Collecting and analyzing load cell data while individuals sleep in their own beds at home presents some unique challenges that are not present in the sleep lab. The current method for connecting the load cells to the bed works well for metal bedframes that are quiet common; however, there are also several other types of bedframes that sleep apnea patients may own. It is possible that some kind of tensioning device could be placed between the load cells and the bedframe. Several load cells could be set under the bedframe in various locations and the tensioning devices used to slightly raise the bedframe, effectively transferring the weight of the bed to the load cells. The development of such a device would allow access to the load cell system for most sleep apnea patients independent of what type of bed they have.

Two other challenges presented by in-home load cell data collection will be determining when the patient is asleep and accounting for multiple individuals sleeping on the bed/mattress system. To address the former, an algorithm that we developed in the lab that was able to accurately distinguish between epochs of sleep and epochs of wake [51] could be utilized. This sleep/wake algorithm utilized more information than just the load cell data so testing will be needed to determine how well it performs when only the

load cell signals are available. For the latter challenge of in-home data collection, I was also able to show in a brief unpublished experiment that by using independent component analysis (ICA) techniques (implemented using the fastICA algorithms [89]) it appears possible to separate the load cell breathing signals from two individuals lying on the bed. Load cell data was collected while two individuals lay down on the bed/mattress system. Using ICA, two breathing signals were extracted from the load cell data. Respiration rates calculated independently for each different load cell breathing signal showed good agreement with the corresponding ground truth respiration rates measured using respiratory inductance plethysmography belts for each subject.

Other elements could also be added to the algorithm presented herein to aid in the automatic detection of sleep apnea using load cell data collected from patients' homes. Many patients with sleep apnea exhibit worsening symptoms when sleeping on their backs compared to sleeping on their sides [76-78], and heart rate changes have been associated with apneic events [90, 91]. In previous work, I was able to develop a method using the load cell signals that could accurately predict whether or not an individual was lying their side [41]. The load cells have also shown potential at detecting heart rate [44, 52-57]. Adding heart rate and lying position detection would likely enhance the load cell systems ability to detect the presence of sleep apnea in individuals as they slept in their own homes.

Conclusions

I have shown that the load cell system can accurately detect the breathing of an individual lying on the bed. I have also shown the potential of using the load cell signals

to diagnose and monitor sleep apnea. The use of other unobtrusive technologies have been studied to extrapolate the breathing signal of person lying on the bed and in some cases make observations about the presence of sleep apnea. However, the limitations of these devices range from restricting where the individual can lie on the bed to altering the sleeping environment which may affect the sleep of the person being monitored. The load cell system does not change the sleeping environment and once in place is at less of a risk of being altered by the subject either intentionally or inadvertently (e.g. during routine bedding changes). The load cell system also has other capabilities outside the realm of detecting breathing and heart rate. For example, in long term care facilities, calibrated load cells could monitor the weight of a resident on a nightly basis and alert caretakers/doctors if sudden weight changes occur that may indicate fluid retention related to heart issues [75]. The load cells could also be used as a presence detector for patients at risk of roaming during the night. The load cell system could also be applied to detecting and monitoring other sleep disorders such as periodic leg movements or circadian rhythm disorders that currently utilize accelerometers placed on the patient if diagnosis outside of the sleep lab is desired.

In particular, I have developed the load cell system and used it to make three significant contributions to the field of unobtrusive breathing monitoring and sleep apnea detection. I used the load cell system to characterize the bed/mattress system for several different types of beds. I have introduced the method of using the load cell *CoP* signal to monitor respiration. I am also the first to demonstrate the ability of the load cell system to detect obstructive sleep apnea and central sleep apnea.

Some groups interested in unobtrusive breathing/heart rate detection have mentioned the possible effects of the bed/mattress system on the signals that they are collecting; however, to my knowledge I am the first to systematically analyze the response of the bed/mattress system to an applied impulse. I was able to show that the bed/mattress system, for several different mattress types, displayed frequency and damping responses that were mass dependent. In unpublished research, I have found the resonance response of the bed to be particularly disruptive to the heart rate detection for several individuals. Heart rate detection using sensors such as the load cells depends on detecting small movements of the individual's body in response to reactionary forces caused by their heart beating. To my knowledge, most methods for detecting heart rate from unobtrusive sensors are centered on finding some kind of peak in the time domain signal that represents the heartbeat. The results from my characterization of the bed/mattress system suggest that heart rate detection difficulty could be increased for persons with higher weight and heart rate. It is possible that individual heart beats would frequently be "hidden" due to temporal summation if several heart beats caused by significant resonance from the bed/mattress system and the lack of attenuation. A reliable unobtrusive technique to detect heart rate would need to take these effects of the bed/mattress system into consideration.

Placing the load cells under all the supports of the bed allows me to uniquely track the mass movements caused by breathing using the load cell *CoP* signal. Other groups using load cells to detect breathing appear to have either only used a single load cell under one support of the bed [58] or have simply summed (i.e. added and subtracted) the output of various load cells to achieve the best results [44]. The optimal combination

of load cell data in order to generate a *CoP* signal allows for accurate representation of mass movement during breathing and the detection of changes due to apneic events.

The ultimate goal of this dissertation was to demonstrate the feasibility of the load cell system to detect sleep apnea. I have shown that load cells can be used as replacements for traditional breathing signals during PSG to diagnose sleep apnea, and I have developed an automatic algorithm to predict the presence of sleep apnea in a patient using only the load cell signals. To my knowledge I was the first to validate the load cells in such a manner and the technology is patent pending.

References

[1] H. R. Colten and B. M. Altevogt, "Sleep Disorders and Sleep Deprivation: An Unmet Public Health Problem." Washington, DC: The National Academies Press (Institute of Medicine of the National Academies), 2006.

[2] M. H. Sanders, "Sleep Breathing Disorders," in *Principles and Practice of Sleep Medicine*, Fourth ed. Philadelphia: Elsevier Saunders, 2005, pp. 969-1156.

[3] C. Iber, S. Ancoli-Israel, A. Chesson, and S. F. Quan, "The AASM Manual for the Scoring of Sleep and Associated Events: Rules, Terminology and Technical Specifications." Westchester, Illinois: American Academy of Sleep Medicine, 2007.

[4] T. Young, M. Palta, J. Dempsey, J. Skatrud, S. Weber, and S. Badr, "The occurrence of sleep-disordered breathing among middle-aged adults," *N Engl J Med*, vol. 328, pp. 1230-5, 1993.

[5] S. Redline, R. Budhiraja, V. Kapur, C. L. Marcus, J. H. Mateika, R. Mehra, S. Parthasarthy, V. K. Somers, K. P. Strohl, L. G. Sulit, D. Gozal, M. S. Wise, and S. F. Quan, "The scoring of respiratory events in sleep: reliability and validity," *J Clin Sleep Med*, vol. 3, pp. 169-200, 2007.

[6] T. Young, L. Evans, L. Finn, and M. Palta, "Estimation of the clinically diagnosed proportion of sleep apnea syndrome in middle-aged men and women," *Sleep*, vol. 20, pp. 705-6, 1997.

[7] H. W. Agnew, Jr., W. B. Webb, and R. L. Williams, "The first night effect: an EEG study of sleep," *Psychophysiology*, vol. 2, pp. 263-6, 1966.

[8] G. Curcio, M. Ferrara, A. Piergianni, F. Fratello, and L. De Gennaro, "Paradoxes of the first-night effect: a quantitative analysis of antero-posterior EEG topography," *Clin Neurophysiol*, vol. 115, pp. 1178-88, 2004.

[9] O. Le Bon, L. Staner, G. Hoffmann, M. Dramaix, I. San Sebastian, J. R. Murphy, M. Kentos, I. Pelc, and P. Linkowski, "The first-night effect may last more than one night," *J Psychiatr Res*, vol. 35, pp. 165-72, 2001.

[10] W. W. Flemons, N. J. Douglas, S. T. Kuna, D. O. Rodenstein, and J. Wheatley, "Access to diagnosis and treatment of patients with suspected sleep apnea," *Am J Respir Crit Care Med*, vol. 169, pp. 668-72, 2004.

[11] J.-Y. Cha, H.-S. Choi, J.-Y. Shin, and K.-J. Lee, "Unconstrained respiration and heart rate monitoring system based on a PPG pillow during sleep," presented at Engineering in Medicine and Biology Society, 2008. EMBS 2008. 30th Annual International Conference of the IEEE, 2008.

[12] W. Chen, X. Zhu, T. Nemoto, Y. Kanemitsu, K. Kitamura, and K. Yamakoshi, "Unconstrained detection of respiration rhythm and pulse rate with one under-pillow sensor during sleep," *Medical and Biological Engineering and Computing*, vol. 43, pp. 306-312, 2005.

[13] T. Harada, A. Sakata, T. Mori, and T. Sato, "Sensor pillow system: monitoring respiration and body movement in sleep," presented at Intelligent Robots and Systems, 2000. (IROS 2000). Proceedings. 2000 IEEE/RSJ International Conference on, 2000.

[14] K. Motoi, S. Kubota, A. Ikarashi, M. Nogawa, S. Tanaka, T. Nemoto, and K. Yamakoshi, "Development of a fully automated network system for long-term

health-care monitoring at home," *Conf Proc IEEE Eng Med Biol Soc*, vol. 2007, pp. 1826-9, 2007.

[15] X. Zhu, W. Chen, T. Nemoto, Y. Kanemitsu, K.-I. Kitamura, and K.-I. Yamakoshi, "Accurate determination of respiratory rhythm and pulse rate using an under-pillow sensor based on wavelet transformation," presented at Annual International Conference of the IEEE Engineering in Medicine and Biology, Shanghai, China, 2005.

[16] X. Zhu, W. Chen, T. Nemoto, Y. Kanemitsu, K.-I. Kitamura, K.-I. Yamakoshi, and D. Wei, "Real-time monitoring of respiration rhythm and pulse rate during sleep," *IEEE Transactions on Biomedical Engineering*, vol. 53, pp. 2553-2563, 2006.

[17] Y. Chee, J. Han, J. Youn, and K. Park, "Air mattress sensor system with balancing tube for unconstrained measurement of respiration and heart beat movements," *Physiol Meas*, vol. 26, pp. 413-22, 2005.

[18] P. Chow, G. Nagendra, J. Abisheganaden, and Y. T. Wang, "Respiratory monitoring using an air-mattress system," *Physiol Meas*, vol. 21, pp. 345-54, 2000.

[19] L. Hernandez, B. Waag, H. Hsiao, and V. Neelon, "A new non-invasive approach for monitoring respiratory movements of sleeping subjects," *Physiol Meas*, vol. 16, pp. 161-7, 1995.

[20] Y. Kurihara, K. Watanabe, T. Kikuchi, T. Namba, and H. Tanaka, "Potentialities of the pneumatic biosensing bed as a network terminal for ubiquitous health

monitoring and medical care," *IEEJ Transactions on Electrical and Electronic Engineering*, vol. 3, pp. 632-641, 2008.

[21] H. Sasaoka, "Detection technologies of sleep condition on bio-signal monitoring system," presented at SICE 2004 Annual Conference, 2004.

[22] K. Watanabe, T. Watanabe, H. Watanabe, H. Ando, T. Ishikawa, and K. Kobayashi, "Noninvasive measurement of heartbeat, respiration, snoring and body movements of a subject in bed via a pneumatic method," *IEEE Trans Biomed Eng*, vol. 52, pp. 2100-7, 2005.

[23] M. Ishijima, "Cardiopulmonary monitoring by textile electrodes without subject-awareness of being monitored," *Medical and Biological Engineering and Computing*, vol. 35, pp. 685-690, 1997.

[24] H. Kimura, H. Kobayashi, K. Kawabata, and H. F. Van der Loos, "Development of an unobtrusive vital signs detection system using conductive fiber sensors," presented at Intelligent Robots and Systems, 2004. (IROS 2004). Proceedings. 2004 IEEE/RSJ International Conference on, 2004.

[25] H. F. M. Van der Loos, N. Ullrich, and H. Kobayashi, "Development of Sensate and Robotic Bed Technologies for Vital Signs Monitoring and Sleep Quality Improvement," *Autonomous Robots*, vol. 15, pp. 67-79, 2003.

[26] V. F. S. Fook, K. P. Leong, E. H. JianZhong, M. Jayachandran, A. A. P. Wai, J. Biswas, L. WeiSi, and P. Yap, "Non-intrusive respiratory monitoring system using Fiber Bragg Grating sensor," presented at e-health Networking, Applications and Services, 2008. HealthCom 2008. 10th International Conference on, 2008.

[27] Y. Nishida, M. Takeda, T. Mori, H. Mizoguchi, and T. Sato, "Monitoring patient respiration and posture using human symbiosis system," presented at Intelligent Robots and Systems, 1997. IROS '97., Proceedings of the 1997 IEEE/RSJ International Conference on, 1997.

[28] M. H. Jones, R. Goubran, and F. Knoefel, "Reliable respiratory rate estimation from a bed pressure array," *Conf Proc IEEE Eng Med Biol Soc*, vol. 1, pp. 6410-3, 2006.

[29] M. H. Jones, R. Goubran, and F. Knoefel, "Identifying movement onset times for a bed-based pressure sensor array," presented at IEEE International Workshop on Medical Measurement and Applications, MeMeA 2006, Benevento, Italy, 2006.

[30] N. Bu, N. Ueno, and O. Fukuda, "Monitoring of Respiration and Heartbeat during Sleep using a Flexible Piezoelectric Film Sensor and Empirical Mode Decomposition," presented at Engineering in Medicine and Biology Society, 2007. EMBS 2007. 29th Annual International Conference of the IEEE, 2007.

[31] J. L. Jacobs, P. Embree, M. Glei, S. Christensen, and P. K. Sullivan, "Characterization of a novel heart and respiratory rate sensor," presented at Engineering in Medicine and Biology Society, 2004. IEMBS '04. 26th Annual International Conference of the IEEE, 2004.

[32] F. Wang, M. Tanaka, and S. Chonan, "A PVDF piezopolymer sensor for unconstrained cardiorespiratory monitoring during sleep," *International Journal of Applied Electromagnetics and Mechanics*, vol. 16, pp. 181-188, 2002.

[33] F. Wang, M. Tanaka, and S. Chonan, "Development of a PVDF piezopolymer sensor for unconstrained in-sleep cardiorespiratory monitoring," *Journal of Intelligent Material Systems and Structures*, vol. 14, pp. 185-190, 2003.

[34] X. L. Aubert and A. Brauers, "Estimation of vital signs in bed from a single unobtrusive mechanical sensor: Algorithms and real-life evaluation," *Conf Proc IEEE Eng Med Biol Soc*, vol. 2008, pp. 4744-7, 2008.

[35] H. Aoki, K. Koshiji, H. Nakamura, Y. Takemura, and M. Nakajima, "Study on respiration monitoring method using near-infrared multiple slit-lights projection," presented at Micro-NanoMechatronics and Human Science, 2005 IEEE International Symposium on, 2005.

[36] K. Nakajima, Y. Matsumoto, and T. Tamura, "A monitor for posture changes and respiration in bed using real time image sequence analysis," presented at Engineering in Medicine and Biology Society, 2000. Proceedings of the 22nd Annual International Conference of the IEEE, 2000.

[37] N. A. Fox, C. Heneghan, M. Gonzalez, R. B. Shouldice, and P. de Chazal, "An evaluation of a non-contact biomotion sensor with actimetry," *Conf Proc IEEE Eng Med Biol Soc*, vol. 2007, pp. 2664-8, 2007.

[38] M. Uenoyama, T. Matsui, K. Yamada, S. Suzuki, B. Takase, S. Suzuki, M. Ishihara, and M. Kawakami, "Non-contact respiratory monitoring system using a ceiling-attached microwave antenna," *Medical and Biological Engineering and Computing*, vol. 44, pp. 835-840, 2006.

[39] J. Alihanka, K. Vaahtoranta, and I. Saarikivi, "A new method for long-term monitoring of the ballistocardiogram, heart rate, and respiration," *Am J Physiol*, vol. 240, pp. R384-92, 1981.

[40] A. M. Adami, T. L. Hayes, and M. Pavel, "Unobtrusive monitoring of sleep patterns," presented at 25th Annual International Conference of the IEEE Engineering in Medicine and Biology Society, Cancun, Mexico, 2003.

[41] Z. T. Beattie, C. C. Hagen, and T. L. Hayes, "Classification of lying position using load cells under the bed," *Conf Proc IEEE Eng Med Biol Soc*, pp. 474-7, 2011.

[42] A. M. Adami, A. G. Adami, G. Schwarz, Z. T. Beattie, and T. L. Hayes, "A subject state detection approach to determine rest-activity patterns using load cells," *Conf Proc IEEE Eng Med Biol Soc*, vol. 2010, pp. 204-7, 2010.

[43] A. M. Adami, M. Pavel, T. L. Hayes, and C. M. Singer, "Detection of movement in bed using unobtrusive load cell sensors," *IEEE Trans Inf Technol Biomed*, vol. 14, pp. 481-90, 2010.

[44] M. Brink, C. H. Muller, and C. Schierz, "Contact-free measurement of heart rate, respiration rate, and body movements during sleep," *Behav Res Methods*, vol. 38, pp. 511-21, 2006.

[45] G. S. Chung, B. H. Choi, K. K. Kim, Y. G. Lim, J. W. Choi, D.-U. Jeong, and K. S. Park, "REM Sleep Classification with Respiration Rates," presented at Information Technology Applications in Biomedicine, 2007. ITAB 2007. 6th International Special Topic Conference on, 2007.

[46] A. M. Adami, A. G. Adami, T. L. Hayes, M. Pavel, and Z. T. Beattie, "A Gaussian model for movement detection during sleep," *Conf Proc IEEE Eng Med Biol Soc*, pp. 2263-6, 2012.

[47] A. M. Adami, A. Adami, C. M. Singer, T. L. Hayes, and M. Pavel, "A System for unobtrusive monitoring of mobility in bed," presented at Proceedings of the 11th IEEE International Conference on Computational Science and Engineering, CSE Workshops 2008, Piscataway, NJ, 2008.

[48] A. M. Adami, T. L. Hayes, M. Pavel, and C. M. Singer, "Detection and classification of movements in bed using load cells," presented at 27th Annual International Conference of the IEEE Engineering in Medicine and Biology Society, Shanghai, China, 2005.

[49] A. M. Adami, M. Pavel, T. L. Hayes, A. G. Adami, and C. Singer, "A method for classification of movements in bed," *Conf Proc IEEE Eng Med Biol Soc*, pp. 7881-4, 2011.

[50] B. H. Choi, J. W. Seo, J. M. Choi, H. B. Shin, J. Y. Lee, U. Jeong do, and K. S. Park, "Non-constraining sleep/wake monitoring system using bed actigraphy," *Med Biol Eng Comput*, vol. 45, pp. 107-14, 2007.

[51] D. Austin, Z. T. Beattie, T. Riley, A. M. Adami, C. C. Hagen, and T. L. Hayes, "Unobtrusive classification of sleep and wakefulness using load cells under the bed," *Conf Proc IEEE Eng Med Biol Soc*, pp. 5254-7, 2012.

[52] G. S. Chung, J. S. Lee, S. H. Hwang, Y. K. Lim, D. U. Jeong, and K. S. Park, "Wakefulness estimation only using ballistocardiogram: nonintrusive method for sleep monitoring," *Conf Proc IEEE Eng Med Biol Soc*, pp. 2459-62, 2010.

[53] B. H. Choi, G. S. Chung, J. S. Lee, D. U. Jeong, and K. S. Park, "Slow-wave sleep estimation on a load-cell-installed bed: a non-constrained method," *Physiol Meas*, vol. 30, pp. 1163-70, 2009.

[54] G. S. Chung, B. H. Choi, D. U. Jeong, and K. S. Park, "Noninvasive heart rate variability analysis using loadcell-installed bed during sleep," *Conf Proc IEEE Eng Med Biol Soc*, vol. 2007, pp. 2357-60, 2007.

[55] G. S. Chung, B. H. Choi, K. K. Kim, Y. G. Lim, J. W. Choi, D.-U. Jeong, and K. S. Park, "Unconstrained heart rate estimation system in bed," presented at Convergence Information Technology, International Conference on, Gyongju, Korea, Republic of, 2007.

[56] J. H. Shin, B. H. Choi, Y. G. Lim, D. U. Jeong, and K. S. Park, "Automatic ballistocardiogram (BCG) beat detection using a template matching approach," *Conf Proc IEEE Eng Med Biol Soc*, vol. 2008, pp. 1144-6, 2008.

[57] J. Paalasmaa, "A respiratory latent variable model for mechanically measured heartbeats," *Physiol Meas*, vol. 31, pp. 1331-44, 2010.

[58] J. Paalasmaa, L. Leppakorpi, and M. Partinen, "Quantifying respiratory variation with force sensor measurements," *Conf Proc IEEE Eng Med Biol Soc*, pp. 3812-5, 2011.

[59] Z. T. Beattie, T. L. Hayes, C. Guilleminault, and C. C. Hagen, "Accurate scoring of the apnea-hypopnea index using a simple non-contact breathing sensor," *J Sleep Res*, vol. 22, pp. 356-62, 2013.

[60] W. F. Riley and L. D. Sturges, *Engineering Mechanics: Statics*, 2nd ed: John Wiley & Sons, Inc., 1996.

[61] J. R. Taylor, *Classical Mechanics*: University Science Books, 2005.

[62] P. D. Welch, "The use of fast Fourier transform for the estimation of power spectra: A method based on time averaging over short, modified periodograms," *Audio and Electroacoustics, IEEE Transactions on*, vol. 15, pp. 70-73, 1967.

[63] J. M. Bland and D. G. Altman, "Statistical methods for assessing agreement between two methods of clinical measurement," *Lancet*, vol. 1, pp. 307-10, 1986.

[64] R. A. Serway and R. J. Beichner, *Physics for Scientists and Engineers* Fifth ed: Harcourt College Publishers, 2000.

[65] D. K. Molina and V. J. DiMaio, "Normal organ weights in men: part II-the brain, lungs, liver, spleen, and kidneys," *Am J Forensic Med Pathol*, vol. 33, pp. 368-72, 2012.

[66] A. Otero, P. Felix, J. Presedo, and M. R. Alvarez, "Is the average duration of apneas, hypopneas and desaturations useful in the diagnosis of SAHS?," presented at Intelligent Signal Processing (WISP), 2011 IEEE 7th International Symposium on, 2011.

[67] V. Tantrakul and C. Guilleminault, "Chronic sleep complaints in premenopausal women and their association with sleep-disordered breathing," *Lung*, vol. 187, pp. 82-92, 2009.

[68] M. Tenhunen, E. Rauhala, J. Virkkala, O. Polo, A. Saastamoinen, and S. L. Himanen, "Increased respiratory effort during sleep is non-invasively detected with movement sensor," *Sleep Breath*, vol. 15, pp. 737-46, 2011.

[69] R. D. Chervin, D. L. Ruzicka, T. F. Hoban, J. L. Fetterolf, S. L. Garetz, K. E. Guire, J. E. Dillon, B. T. Felt, E. K. Hodges, and B. J. Giordani, "Esophageal

Pressures, Polysomnography, and Neurobehavioral Outcomes of Adenotonsillectomy in Children," *Chest*, 2012.

[70] Z. T. Beattie, C. C. Hagen, M. Pavel, and T. L. Hayes, "Classification of breathing events using load cells under the bed," *Conf Proc IEEE Eng Med Biol Soc*, vol. 2009, pp. 3921-4, 2009.

[71] J. N. Murthy, J. van Jaarsveld, J. Fei, I. Pavlidis, R. I. Harrykissoon, J. F. Lucke, S. Faiz, and R. J. Castriotta, "Thermal infrared imaging: a novel method to monitor airflow during polysomnography," *Sleep*, vol. 32, pp. 1521-7, 2009.

[72] O. Polo, L. Brissaud, B. Sales, A. Besset, and M. Billiard, "The validity of the static charge sensitive bed in detecting obstructive sleep apnoeas," *Eur Respir J*, vol. 1, pp. 330-6, 1988.

[73] M. Kobayashi, K. Namba, S. Tsuiki, M. Nakamura, M. Hayashi, Y. Mieno, H. Imizu, S. Fujita, A. Yoshikawa, H. Sakakibara, and Y. Inoue, "Validity of sheet-type portable monitoring device for screening obstructive sleep apnea syndrome," *Sleep Breath*, vol. 17, pp. 589-95, 2012.

[74] C. Acebo, R. K. Watson, L. Bakos, and E. B. Thoman, "Sleep and apnea in the elderly: reliability and validity of 24-hour recordings in the home," *Sleep*, vol. 14, pp. 56-64, 1991.

[75] "Consensus recommendations for the management of chronic heart failure. On behalf of the membership of the advisory council to improve outcomes nationwide in heart failure," *Am J Cardiol*, vol. 83, pp. 1A-38A, 1999.

[76] R. D. Cartwright, "Effect of sleep position on sleep apnea severity," *Sleep*, vol. 7, pp. 110-4, 1984.

[77] C. F. George, T. W. Millar, and M. H. Kryger, "Sleep apnea and body position during sleep," *Sleep*, vol. 11, pp. 90-9, 1988.

[78] B. A. Phillips, J. Okeson, D. Paesani, and R. Gilmore, "Effect of sleep position on sleep apnea and parafunctional activity," *Chest*, vol. 90, pp. 424-9, 1986.

[79] R. O. Duda, P. E. Hart, and D. G. Stork, *Pattern Classification*, 2nd ed. New York, NY: John Wiley & Sons, Ltd., 2001.

[80] S. E. Martin, H. M. Engleman, R. N. Kingshott, and N. J. Douglas, "Microarousals in patients with sleep apnoea/hypopnoea syndrome," *J Sleep Res*, vol. 6, pp. 276-80, 1997.

[81] C. J. Stepnowsky, Jr., C. Berry, and J. E. Dimsdale, "The effect of measurement unreliability on sleep and respiratory variables," *Sleep*, vol. 27, pp. 990-5, 2004.

[82] A. Zaffaroni, P. de Chazal, C. Heneghan, P. Boyle, P. Ronayne, and W. T. McNicholas, "SleepMinder: an innovative contact-free device for the estimation of the apnoea-hypopnoea index," *Conf Proc IEEE Eng Med Biol Soc*, pp. 7091-4, 2009.

[83] T. Agatsuma, K. Fujimoto, Y. Komatsu, K. Urushihata, T. Honda, T. Tsukahara, and T. Nomiyama, "A novel device (SD-101) with high accuracy for screening sleep apnoea-hypopnoea syndrome," *Respirology*, vol. 14, pp. 1143-50, 2009.

[84] R. B. Berry, R. Budhiraja, D. J. Gottlieb, D. Gozal, C. Iber, V. K. Kapur, C. L. Marcus, R. Mehra, S. Parthasarathy, S. F. Quan, S. Redline, K. P. Strohl, S. L. Davidson Ward, and M. M. Tangredi, "Rules for scoring respiratory events in sleep: update of the 2007 AASM Manual for the Scoring of Sleep and Associated

Events. Deliberations of the Sleep Apnea Definitions Task Force of the American Academy of Sleep Medicine," *J Clin Sleep Med*, vol. 8, pp. 597-619, 2012.

[85] N. Ahmadi, G. K. Shapiro, S. A. Chung, and C. M. Shapiro, "Clinical diagnosis of sleep apnea based on single night of polysomnography vs. two nights of polysomnography," *Sleep Breath*, vol. 13, pp. 221-6, 2009.

[86] O. Le Bon, G. Hoffmann, J. Tecco, L. Staner, A. Noseda, I. Pelc, and P. Linkowski, "Mild to moderate sleep respiratory events: one negative night may not be enough," *Chest*, vol. 118, pp. 353-9, 2000.

[87] D. J. Levendowski, N. Zack, S. Rao, K. Wong, M. Gendreau, J. Kranzler, T. Zavora, and P. R. Westbrook, "Assessment of the test-retest reliability of laboratory polysomnography," *Sleep Breath*, vol. 13, pp. 163-7, 2009.

[88] J. Newell, O. Mairesse, P. Verbanck, and D. Neu, "Is a one-night stay in the lab really enough to conclude? First-night effect and night-to-night variability in polysomnographic recordings among different clinical population samples," *Psychiatry Res*, vol. 200, pp. 795-801, 2012.

[89] A. Hyvarinen, "Fast and robust fixed-point algorithms for independent component analysis," *IEEE Trans Neural Netw*, vol. 10, pp. 626-34, 1999.

[90] C. Guilleminault, S. Connolly, R. Winkle, K. Melvin, and A. Tilkian, "Cyclical variation of the heart rate in sleep apnoea syndrome. Mechanisms, and usefulness of 24 h electrocardiography as a screening technique," *Lancet*, vol. 1, pp. 126-31, 1984.

[91] P. K. Stein and Y. Pu, "Heart rate variability, sleep and sleep disorders," *Sleep Med Rev*, vol. 16, pp. 47-66, 2012.

Appendix A

The following protocol was followed separately for each different mattress. During the experiments using the adjustable air-filled mattress, the "Comfort Select Level" was set at 75. Load cell data was collected for each iteration of the experiment using a sampling rate of 500 Hz for each individual load cell.

1. One minute of load cell data was collected with nothing on the mattress.
2. The wooden platform was placed on the bed.
3. The bed/mattress system was allowed to settle for approximately 15 seconds.
4. One minute of load cell data was collected.
    a. At approximately 25 seconds after the start of the data collection, the impulse weight (0.77 kg) was dropped onto the mattress in the approximate center of the hole cut out of the wooden platform from a height of about 30 cm.
    b. The impulse mass was allowed to only "bounce" once on the mattress before being caught and removed. The exception being the experiments performed using the foam mattress where the impulse mass did not physically "bounce" off the mattress and was therefore simply dropped and left.
5. Two masses (≈ 2.3 kg each) were loaded onto the wooden platform.
    a. For all mass loadings of the wooden platform, one mass was placed on the platform above the hole cutout (i.e. towards the head of the bed), and the other was placed below the impulse hole (i.e. towards the foot of the bed).
6. Steps 3 and 4 were repeated.
7. The two masses from step 5 were removed from the wooden platform and were replaced with two larger masses (≈ 11 kg each).

8. Steps 3 and 4 were repeated.
9. Two more masses (≈ 11 kg each) were added to the wooden platform, and steps 3 and 4 were repeated.
10. Two more masses (≈ 11 kg each) were added to the wooden platform, and steps 3 and 4 were repeated.
11. Two more masses (≈ 11 kg each) were added to the wooden platform, and steps 3 and 4 were repeated.
12. Two more masses (≈ 11 kg each) were added to the wooden platform, and steps 3 and 4 were repeated.
13. Two more masses (≈ 11 kg each) were added to the wooden platform, and steps 3 and 4 were repeated.
14. Steps 3 through 13 were repeated with the exception that during each iteration two masses were removed from the wooden platform as opposed to being loaded on the wooden platform.
15. Steps 3 through 14 were repeated so that one minute of data was collected four times for each specific mass loading of the wooden platform.

Biographical Sketch

Zachary Todd Beattie was born on September 18th, 1979 in Idaho Falls, Idaho to his parents Todd and Vicki Beattie. On June 28th, 2003 he married Jacklyn Sharlee Glasmann and they are the proud parents of three very rambunctious boys: Keegan, Kayden, and Kyler.

Growing up Zach was very involved in sports and scouting. He achieved the highest rank of Eagle Scout in the Boy Scouts of America. Zach attended Hillcrest High School where he lettered in baseball, football, and cross country. In 1998, he graduated as a valedictorian. After high school, Zach lived in Japan for two years while he served as a missionary for the Church of Jesus Christ of Latter-Day Saints.

Zach started his undergraduate studies at Brigham Young University Idaho where graduated *summa cum laude* with his Associate of Science in Mechanical Engineering in 2004. He then transferred to the University of Utah where he again graduated *summa cum laude* with his Bachelor of Science in Bioengineering in 2006. As an undergraduate at the University of Utah, Zach worked in the lab of Kenneth Horch, Ph.D. where he developed a method for transforming the implanted portion of a cochlear implant so that it could be used as implantable nerve stimulation electrodes for neural prosthetic arms.

Zach started his graduate work in the Department of Biomedical Engineering at OHSU in the fall of 2006. While at OHSU, Zach was awarded a scholarship from the Achievement Rewards for College Scientists (ARCS) Foundation, Portland Chapter. He is currently an ARCS Scholar Alumnus. Along with his advisor Tamara Hayes, Ph.D. and mentor/collaborator Chad Hagen, M.D., he developed a load cell system that can be used to unobtrusively detect sleep apnea. The technology is currently patent pending.

Publications

1. **Beattie ZT**. Algorithm for automatic beat detection of cardiovascular pressure signals. *Proceedings of the Annual International Conference of the IEEE Engineering in Medicine and Biology Society,* 2008. 2594-2597.

2. **Beattie ZT**, Hagen CC, Pavel M, Hayes TL. Classification of breathing events using load cells under the bed. *Proceedings of the Annual International Conference of the IEEE Engineering in Medicine and Biology Society,* 2009. 3921-3924.

3. Adami AM, Adami AG, Schwarz G, **Beattie ZT**, Hayes TL. A subject state detection approach to determine rest-activity patterns using load cells. *Proceedings of the Annual International Conference of the IEEE Engineering in Medicine and Biology Society*, 2010. 204-207.

4. **Beattie ZT**, Hagen CC, Hayes TL. Classification of lying position using load cells under the bed. *Proceedings of the Annual International Conference of the IEEE Engineering in Medicine and Biology Society*, 2011. 474-477.

5. Adami AM, Adami AG, Hayes TL, Pavel M, **Beattie ZT**. A Gaussian model for movement detection during sleep. *Proceedings of the Annual International Conference of the IEEE Engineering in Medicine and Biology Society,* 2012. 2263-2266.

6. Austin D, **Beattie ZT**, Riley T, Adami AM, Hagen CC, Hayes TL. Unobtrusive classification of sleep and wakefulness using load cells under the bed. *Proceedings of the Annual International Conference of the IEEE Engineering in Medicine and Biology Society*, 2012. 5254-5257.

7. **Beattie ZT**, Hayes TL, Guilleminault C, Hagen CC. Accurate scoring of the apnea–hypopnea index using a simple non-contact breathing sensor. *Journal of Sleep Research*, 2013, 22: 356–362.

Abstracts

1. **Beattie ZT**, Hagen CC, Pavel M, Hayes TL. Unobtrusive monitoring of sleep apnea. *SLEEP 2011, 25th Annual Meeting of the Associated Professional Sleep Societies LLC (APSS)*, Minneapolis, Minnesota (June 2011).

2. **Beattie ZT**, Hagen CC, Hayes TL. Detecting sleep apnea using load cells installed under the bed. *SLEEP 2012, 26th Annual Meeting of the Associated Professional Sleep Societies LLC (APSS)*, Boston, Massachusetts (June 2012).

Presentations

1. "Unobtrusive Monitoring of Sleep", Student Research Forum, Oregon Health & Science University, Portland, OR (May, 2008).

2. "Automatically Detecting Sleep Apnea using Load Cells placed under the Bed", Annual May meeting of the members of the Achievement Rewards for College Scientists (ARCS), Oregon Chapter (May, 2009).

3. "Automatically Detecting Sleep Apnea using Load Cells placed under the Bed", Student Research Forum, Oregon Health & Science University, Portland, OR (May, 2009).

4. "Automatically Detecting Sleep Apnea: Unobtrusive Heart Rate Detection", Student Research Forum, Oregon Health & Science University, Portland, OR (May, 2010).

5. "Automatically Detecting Sleep Apnea using Load Cells placed under the Bed", MBA Program, Oregon State University, Corvallis, OR (Sept, 2010).

6. "Classification of Lying Position Using Load Cells Under the Bed", Student Research Forum, Oregon Health & Science University, Portland, OR (May, 2011).

7. "Classification of Lying Position Using Load Cells Under the Bed", Annual International Conference of the IEEE Engineering in Medicine and Biology Society, Boston, MA (Aug, 2011).

8. "Unobtrusive Monitoring of Sleep using Load Cells under the Bed", Department of Biomedical Engineering, Oregon Health & Science University, Portland, OR (Dec, 2011).

9. "Unobtrusive Monitoring of Sleep using Load Cells under the Bed", Healthy Aging Alliance conference, Portland, OR (Oct, 2012).